DOCTOR OF PHILOSOPHY

Optical pulse generation using an optically injected Nd:YVO4 laser

Kamel, Nada

Award date:
2015

Awarding institution:
Bangor University

PRIFYSGOL
BANGOR
UNIVERSITY

Optical Pulse Generation using an Optically Injected Nd:YVO_4 Laser

Submitted by Nada A. Kamel

for the degree of

Doctor of Philosophy

Bangor University

2015

Declaration and Consent

Details of the Work

I hereby agree to deposit the following item in the digital repository maintained by Bangor University and/or in any other repository authorized for use by Bangor University.

AuthorName: …Nada A. Kamel

Title: Optical Pulse Generation using an OpticallyInjected Nd:YVO_4 Laser

Supervisor/Department: Prof. K. Alan Shore/School of Electronic Engineering

Funding body (if any): ……/……

Qualification/Degree obtained: PhD In Electronic Engineering

This item is a product of my own research endeavours and is covered by the agreement below in which the item is referred to as "the Work". It is identical in content to that deposited in the Library, subject to point 4 below.

Non-exclusive Rights

Rights granted to the digital repository through this agreement are entirely non-exclusive. I am free to publish the Work in its present version or future versions elsewhere. I agree that Bangor University may electronically store, copy or translate the Work to any approved medium or format for the purpose of future preservation and accessibility. Bangor University is not under any obligation to reproduce or display the Work in the same formats or resolutions in which it was originally deposited.

Bangor University Digital Repository

I understand that work deposited in the digital repository will be accessible to a wide variety of people and institutions, including automated agents and search engines via the World Wide Web.I understand that once the Work is deposited, the item and its metadata may be incorporated into public access catalogues or services, national databases of electronic theses and dissertations such as the British Library's EThOS or any service provided by the National Library of Wales.

I understand that the Work may be made available via the National Library of Wales Online Electronic Theses Service under the declared terms and conditions of use (http://www.llgc.org.uk/index.php?id=4676). I agree that as part of this service the National Library of Wales may electronically store, copy or convert the Work to any approved medium or format for the purpose of future preservation and accessibility. The National Library of Wales is not under any obligation to reproduce or display the Work in the same formats or resolutions in which it was originally deposited.

Statement 1:

This work has not previously been accepted in substance for any degree and is not being concurrently submitted in candidature for any degree unless as agreed by the University for approved dual awards.

Signed …….. (candidate)

Date ……..

Statement 2:

This thesis is the result of my own investigations, except where otherwise stated. Where correction services have been used, the extent and nature of the correction is clearly marked in a footnote(s).

All other sources are acknowledged by footnotes and/or a bibliography.

Signed …….. (candidate)

Date ……..

Statement 3:

I hereby give consent for my thesis, if accepted, to be available for photocopying, for inter-library loan and for electronic storage (subject to any constraints as defined in statement 4), and for the title and summary to be made available to outside organisations.

Signed …….. (candidate)

Date ……..

NB: Candidates on whose behalf a bar on access has been approved by the Academic Registry should use the following version of **Statement 3:**

Statement 3 (bar):

I hereby give consent for my thesis, if accepted, to be available for photocopying, for inter-library loans and for electronic storage (subject to any constraints as defined in statement 4), after expiry of a bar on access.

Signed …….. (candidate)

Date ……

Statement 4:

Choose **one** of the following options

a) I agree to deposit an electronic copy of my thesis (the Work) in the Bangor University (BU) Institutional Digital Repository, the British Library ETHOS system, and/or in any other repository authorized for use by Bangor University and where necessary have gained the required permissions for the use of third party material.	✓
b) I agree to deposit an electronic copy of my thesis (the Work) in the Bangor University (BU) Institutional Digital Repository, the British Library ETHOS system, and/or in any other repository authorized for use by Bangor University when the approved bar on access has been lifted.	
c) I agree to submit my thesis (the Work) electronically via Bangor University's e-submission system, however I opt-out of the electronic deposit to the Bangor University (BU) Institutional Digital Repository, the British Library ETHOS system, and/or in any other repository authorized for use by Bangor University, due to lack of permissions for use of third party material.	

Options B should only be used if a bar on access has been approved by the University.

In addition to the above I also agree to the following:

1. That I am the author or have the authority of the author(s) to make this agreement and do hereby give Bangor University the right to make available the Work in the way described above.
2. That the electronic copy of the Work deposited in the digital repository and covered by this agreement, is identical in content to the paper copy of the Work deposited in the Bangor University Library, subject to point 4 below.
3. That I have exercised reasonable care to ensure that the Work is original and, to the best of my knowledge, does not breach any laws – including those relating to defamation, libel and copyright.
4. That I have, in instances where the intellectual property of other authors or copyright holders is included in the Work, and where appropriate, gained explicit permission for the inclusion of that material in the Work, and in the electronic form of the Work as accessed through the open access digital repository, *or* that I have identified and removed that material for which adequate and appropriate permission has not been obtained and which will be inaccessible via the digital repository.
5. That Bangor University does not hold any obligation to take legal action on behalf of the Depositor, or other rights holders, in the event of a breach of intellectual property rights, or any other right, in the material deposited.
6. That I will indemnify and keep indemnified Bangor University and the National Library of Wales from and against any loss, liability, claim or damage, including without limitation any related legal fees and court costs (on a full indemnity bases), related to any breach by myself of any term of this agreement.

Signature: …… Date : ……..

Acknowledgments

It is my pleasure to have here the opportunity to warmly acknowledge all those who have supported me during my PhD at Bangor University. I would first like to express my gratitude for my supervisor Professor K. Alan Shore for his encouragement and endless patience with me throughout the research and writing this thesis. I would like to express my appreciation for Professor Deb Kane, of Macquarie university, Sydney, for her short visits, but valuable to provide me an important direction towards my research. I am grateful to Dr. Yanhua Hong for her guidance, discussions, and for the support in lab experiments. My thanks and acknowledgement to Dr. Tomas Fordell who provided me with his computational program to generate the dynamical map of the system used in the thesis. I would also like to thank my friend and colleague Dr. Zubaida Abdul Sattar for her support and assistance whenever I need her help during my PhD.

My thanks and acknowledgements to the authority of Bangor University for providing a good environment and facilities, especially the staff at school of electronic engineering for their assistance and friendly environment.

Last, I would also like to offer my kind regards to my husband Salama, my sister Basma, my daughter Haya and friends for their motivation and moral support.

Abstract

This thesis experimentally investigates the use of the optically injected solid state-laser system as a new approach to generate optical pulses with a continuous range of pulse repetition frequency. The construction of the system, the basic requirements and various performance characteristics of different dynamical states resulted from the optical injection are introduced and discussed.

One of the objectives of this research is to investigate control over the pulse repetition frequency (PRF) of the nonlinear dynamics of solid state laser, by varying the frequency detuning between the free running injection and the main lasers. For this purpose, the response of the pulse repetition frequency to the changes in the detuning is evaluated for the main dynamical regimes that operate in this system. The results showed a high level of response of PRF to the changes in detuning for the period-doubling regime and for the limit cycle regime with a correlation coefficient between the PRF and the detuning of around 0.99. A very low correlation coefficient for the same variables, of 0.2 and less are determined in the spiky regime, showing low response to the detuning change. While different correlation coefficients of PRF and detuning were obtained in the quasi-periodic regime. The results revealed a bistable behaviour of periodic and quasi-periodic waveforms in the spiky regime.

Pulses with a continuously variable pulse repetition frequency and intensity, are obtained by adjusting the frequency detuning between the frequencies of the injection laser and main laser. The accessible range of pulse repetition frequency in this system is from approximately 200 kHz up to 7.5 MHz. The experimental curves reveal that the relationship between PRF, intensity and detuning is a piecewise function which means that different parts have different properties.

The thesis includes also, an evaluation of the frequency instability of the optically pumped solid state laser that leads to stabilise the optically injected solid state-laser system. In this regards, normalised root Allan variance is used as a measure of the instability. The lowest frequency instability of the free running Nd:YVO_4 laser was measured to be 10^{-11} for evaluating time less than 1ms. The frequency instability of the optically pumped Nd:$GdVO_4$ is also evaluated, showing approximately a similar level of instability as Nd:YVO_4. The two lasers show a normal level of frequency instability compared to other kinds of optically pumped solid-state lasers. The investigation

reveals the existence of many kinds of systematic noise mostly related to the temperature controlling system.

This work paves the way to employ the nonlinear dynamics of an optically injected Nd:YVO_4 laser as a source of optical pulses.

Contents

Chapter 1

Introduction

1.1. General introduction

The research described in this thesis represents a new approach for generating laser light pulses having a controllable repetition frequency. The approach exploits the relaxation oscillation resonance which is the exchange of energy between the electric field and the population inversion density. The relaxation oscillation resonance is damped for free running laser, exciting this resonance by an external field, such as optical injection or external optical feedback causes undamped oscillations [1].

In this approach, an external injection beam modifies the dynamical behaviour of the solid-state laser. As a result, continuous wave operation is changed to pulsed output, with a pulse repetition frequency variable in a continuous range from a few hundred kHz to a few MHz and with pulse durations of a few tens of nanoseconds.

Many applications that require optical pulses need a waveform of a specific pulse duration, a specific pulse repetition rate, or even a specific pulse shape. It is usually difficult to design a laser with these specific performances. A laser with variable characteristics can play a role in producing these exact requirements. Few kinds of lasers have this feature, and most of them either have poor beam quality and high jitter or need to change a design parameter, which is not preferable in general [2,3].

The work of this thesis is concerned with an optically injected solid-state laser and stands in contrast to other kinds of laser pulse generators, such as Q-switched and gain-switched lasers, that also can provide the continuous ranges of pulse repetition frequency in MHz range. However, it is premature to compare these two techniques that have received interest for many decades with optically injected solid-state laser, which has not yet reached its state of maturity.

Using optically injected lasers to generate laser pulses offers many features including generating different waveforms of laser pulses, as well as, controlling the pulse

repetition frequency, pulse power, and possibly pulse duration continuously by a single parameter.

From a dynamical point of view, lasers can be classified depending on the decay rate of three relevant variables, the electric field, the population inversion and the material polarization, in the laser resonator. According to this classification, there are three classes, named as class A, class B and class C lasers. Lasers like solid state lasers are class B lasers in which the polarization decays faster than the two other variables. Therefore the dynamical behaviour of single-mode class B lasers can be described by two equations, one for the electric field and the other for the population inversion (explained in chapter 3, section 3.2). Generating regular oscillation is possible with class B lasers with additional external perturbation like injection field [1].

The process of optical injection is illustrated in figure 1.1. In this system, two single-frequency lasers operate in a master-slave configuration, in which one of the two

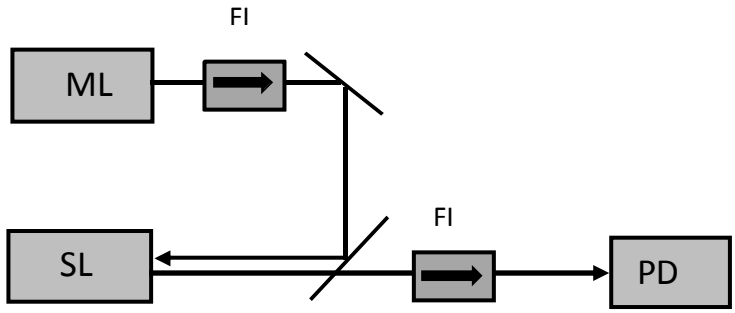

Figure 1.1. Schematic of optically injected laser: ML, master laser; SL, slave laser; FI, Faraday isolator; PD, photo detector.

lasers (the master) is used to inject the second laser (the slave). The optical injection has a variety of effects on the slave laser's output characteristics. The main effects are locking the frequency and the phase of the slave laser to the frequency and the phase of the master laser (injection locking), producing various dynamical instabilities, such as periodic, quasi-periodic, and chaotic behaviour. The system output characteristics depend on two operational parameters: the normalised injection strength (K), which represents the rate of the injected field that enters the slave laser cavity to the slave laser field normalized to the relaxation oscillation frequency of the slave laser. The second operational parameter is the normalised frequency detuning ($\Delta\omega$), which is

the frequency offset between the free running master and slave lasers normalised to the relaxation oscillation frequency of the slave laser. Changing these parameters caused dynamical changes in the system output.

The solutions of the rate equations with injection, can describe the dynamical changes in the laser output. These changes can be a quantitative or a qualitative changes, the qualitative changes in the dynamical behaviour called bifurcations. A bifurcation diagram which is, a visual summary of the possible solutions of the rate equations, is used to demonstrate different kinds of bifurcations as a function of the operational parameters of the injected system [4].

Optical injection is widely used in injection locking [5,6]. In many high power lasers, it is difficult to achieve a low-noise performance or a single frequency operation due to the high noise of the pumping source and the unavoidable thermal influences. Using the injection locking technique, the high power laser will be forced to operate on the injected frequency exactly, with relatively low intensity and phase noise. Using the same concept optical injection is used to synchronize one (or several) free running lasers to a stabilize master laser [7]. Optically injected lasers are also used to generate chaos. The chaotic behaviour used in many applications like secure communications [8].

The two applications introduced above, used the extreme states of the nonlinear dynamics which are a stable dynamics and a highly unstable dynamics. In between these two states optically injected laser could be used to produce controllable pulses. This thesis paves the way to employ the unstable dynamics as a source of optical pulses, using optically injected Nd:YVO_4 laser.

1.2. Thesis outline

Chapter 2 gives an overview of the early studies of unlocked dynamics generated by optical injection. A detailed review of the experimental and analytical studies of the nonlinear dynamics of a single mode Nd:YVO_4 solid-state laser is introduced. The chapter demonstrates the dynamical maps of the optically injected Nd:YVO_4 solid-state laser. These dynamical maps are used as a guide in the present work. The chapter also presents two kinds of instability related to this system (not to be confused with the dynamical instability), the first is the detuning fluctuations due to the unstable

frequencies of the two solid state laser and the second is the variation of the time interval between pulses.

Chapter 3 provides the necessary concepts that support operating and designing optically injected solid-state lasers. The rate equation model, the parameters that could be used to generate the pulses and the basic bifurcations in the bifurcation diagram are included. The chapter describes a diode end-pumped Nd:YVO_4 laser, the configuration used in pumping the lasers, and the properties of diode end-pumped Nd:YVO_4 lasers. The main requirements for the use of an optically pumped solid state laser in an optically injected-solid state laser system as a pulse generator are also discussed.

Chapter 4 explains the the optically injected Nd:YVO_4 system. The experimental setup is given. Controlling the frequency offset between the master and the slave lasers and controlling the injected beam using an acousto-optic modulator are explained in detail. The chapter includes practical information about operating the system and generating the pulses, and it explains two methods used to calculate the injection strength. Furthermore, the chapter includes procedures to facilitate optically injected-solid state laser system.

Chapter 5 provides a study of the characteristics of different dynamical regions. An experimental demonstration of the dynamics belonging to the dynamical states is introduced. To identify the regions of the dynamical map that are appropriate for generating a variable pulse repetition frequency, the response of the pulse repetition frequency to the frequency detuning changes is studied. For this purpose, a specific points on the (detuning, injection strength)-plane are chosen to represent different regions of the dynamical map. The chapter also investigates the existence of an unexplained large pulse-timing jitter spread throughout a wide region in the (detuning, injection strength)- plane.

Chapter 6 includes operating the system to produce a continuous variable pulse repetition frequency by varying the frequency detuning between the free-running master and slave lasers. This chapter investigates two ranges of injection strength specified in Chapter 5 and shows the accessible ranges of pulse repetition frequency this system can attain.

Chapter 7 presents a study of the optical frequency instability of the optically pumped solid-state lasers that are used in an optically injected solid-state laser system. The chapter introduces Nd:$GdVO_4$ crystal as a competent alternative to Nd:YVO_4 with additional good performance. The frequency noise in free running optically pumped Nd:YVO_4 and Nd:$GdVO_4$ lasers is evaluated.

Chapter 8 provides an overview of the main results of the previous chapters and makes suggestions for developing the optically injected solid-state laser system.

References

1. Ohtsubo, Junji. Semiconductor lasers: stability, instability and chaos. Vol. 111. Taylor & Francis, 2006.
2. Rabek, Jan F., and Jean-Pierre Fouassier. Lasers in polymer science and technology: applications. Vol. 1. CRC Press, 1989.
3. Kane, D. M., and J. P. Toomey. "Variable pulse repetition frequency output from An optically injected solid state laser." Optics Express, vol. 19,no. 5, pp. 4692-4702, 2011.
4. Drazin, P. G. "Nonlinear Systems, Cambridge texts in applied mathematics." (1992).
5. Mogensen, Finn, Henning Olesen, and Gunnar Jacobsen. "Locking conditions and stability properties for a semiconductor laser with external light injection." IEEE Journal of Quantum Electronics, vol 21, no. 7 ,pp. 784-793, 1985.
6. Lariontsev, E. G., I. Zolotoverkh, P. Besnard, and G. M. Stéphan. "Injection locking properties of a microchip laser." The European Physical Journal D-Atomic, Molecular, Optical and Plasma Physics, vol. 5, no. 1,pp. 107-117, 1999.
7. Mogensen, Finn, Henning Olesen, and Gunnar Jacobsen. "Locking conditions and stability properties for a semiconductor laser with external light injection." IEEE Journal of Quantum Electronics,vol. 21, no. 7, pp. 784-793, 1985.
8. Uchida, Atsushi. Optical communication with chaotic lasers: applications of nonlinear dynamics and synchronization. John Wiley & Sons, 2012.

Chapter 2

Background

2.1. Historical review

In 1984, Tredice et al. studied theortically, the dynamics of an optically injected class B laser, discussing the stability of the steady-state and the time-dependent state [1]. This work showed if the injected field does not satisfy an injection locking condition, the system will destabilize. The numerical results showed under specific conditions the laser pulses with a damping oscillation became undamped. In this work the process of producing undamped oscillation instigated by an external field, called self-Q-switching. The pulse repition frequency of the pulses is related to the amplitude of the external field.

In 1993, Simpson and Liu [2] introduced a theoretical analysis in terms of the phase and amplitude modulations caused by mixing of the optical fields in the injected laser. They used a model of an unlocked injected laser, which takes into account the effect of the Fabry-Perot resonant cavity. The model is applicable to most class B lasers .

Yeung and Strogatz [3] studied the rate equation model of a solid-state laser with injection. The paper reports three unlocking mechanisms (or three routes to locking) in this kind of laser. They report a route to locking in an intermediate regime between locking via a saddle-node bifurcation and locking via a Hopf bifurcation. This route to locking involves cascades of periodic orbits and was identified later as a period-adding sequence.

Such work gave motivation for more studies in the field of nonlinear behaviour in lasers. In 2002, Krauskopf and Wieczorek performed an important Investigation [4, 5]. This research studied the route to locking in class B lasers subjected to optically injected light and introduced a deeper understanding of the optical injection phenomena. Although the study intended to explain the dynamical complexity of a semiconductor laser, it was used to explain the behaviour of other kind of injected laser systems.

The study considered the linewidth enhancement factor (α) (the amplitude-phase coupling), as the most important parameter that specifies the dynamical behaviour of

the lasers. The work is concerned with the bifurcation diagram in the injection strength and detuning (K, Δω)-plane for different fixed values of a linewidth enhancement factor, while the other material parameters remain fixed. Some of the important results are shown in figure 2.1. The figure shows the bifurcation curves associated with the accumulation of large regions of periodic orbits. The bifurcation curves are: saddle-node bifurcation (SN) (a transition mechanism between synchronization (phase locking) and modulation (beating oscillations)), Hopf bifurcation (H) (a bifurcation to a limit cycle (periodic behaviour)) and torus bifurcation (T) (a bifurcation to quasi-periodic oscillation).

The periodic orbits are: saddle-node of limit cycle orbits (SL^j) (limit cycle oscillation) and period-doubling orbits (P^j)(orbits include bifurcation which occurs when a new limit cycle emerges from an existing limit cycle, and the period of the new limit cycle is twice that of the old one), where (j = 1, 2, . ..).

According to Krauskopf and Wieczorek's results, and considering the linewidth enhancement factor (α) for solid-state lasers = 0, the behaviour of the optically injected solid-state laser is represented by the figures 2.1 A(a) and 2.1 B(a) .

(A)

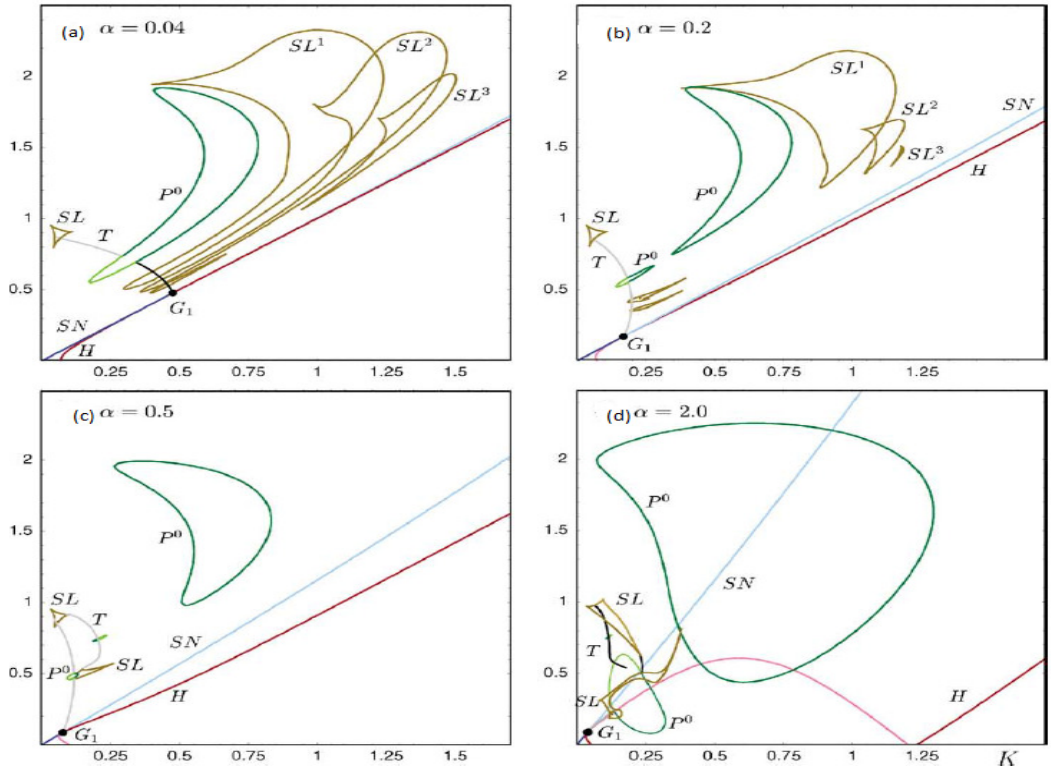

(B)

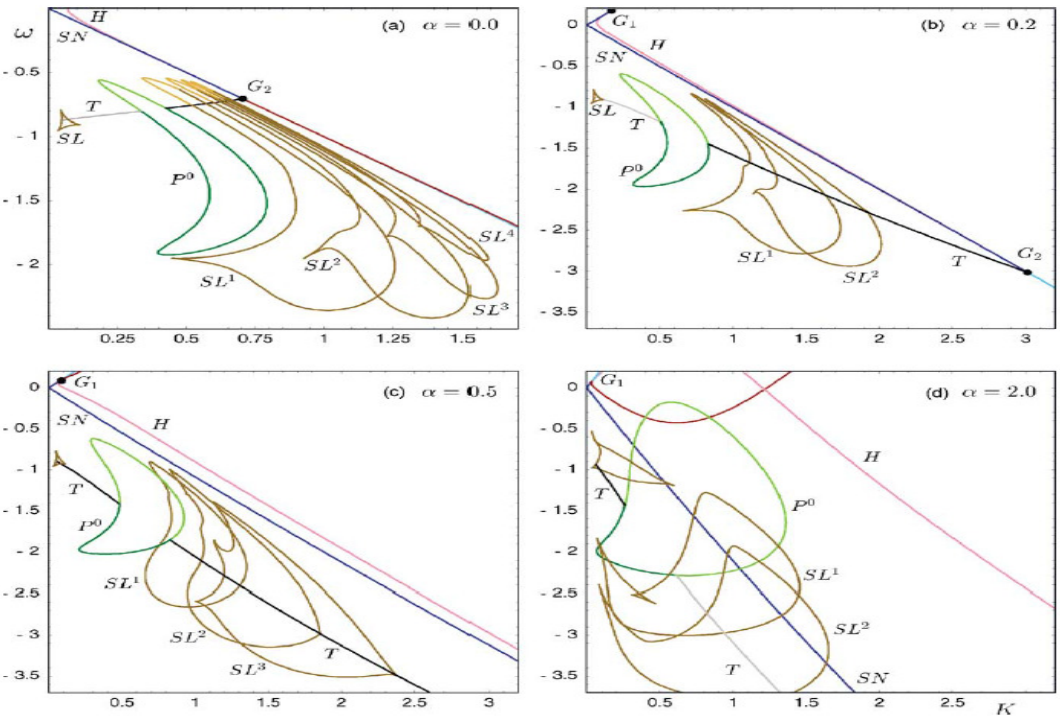

Figure 2.1. Transition of the accumulating regions in the (K, Δω)-plane with increasing α; from (a) to (d) α takes the values 0.04, 0.2, 0.5, and 2.0. The bifurcation curves are: Saddle-node bifurcation (SN), Hopf bifurcation (H) and torus bifurcation (T). The winding Periodic orbits are: saddle-node of limit cycle orbits (SL^j) and Period-doubling orbits (P^j) for j = 1, 2, . . ., Points G1 and G2 represent SN-Hopf bifurcation points. (A) for positive detuning, (B) for negative detuning. After [5].

2.2. An optically injected $Nd:YVO_4$ solid state laser studies

Optically injected solid state laser (OISSL) has been investigated by S. Valling et al. [6,7,8,15] and by Toomey and Kane. [9,10,11].

In [6], the dynamics of an optically injected solid state laser has been investigated both experimentally and numerically using intensity time series analysis. The experimental time series have been generated by keeping the frequency detuning ($\Delta\omega$) constant and controlling the injection strength (K). Intensity time series are also obtained numerically with a rate equation model for comparison with the experimental results. In this study different dynamical pulses have been generated and compared to the simulated results. The simulated results showed good agreement with the experimental results if the linewidth enhancement factor (α) is chosen to be between 0.2 and 0.35.

These results established that the linewidth enhancement factor in solid state laser is non-zero. According to this result the expected dynamical map of solid state laser in figure 2.1, should be closed to panel (b) or (c) with small α value rather than (a) with α equal zero.

In [7,15] maps of the dynamics of an optically injected $Nd:YVO_4$ laser are generated numerically and experimentally (a complete set of data) for all dynamical regions. The experimental map (figure 2.2 a), is generated from the measured intensity time series by plotting the maximum of intensity. For this purpose, a long time series of the laser intensity with increasing K and several fixed values of $\Delta\omega$ were measured. The results, normalized to the steady state value are plotted in the K-ω plane as a colour coding of the maximum intensity. The red colour on the map corresponds to a large amplitude whereas the blue colour corresponds to a small amplitude. The value one (dark blue) means that the laser has the same output as in the free running case. The highest peaks are about 12 times higher than the free running laser intensity.

The numerical map (figure 2.2 b) which represents the maximum of the intensity time series is plotted in the same way. Each value of intensity is found by direct integration of the model equations at numerous points in the K-ω plane. Experimental and numerical maps are shown to be in a good agreement with each other. Full details of the rate equation model used to generate the the numerical map shown above can be

found in reference [7]. The model describes the dynamics of a single mode solid state laser subject to external optical injection:

$$\frac{dE}{dt} = \left[\frac{1}{2} (1 - i\alpha) \frac{\gamma_c \gamma_n}{\gamma_s J} (N - 1) - \frac{1}{2} \gamma_p (E^2 - 1) + i(\Delta\omega)\Omega_R \right] E + K\Omega_R \quad (2.1)$$

$$\frac{dN}{dt} = \gamma_s(1 - N) + \gamma_s J (1 - E^2) + \gamma_n E^2 (1\text{- N}) + \frac{\gamma_p \gamma_s J}{\gamma_c} E^2(E^2 - 1) \quad (2.2)$$

Here, E is the electric field envelope, N is the population inversion density, both E and N are normalized to their steady state values (no injection), $J = (J_o - J_{th}) / J_{th}$ is the pump power J_o normalized to its threshold value J_{th}, γ_c is the decay rate of the cavity, γ_s is the decay rate of upper state level, γ_n is the relaxation rate of the differential gain, γ_p is the relaxation rate of the nonlinear gain, α is the linewidth enhancement factor, $\boldsymbol{\Omega}_R$ is the angular relaxation oscillation frequency of the slave laser, $\Delta\omega = 2\pi (\nu_{ML} - \nu_{SL}) / \boldsymbol{\Omega}_R$ is the normalized frequency detuning between the master and the slave laser where ν_{ML} is the master laser frequency and ν_{SL} is the slave laser frequency, K is the normalized injection strength ($K = (\boldsymbol{\eta} / \boldsymbol{\Omega}_R) (|E_i| / |E_o|)$, where $\boldsymbol{\eta}$ is the coupling rate, E_i and E_O are the injected and the free running oscillating field amplitudes). The dimensionless parameters Δω, K are used in equation 2.1, 2.2 to characterise the dynamic performance. The numerical model used to generate intensity stability maps shown in chapter 4 (section 4.4) is taken from reference [7]. The maps were generated using the rate equation model outlined above.

Equation 2.1, 2.2 includes nine parameters, two of them, which can be changed experimentally, are the detuning and the injected strength. The five parameters α, γ_c, γ_s, γ_n and γ_p are called the material parameters and are fixed for a certain laser. The normalized pump power J and the relaxation oscillation frequency $\boldsymbol{\Omega}_R$ can be optimized for a given experiment. The solutions of equations 2.1 and 2.2 display a number of diverse dynamics.

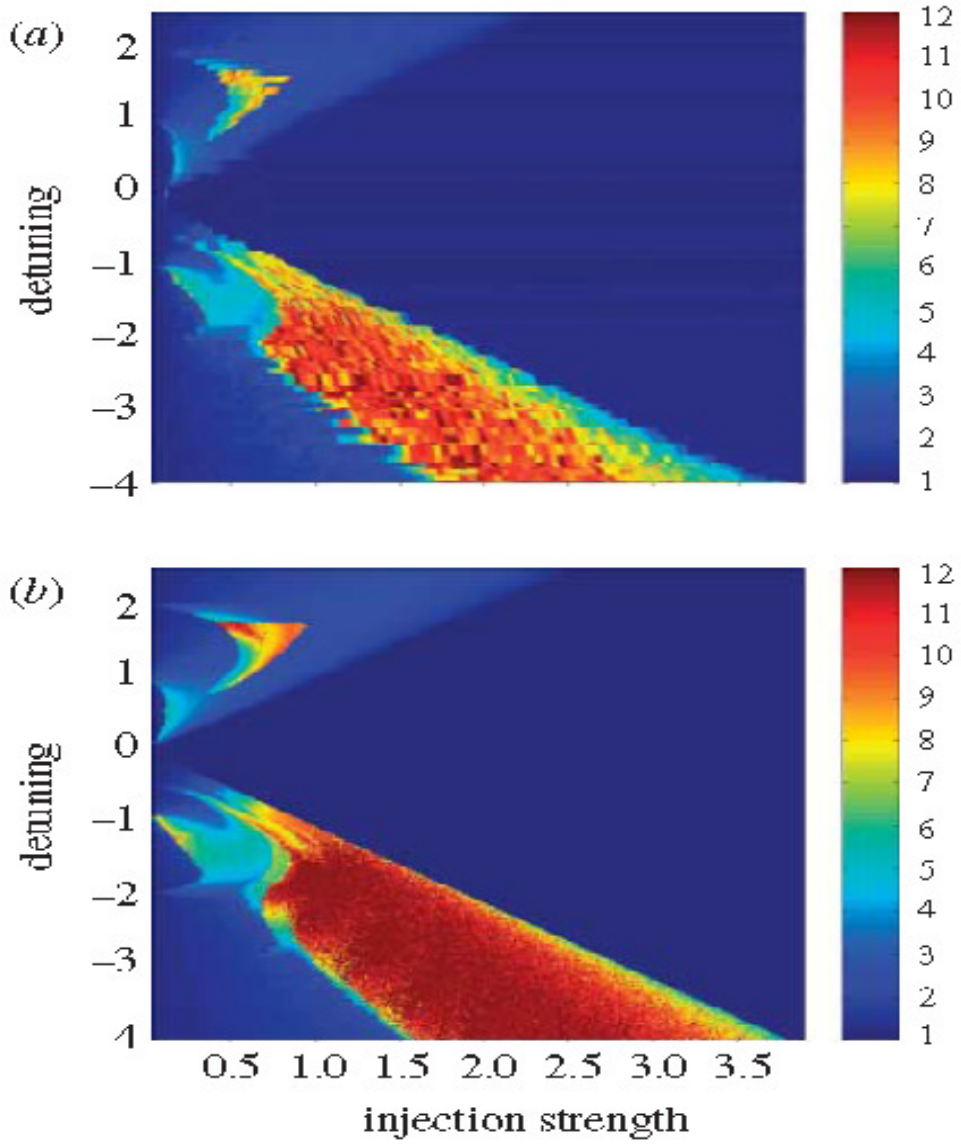

Figure 2.2: (a) Experimental map, where the color coding reveals the intensity time series maxima for certain (K, Δω). (b) Numerical map of intensity time series maxima with α=0.35. After [15].

To identify different types of dynamical behaviour, the bifurcation diagram (figure 2.3) is determined by solving equation 2.1, 2.2 [7]. The diagram represents the basic bifurcations of the optically injected solid state laser in the K-Δω plane consisting of saddle-node bifurcations (SN), Hopf bifurcations (H), period-doubling bifurcations (PD), and torus bifurcations (T). The bifurcation curves in the (K,ω)-plane are the boundaries at which the laser's behaviours changes qualitatively. In figure 2.3 there

are two bifurcation curves confining a locking region (the cone-like region in the middle) in which the laser locks to the injection laser showing relatively constant power and oscillating with the master laser frequency. The two curves are the saddle-node bifurcation and the Hopf bifurcation.

In the positive detuning region and along the Hopf bifurcation H, a limit cycle is created. By changing the experimental parameters, the limit cycle changes stability through the period doubling regime. In the negative detuning region, crossing the saddle-node bifurcation results in a sudden change in the amplitude and the frequency of the oscillation.

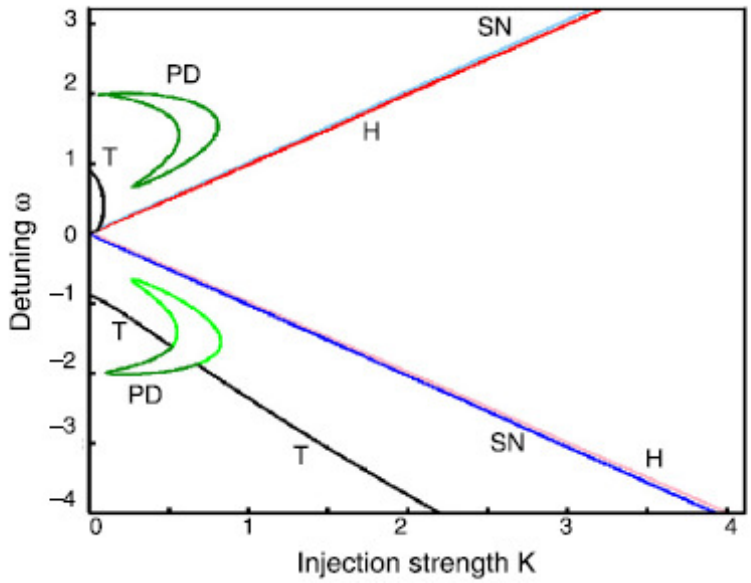

Figure 2.3. Theoretical bifurcation diagram of the rate equation model showing the basic bifurcations. Saddle-node (SN) bifurcations in blue, Hopf (H) bifurcations in red, period-doubling (PD) bifurcations in Green, and torus (T) bifurcations in black. After [7].

Two crescent-shaped regions above and below the locking region represent period-doubling regimes. The limit-cycle regime dominates in the area above the Hopf bifurcation curve for positive detuning and below the torus bifurcation curve for negative detuning. Far outside these areas, for higher frequency detuning range, a noisy free-running regime dominates with an oscillation frequency equal to the relaxation oscillation frequency of the injected laser.

An experimental bifurcation diagram of optically injected solid state laser was determined in [8]. A new method to construct the experimental bifurcation diagram of

an optically injected Nd:YVO4 solid state laser in the (K-Δω) plane was presented. The approach is to characterize the different bifurcations in terms of indicators determined from the experimental map. Different dynamics and bifurcation curves were deduced from the different properties of long time series maxima.

In [9] the correlation dimension (a statistical index of complexity of a nonlinear system) which provides a tool to quantify self-similarity contained in nonlinear behaviour was used to study the degree of the complexity of the output of OISSL system. In this research, a map of the correlation dimension as a function of the injection strength and frequency detuning are extracted from the time-series data of the laser output power that was been used in [7,8]. The map is in agreement with prior investigations of this laser system (figure 2.4). It also gives further insight into the

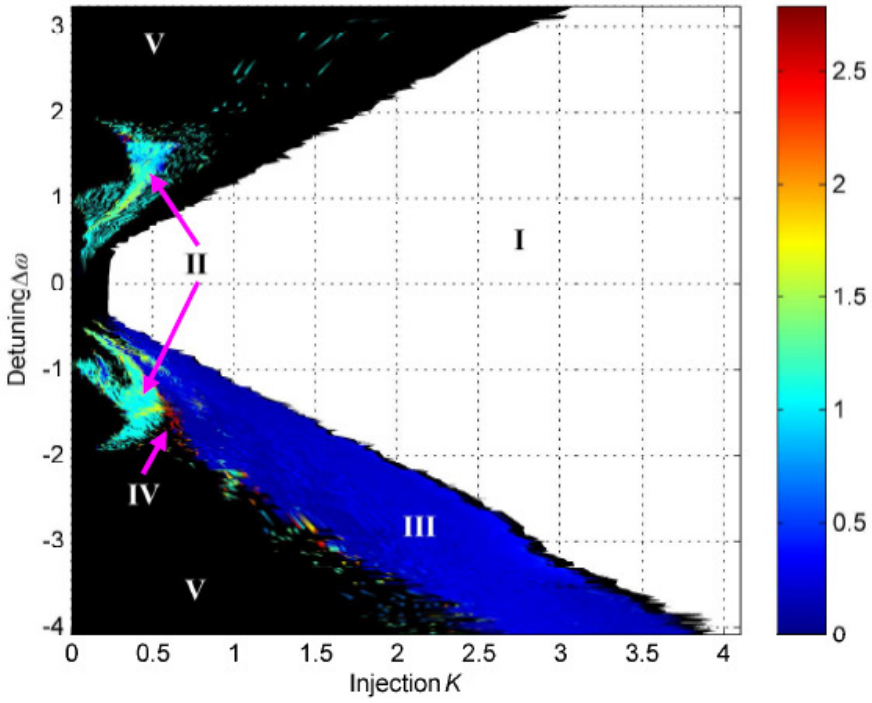

Figure 2.4. Correlation dimension (CD) map in the (K, Δω) plane of experimental data. The different dynamical region is identified as I: Locked (no data), II: Periodic (CD = 1), III: Spiky output (CD < 1), IV: Chaotic (CD > 2), V: Noisy (CD = ∞). After [9].

level of complexity of the different nonlinear dynamics. Details such as the small chaos regions (the red regions in figure 2.4) that are predicted in [5] are manifested clearly in the correlation dimensional map. The correlation dimension map was constructed

also from a simulated time series generated from the rate equation model. Both the experimental and simulated laser maps showed similar structure.

The using of the optically injected solid state Nd:YVO_4 laser as a pulse generator was demonstrated for the first time in [10] This work showed that the OISSL system can be operated as a source of laser pulses with a pulse repetition frequency (PRF) that can be continuously varied by a single control, ranging from 200 kHz up to 4 MHz and pulse durations between 10 and 100 ns. The map of the dominant frequency, identified as the inverse of the average pulse period of the peaks, was generated for all injection strengths and frequency detuning. The dominant frequency are represented by a colour bar (figure 2.5). The same experimental intensity time series used in [7] was employed in this work. The same map with a rescaled coloured bar, to show details in the range 0 to 4 MHz is shown in figure 2.6.

The results obtained also included maps of the dominant frequency from simulated time series in the (K, $\Delta\omega$) plane for full pulse repetition frequency scale and a map scaled to highlight PRF between 0 and 4 MHz. The simulated map was generated from a single mode, rate equation model as described in [9,10]. The range of pulse repetition frequency attainable from this system as a function of the injection strength for fixed detuning is shown and discussed in detail in chapter 6.

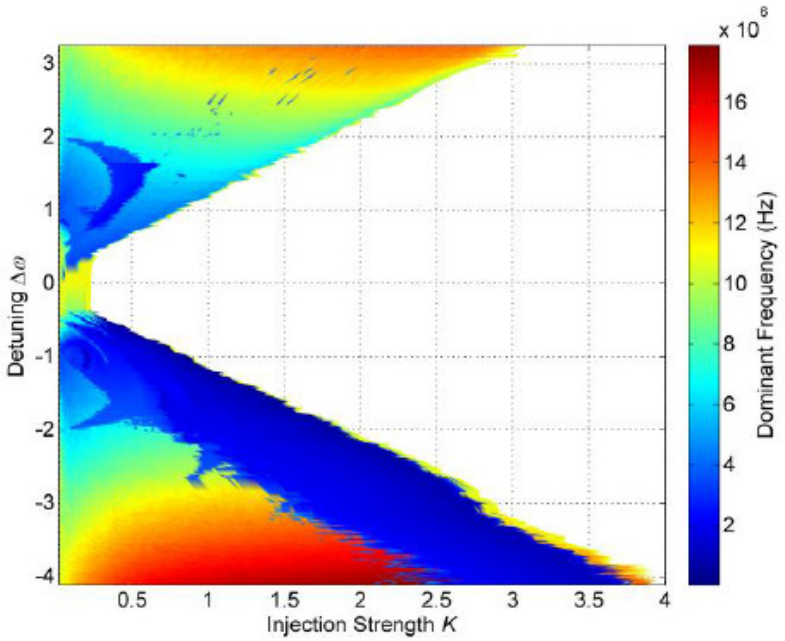

Figure 2.5. Dominant frequency from experimental intensity time series in the (K, Δω) plane. After [10].

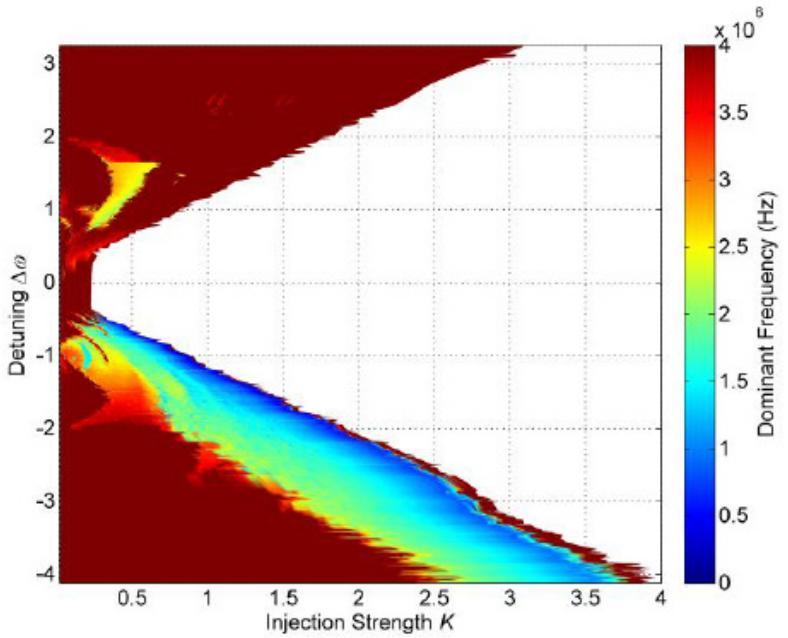

Figure 2.6. The same map of the (K, Δω) plane as in figure 2.4 with a rescaled colour bar to highlight features in the 0 to 4 MHz scale. After [10].

2.3. Instability of optically injected solid-state laser system

2.3.1. Detuning Instability of solid-state laser system

The optical frequencies of the two solid state lasers are not stable. The fluctuation in the optical frequencies can limit the performance of the system because the pulse repetition frequency of an optically injected laser system depends directly on the detuning between the optical frequencies of the main laser and the injected field.

The instability of the detuning has been discussed by T. Fordell [14]. The low characteristic frequency of these lasers (in MHz range) implies that the frequency stability of these lasers caused a problem in the experiments to generate the dynamical map of OISSL (figuure2.2) [7, and 8]. In this work, the map of dynamics of OISSL is generated by recording the intensity time series as a function of the injection power while keeping the detuning constant. By repeating this process for many detuning values it was possible to generate the map of intensity in a K-Δω plane. The sweep time should be long enough to register a suitable amount of time series data. Because it is

difficult to keep the beat frequency (detuning) between the lasers constant during the sweep of the injection power (with fluctuation approximately 200 kHz in10 ms in that system), a fast sweeping is used to provide a change in the normalized injection strength of 4 in 10 ms. Long term stability in this system is difficult to achieve, because no active stabilization methods can be allowed for the slave laser in the optically injected system This issue is investigated in chapter 7.

2.3.2. Instability of the time periods in different regions on the dynamical map

To study the constancy of the dynamics in OISSL, the standard deviation of the time period between pulses (given as a percentage ratio) is mapped in [11]. The map showed regions with very little variation in the inter pulse period like the two crescent shaped regions which correspond to the regions bounded by period doubling bifurcations [7,8]. The region just above the period doubling bifurcation boundary for negative detunings showed high standard deviation values. The reason of this high standard deviation of the time period, which occupy a wide area on the map, is not clear and needs more investigation. Figure 2.7 shows the standard deviation of the pulse period in the different regions of the map.

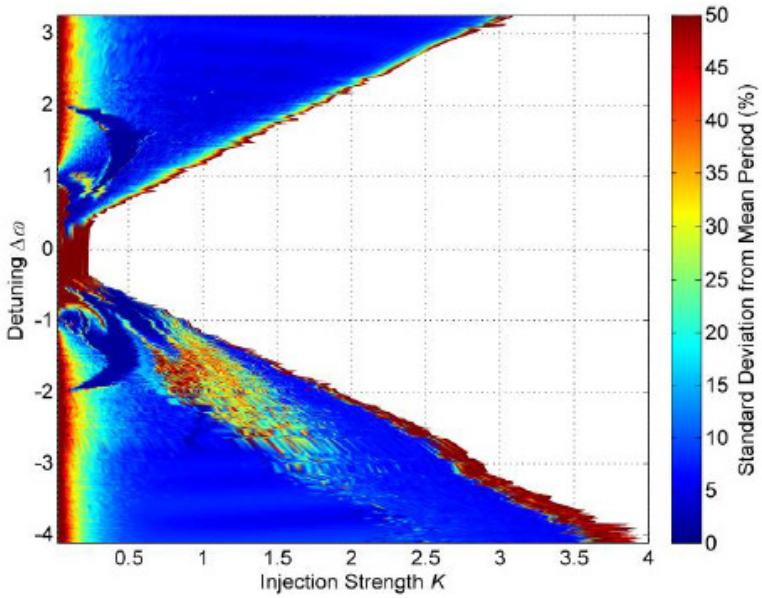

Figure 2.7: Showing the standard deviation in pulse period for all time series in the (K, Δω) plane. Red regions correspond to unstable pulses [11].

2.4. Conclusion

This chapter introduced the main previous studies on unlocking dynamics of optically injected lasers. In the second section, the nonlinear dynamics of an optically injected $Nd:YVO_4$ solid state laser studies are explained in details. The chapter introduced also the background of two important issues in an optically injected solid state laser system that can determine the performance of the system: the detuning Instability of solid state laser systems and the high instability of the time periods in a specific region on the dynamical map of the system.

References

1. Tredicce, J. R., et al. "Instabilities in lasers with an injected signal." Journal of the Optical Society of America B, vol. 2, no.1, pp. 173-183, 1985.
2. Simpson, T. B., and J. M. Liu. "Phase and amplitude characteristics of nearly degenerate four-wave mixing in Fabry–Perot semiconductor lasers." Journal of Applied Physics, vol. 73, no. 5, pp. 2587-2589, 1993.
3. Yeung, MK Stephen, and Steven H. Strogatz. "Nonlinear dynamics of a solid-state laser with injection." Physical Review E, vol. 58, no. 4, pp. 4421, 1998.
4. Krauskopf, Bernd, and Sebastian Wieczorek. "Accumulating regions of winding periodic orbits in optically driven lasers." Physica D: Nonlinear Phenomena, vol. 173, no. 1, pp. 97-113, 2002.
5. Wieczorek, Sebastian, et al. "The dynamical complexity of optically injected emiconductor lasers." Physics Reports, vol. 416, no. 1, pp. 1-128, 2005.
6. Valling, S., T. Fordell, and Å. M. Lindberg. "Experimental and numerical Intensity time series of an optically injected solid state laser." Optics Communications, vol. 254, no. 4, pp. 282-289, 2005.
7. Valling, Simo, Thomas Fordell, and Åsa Marie Lindberg. "Maps of the dynamics of an optically injected solid-state laser." Physical Review A, vol. 72, no. 3, pp. 033810 (1-7), 2005.
8. Valling, S., et al. "Experimental bifurcation diagram of a solid state laser with optical injection." Optics Communications, vol. 271, no. 2, pp. 532-542, 2007.

9. Toomey, J. P., et al. "Automated correlation dimension analysis of optically injected solid state lasers." Optics Express, vol. 17,no. 9, pp. 7592-7592, 2009.
10. Kane, D. M., and J. P. Toomey. "Variable pulse repetition frequency output from an optically injected solid state laser." Optics Express, vol. 19,no. 5, 4692- 4702, 2011.
11. Toomey, J. P., C. Nichkawde, and D. M. Kane. "Uncertainty in interpulse time interval evaluated as a new measure of nonlinear laser dynamics." Conference on Lasers and Electro-Optics/Pacific Rim. Optical Society of America, 2011.
12. Simpson, T. B., et al. "Period-doubling route to chaos in a semiconductor laser subject to optical injection." Applied Physics Letters, vol. 64, no. 26, pp. 3539-3541, 1994.
13. Fordell, T., and Å. M. Lindberg. "Numerical stability maps of an optically injected semiconductor laser." Optics Communications, vol. 242, no. 4, pp. 613-622, 2004.
14. Fordell, Thomas. "Dynamics of free-running, pump-modulated and coupled semiconductor and solid-state lasers.", PhD thesis, University of Helsinki, 2007.
15. Lindberg, Åsa Marie, Thomas Fordell, and Simo Valling. "Dynamics, bifurcations and chaos in coupled lasers." Philosophical Transactions of the Royal Society A: Mathematical, Physical and Engineering Sciences, vol. 366, no. 1864, pp. 427- 435, 2008.

Chapter 3

Basic concepts

3.1. Introduction

The aim of this chapter is to provide the necessary concepts that support operating and designing optically injected solid-state lasers (OISSL). The section discusses the characteristics of the highly efficient diode-pumped solid-state laser of Nd:YVO_4, including the basic laser operation process, the configuration used in the end pumping, and some of the most important optical and thermal properties of the diode end-pumping Nd:YVO_4 laser. The section also discusses the basic requirements of optically injected solid-state lasers.

3.2. Diode end-pumped Nd:YVO_4 laser

The improvements of diode lasers have led to the development of optically-pumped solid state lasers. The developments in material science and optics fields also enhanced the development of optically-pumped solid state lasers. A varies kinds of diode lasers and novel crystals led to test hundreds of laser transitions and to select the most efficient kinds [1,2].

Nd:YVO_4 (Neodymium-yttrium vanadate) has been selected as a laser gain element due to many characteristics, such as its large stimulated emission cross section, low fluorescence lifetime and strong broadband absorption at 809 nm. The large stimulated emission cross section and the low fluorescence lifetime are useful for efficient, high repetition rate pulsed operation [1,2]. Growing big Nd:YVO_4 crystals is rather difficult, with the emergence of diode pumping, Nd:YVO_4 has become an important solid-state laser material because small crystals are required with this pump source [2,3].

Diode-pumped solid state lasers of Nd:YVO_4 are considered the most efficient diode-pumped lasers for both side and longitudinal pumping modes, because of their high absorption efficiency (the peak absorption cross section is about five times larger than

of Nd:YAQ at 808 nm) which explains why Nd:YVO_4 laser is used as a microchip laser. The broad absorption spectrum makes Nd:YVO_4 more suitable for diode-laser pumping than other materials as a low-threshold laser material at emitting wavelength 1064 nm [2,4].

A solid state laser system is a combination of a doped ion and a hosting crystal. The type of doped ion determines the emission peak of the laser wavelength. At the same time, the emission peak is affected by the field of the host crystal, which causes a spectral shift of the peak due to the stark effect. As a one of the solid state lasers, Nd:YVO_4 consists of a host of YVO_4 with a small amount of Nd ions (Nd^{+3}) [5,7]. Figure 3.1 shows the operation of this kind of laser. The pump light raises electrons from the ground state, E (0), to the pump band metastable level (level with a relatively long lifetime) E (3).

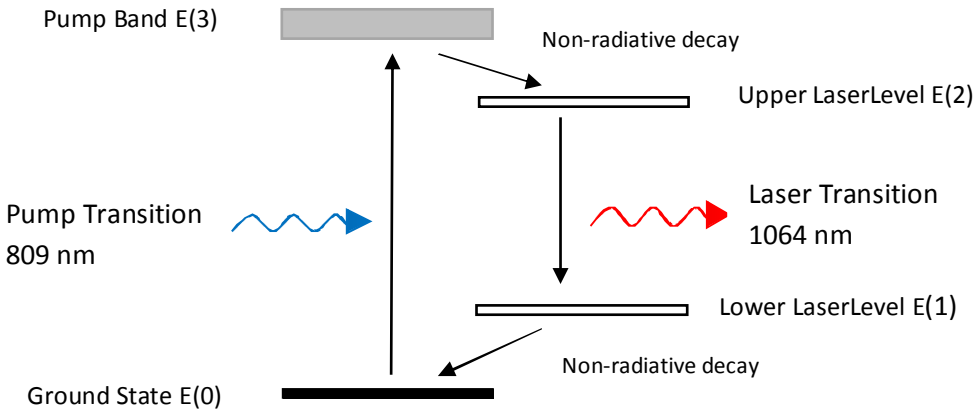

Figure 3.1. Energy levels diagram for four level lasers

The pumping band is a wide absorption band made up of a number of bands, so that optical pumping can be accomplished over a broad spectral range. The excited electrons are transferred into the sharp level E(2) by fast nonradiative transitions. The laser transition, however, proceeds to a fourth level E(1) by the emission of the photons. Therefore the laser transition takes place between the excited laser level E(2) and level E(1). Finally, the electron returns to the ground level E(0) by a rapid nonradiative transition. In this system, the existence of the metastable level E(3) is very important because this level with the relatively long lifetime provides a

mechanism by which an inverted population can be achieved. In the Nd:YVO_4 solid state laser, the transition from manifold $^4F_{3/2}$ to manifold $^4I_{11/2}$ of the Nd^{+3} ions is responsible for emitting the laser line at 1064 nm [3,5].

3.2.1 Basic configuration of a diode end-pumped Nd:YVO_4 laser

The basic configuration of a diode end-pumped Nd:YVO_4 laser (figure 3.2) consists of a diode-pumping source, coupling optics that direct the diode light into laser crystal, a monolithic laser crystal (crystal with coated mirrors on the crystal surfaces), and a collimating lens.

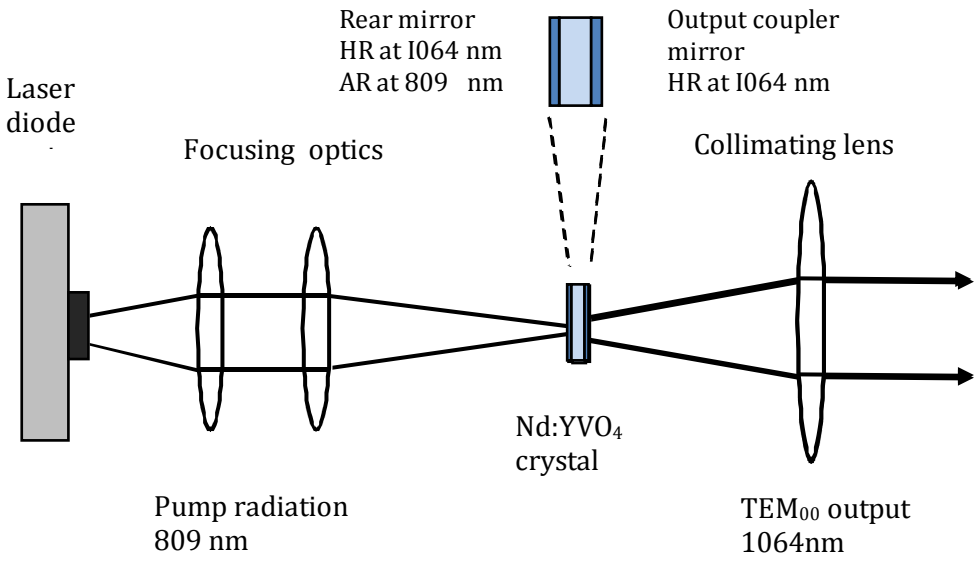

Figure 3.2. The basic configuration of a diode end-pumped Nd:YVO_4

The diode laser which emits a wavelength at about 809 nm (at 27°C) is used as a pumping source in this configuration because this wavelength has a large absorption cross section by the Nd^{+3} ions in YVO_4. The two end mirrors, the output coupler and the back mirror represent a plane-parallel optical resonator.

In this configuration a laser diode beam is focused to a small spot on the end of a laser crystal, and is directed along the laser axis. The high density of the pump beam

produces a low laser threshold and a high slope efficiency operation because both the threshold pump power and the pumping efficiency of the laser are related to the diameter of the pump beam [6]. This geometry produces a natural aperture (figure 3.3) operating on the fundamental transverse mode (TEM_{00}) in which the intensity distribution is approximated by a Gaussian profile.

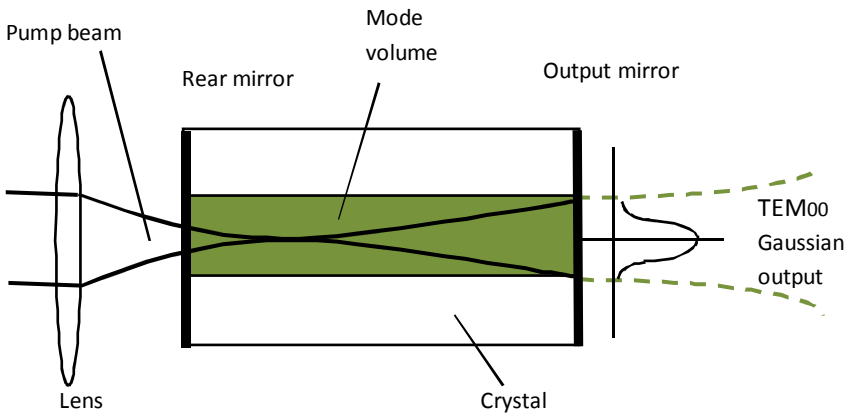

Figure 3.3. An end-pumped solid-state laser, the focused pumping beam causes confine oscillation in small volume and produce a natural aperture operating on the fundamental transverse mode (TEM_{00}).

This configuration allows the maximum use of the energy of the laser diode, first because high power density produces a high threshold and a high slope efficiency, as disscused. Second, the pump light can be deposited entirely within the crystal volume if a right crystal length is chosen. As an example using crystal length of 1mm, the fraction of the light (A) in which the crystal can absorb, can be determined using Beer's law [2,3].

$$A = 1 - e^{-\alpha \ell} \qquad (3.1)$$

where (ℓ) is the pathlength in the crystal, and (α) is the absorption coefficient.

The absorption coefficient for π direction (discussed in the next section) at wavelength 809 nm with a doping level of 1 % at. Nd, is approximately 34 cm^{-1} [2]. With a pathlength of 1 mm, the crystal can absorb approximately 96% of the pumping light.

3.2.2. Properties of diode end-pumping Nd:YVO_4 laser

3.2.2.1. Optical properties

Nd:YVO_4 is a uniaxial crystal, which means it has one optical axis in which the refraction does not depend on the polarization of light. For the other two axes, birefringence occurs; in this case, the refractive index depends on the polarization direction of the electric field causing the existence of two polarization states. The best absorption of light by this crystal is satisfied when a polarized light (like the diode laser) propagates in any of the polarized dependent axis. In addition, the maximum absorption is satisfied when an electric field of the incident light is parallel to the optical axis of the crystal (π polarization), rather than when the electric field of the incident light is perpendicular to the optical axis of the crystal (σ polarization).

3.2.2.2. Thermal properties

Figure 3.2 shows the existence of two nonradioactive transitions. The first is from the pumped band to the upper laser level and the second is from lower laser level to the ground state. These two transitions emit heat and are within the frequency range of the vibration spectrum of the host crystal lattice which in turn absorb this heat. Therefore, these two transitions represent the major source of heating in the optical pumping of Nd:YVO_4 laser. The thermal properties of the laser crystals are dominated by the nature of the host laser material through the thermal conductivity coefficient and thermal expansion coefficient.

In an optically injected solid state laser system, it is important to use an efficient heat removal to keep the crystal temperature stable with time. Any oscillation in the crystal temperature causes oscillation in the crystal optical path and translates to phase and frequency noise [7, 8].

In contrast to other kinds of pumping, the end-pumped laser produces heat in a small volume, along the pumping focused beam. For pump power close to the threshold, the thermo-optic effect (the change of the refractive index due to the change in the temperature) is less important [9]. However, this effect could increase the transverse

modes in the laser output due to the thermal lensing. These effects show the essential need for an effective technique to control and eliminate the generated heat through the lasing process.

3.3. Main requirements of OISSL as an optical pulse generator

There are three basic requirements of optically injected solid-state laser as an optical pulse generator, that should be available in the optically pumped solid-state lasers:

3.3.1. High laser power

In optically injected solid-state laser system, the high slave laser power is important for two reasons [10]. First, it is known that the experimental parameters K and Δω drive the laser close to the relaxation oscillation frequency ($\boldsymbol{\Omega}_r$) or its multiples ($2\boldsymbol{\Omega}_r$, $3\boldsymbol{\Omega}_r$,--, etc.) This is because the appearance of different oscillation states means some resonance oscillation states get excited in the laser. Therefore a large relaxation oscillation frequency provides a wider modulation range.

The relaxation oscillation frequency in solid-state laser depends on the average power, where:

$$\Omega_r = \frac{1}{2\pi} \sqrt{\frac{r-1}{\tau_c \tau_2}} \qquad (3.2)$$

Where τ_c is the cavity lifetime, τ_2 is the upper laser level lifetime, and r is the pumping rate, which is the ratio of the pumping power to the threshold pump power. If the laser operates far from the threshold power, it will oscillate with a higher relaxation oscillation frequency.

Second, the power of the OISSL system which is approximately the slave laser power, is required for different applications.

3.3.2. Single longitudinal mode operation

In many laser systems, there is a need to employ a single longitudinal mode laser with high power. Offering these two characteristics at the same time (without using additional techniques) is very difficult, because the length of the resonator required to produce a high power usually allows for many longitudinal modes to oscillate. The solution in such a case is to delay achieving higher power to a next stage, in which an optical amplifier can be used. However, this does not mean power should be ignored when operating the laser; it means priority should be given to maintain single mode operation and optimizing the power as possible.

Optically injected solid-state lasers operate ideally with a single-longitudinal mode. If the system operates with more than one mode, and the oscillation frequencies of these modes are not interacting with each other and not close to each other, it is possible to select one of the modes to interact with the injected beam. The extra modes, operate far from the selected mode will not affect the interaction between the injected mode and the selected mode of the slave laser. The drawback is the extra modes generate a heat (in the same way explained in subsection 3.2.2.2) in the laser crystal in addition to the heat generated from the selected mode. The additional heat can change the spectral properties of the selected mode and the system output.

Single-mode oscillation could be obtained using a variety of techniques, most of them involve the insertion of additional components into the laser resonator. Adding additional components in the laser cavity needs long laser cavity, which produces more noise. Single-mode oscillation can also be achieved by using diode end-pumping microchip (cavity length of less than 1 mm) lasers [1,2]. The microchip lasers are used in the recent work.

3.3.3. Low noise lasers

When using the OISSL as a pulse generator with destabilized region, any small change in the injection parameters due to noise, will translate directly to a change in the output characteristics. The high sensitivity to noise in OISSL as a pulse generator means design considerations for the noise effects (in particular, crystal length) must be considered, in addition to the need of the high power slave laser.

3.4. Conclusion

The chapter discussed the operating principle and the system requirements of the optically injected solid-state laser as a pulse generator. The second section explained the operation of the diode end-pumped Nd:YVO_4 laser, the basic configuration of this kind of laser, the properties of diode end-pumping Nd:YVO_4 laser including Optical and thermal properties.

The third section discusses the basic requirements of an optically injected solid-state laser system as an optical pulse generator that should be available in the optically pumped solid-state lasers. The requirements include, high laser power, single longitudinal mode operation and low noise lasers.

References

1. Taira, Takunori, Akira Mukai, Yukihiro Nozawa, and Takao Kobayashi. "Single-mode oscillation of laser-diode-pumped Nd:YVO_4 microchip lasers." Optics letters, vol. 16, no. 24, pp. 1955-1957, 1991.
2. Koechner, Walter. “Solid-state laser engineering”, vol. 1. Springer Science, 2006.
3. Scheps, Richard.” Introduction to laser diode-pumped solid state lasers”. SPIE Press, 2002.
4. Koechner, Walter, and Michael Bass.” Solid-State Lasers: A Graduate Text”, Springer Science, 2003.
5. Kalisky, Yehoshua Y.” The physics and engineering of solid state lasers”. vol. 71. SPIE Press, 2006.
6. Laporta, Paolo, and Marcello Brussard. "Design criteria for mode size optimization in diode-pumped solid-state lasers." IEEE Journal of Quantum Electronics, vol. 27, no. 10, pp. 2319-2326, 1991.
7. Ohtsubo, Junji.” Semiconductor lasers: stability, instability and chaos”. Taylor & Francis, 2006.
8. Siegman, Anthony E. "Lasers University Science Books." Mill Valley, CA 37, 1986.

9. Fields, R. A., M. Birnbaum, and C. L. Fincher. "Highly efficient Nd: YVO4 diode-laser end-pumped laser." Applied physics letters, vol. 51, no. 23, pp. 1885-1886, 1987.
10. Kemp, Alan J., Richard S. Conroy, Graham J. Friel, and Bruce D. Sinclair. "Guiding effects in Nd: YVO 4 microchip lasers operating well above threshold." IEEE Journal of Quantum Electronics, vol. 35, no. 4, pp. 675-681, 1999.

Chapter 4

Optically injected solid-state laser system

4.1. Introduction

In this chapter, a full description of the optically injected Nd:YVO_4 solid-state laser system is provided. The practical requirements to control the optical frequency offset between the crystals and to control the injection strength are discussed. The method used to quantify the normalized injection strength values is also explained. Finally, solutions to facilitate the system operation are presented.

4.2. Experimental setup and measurements

This system is established to study the characteristic of the OISSL system as an optical pulse-generator. The main purpose of this system is to produce pulses with changeable pulse repetition frequency (PRF) using fewer parameters. The experimental parameters that can be used to change the pulse repetition frequency of the pulses generated by the system are: the normalized frequency detuning between master and slave laser ($\Delta\omega$) and the normalised injection strength (K). In an optically injected solid-state Nd:YVO_4 laser, the optical frequencies can be controlled by changing the temperature of the crystals, and the injection strength can be controlled using any intensity attenuator. The basic requirements of the OISSL system are: two single mode lasers with two close optical frequencies of which at least one can be controlled.

4.2.1. The setup

The experimental setup is shown in figure 4.1. Two monolithic Nd:YVO_4 solid-state lasers are operated in a master-slave configuration (explained in chapter 1, section 1.1) in which the laser beam from one of the two lasers (the master) is directed to the second laser (the slave). The two solid state lasers are pumped using a single mode 809 nm SDL- 5421 diode laser (DL) using end pumping configuration explained in chapter 3.

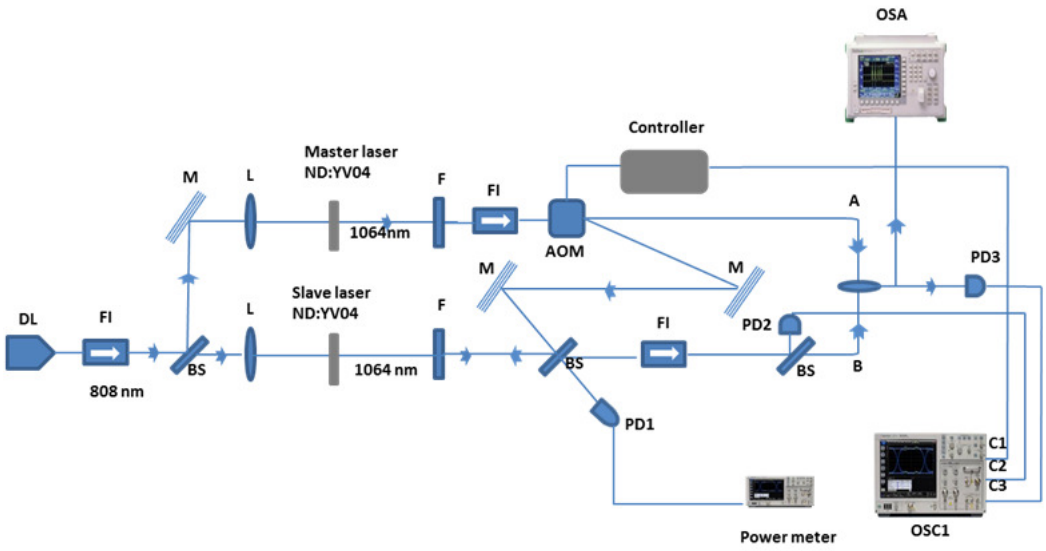

Figure 4.1. Experimental setup used to study the charicteristics of OISSL, showing the basic apparatus: DL, Diode laser; BS, beam splitter; F, filter; FI, Faraday isolator; L, lense; M, mirror; AOM, acousto-optic modulator; OSC, oscilloscope; OSA, Optical spectrum analyzer; A, B fiber heads; C1, C2, C3 are oscilloscope chanels, PD1, PD2, PD3 photo detectors.

The maximum output power of the diode laser is 150 mW. The diode laser collimated output beam is splited into two beams using a beam splitter (BS) to pump each of the solid-state lasers. Both Nd:YVO_4 crystals are 1 mm thick and 3x3 mm^2 area. The Nd:YVO_4 crystals are 1% Nd^{3+} doping and 5% output coupling at the end facet. To protect the DL from optical feedback, a Faraday isolator (FI) is placed between the pump laser and the beam splitter. The two pumping beams are focused into the crystals using a 25 mm objective lens (L). Two copper mounts with XYZ stages are used to fix and align the crystals with the pumping beam. A linearly π-polarised beam is used to pump each of the crystals along their pumping axis (chapter 3, section 3.3.2.1). To remove the pump light from the 1064-nm laser, two interference filters are used (F). The master laser output was directed to the slave laser through an acousto-optic modulator (AOM) with an operating frequency of 80 MHz. Two other Faraday Isolators are used in the setup to ensure the unidirectional injection operation and to prevent unwanted feedback reflected from the different optical apparatus.

An Optical spectrum analyser (ANRITSU MS9001B1) was used to enable coarse frequency tuning (few GHz range). To enable fine frequency tuning (few MHz range)

and to measure the beat frequency, 400-MHz photodeetector (PD3) connected to a Wave MASTER 8600A oscilloscope was used. The beat frequency was measured by finding the fast Fourier transformation (FFT) for the beat time series. A New Focus 1554-B-12 GHz photodetector (PD2) connected to the same oscilloscope was used to register the intensity time series of the injected laser. A detector PD1 was used to monitor the injected beam. This detector was connected to a LeCroy LC564A oscilloscope. To ensure the single mode operation of both lasers, a Fabry-Perot interferometer (Burleigh TL-15) was used. Finally, a power meter (THORLABS PM30) was used to measure the power.

4.2.2. Single mode operation

The spectral output of the laser is determined by the gain-bandwidth of the active material and the properties of the resonator. By considering the monolithic resonator as a Fabry–Perot system, the separation of the longitudinal modes ($\Delta\nu_m$) is given by

$$\Delta\nu_m = c/(2nd\cos\theta), \quad (4.1)$$

where θ is the incident beam angle, c is the speed of light, d is the length of the cavity and n is the refractive index of the cavity medium [1]. The longitudinal mode

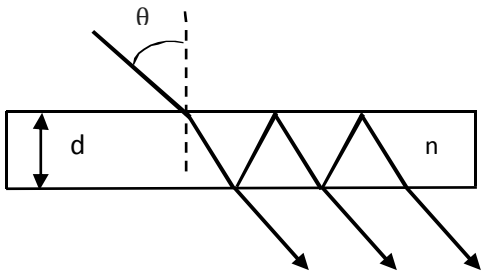

Figure 4.2. Fabry–Perot resonator where θ is the incident beam angle, d is the cavity length and n is the refractive index of the cavity medium.

separation of a 1mm monolithic Nd:YVO4, where n = 2.16 [2], considering a normal incidence of light, is 69 GHz. The number of oscillating modes (m) is given by

$$m = \Delta\nu_g/\Delta\nu_m \quad (4.2)$$

where $\Delta\nu_g$ is the gain bandwidth. The gain bandwidth for 1% at. Nd doping is 200 GHz, Using this relation the number of the oscillating modes is 2.8, which means that two

longitudinal modes will oscillate in this laser. Equation 4.1 illustrated in figure 4.2, shows the possibility of using the incidence angle to obtain single mode operation. This method is used successively in controlling the modes in this study.

4.2.3. Effect of the pumping beam alignment on the OISSL system

The pumping beam alignment plays an important role in the OISSL system performance because both the threshold pump power and the pumping efficiency of the laser are related to the diameter of the incident beam [3], The relaxation oscillation frequency ($\boldsymbol{\Omega}_r$) is affected also by the location of the focusing point of the pumping beam on the crystal. Equation 3.2 in chapter 3 shows the effect of the pumping parameters on the $\boldsymbol{\Omega}_r$ value. The relaxation oscillation frequency in the OISSL system as a pulse generator is very important because generating the pulse depends on the interaction between the injected electric field and the relaxation oscillation process. A high relaxation oscillation frequency offers a wide range of pulse repetition frequency.

4.2.4. Controlling the optical frequency offset between the crystals

The frequency offset (detuning) between the master and slave lasers in an optically injected solid-state laser can be controlled by changing the crystal temperature. To control the temperature of either crystal, Peltier elements are fixed inside the mounts and connected to temperature controllers. By changing the temperature, the frequency of each solid-state laser can be tuned. The temperature of the injected laser (the slave laser) is kept near room temperature, while the injection laser (master laser) operates at $\sim 12^0$C. The master laser is chosen for adjustment in order not to disturb the slave laser for as long as possible. Figure 4.3 shows the response of the master laser central frequency to the change in temperature. For a better control, the temperature controller can be connected to a DC source, to produce small changes in the temperature. To clarify this point, the temperature coefficient of oscillation frequency ($d\nu/dT$) for Nd:YVO_4 is -1.6 GHz $^oK^{-1}$ [4]. To produce a change in the detuning of 1 MHz, The crystal temperature should be changed by 0.62 m ^{o}K, this range of change is

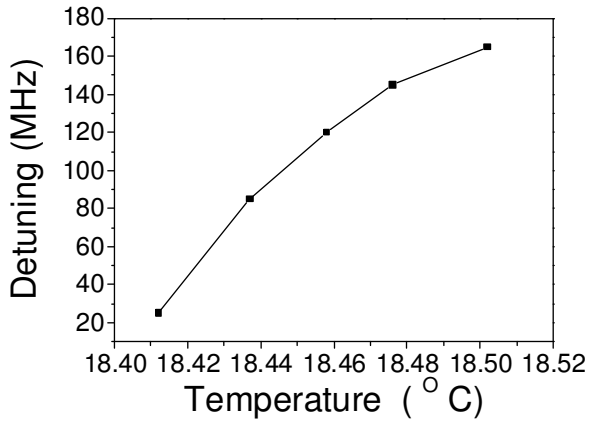

Figure 4.3. The detuning response to the change in the temperature of the master laser crystal.

possible by varying the connected DC voltage in a range of milivolt.

4.2.5. Solid-state laser pumping

The frequency detuning between the two lasers is a main parameter that could be used to control the OISSL. One of the most important types of noise in the detuning due to the unstable frequencies of the two lasers, is the low-frequency random walk noise [5]. This noise is shown in Figure 4.4, a, b. Figure 4.4 a, shows another kind of noise as a regular change (ripple) in the offset between the laser frequencies due to relative change of one of the frequencies to the other. Using a single optical pumping beam to

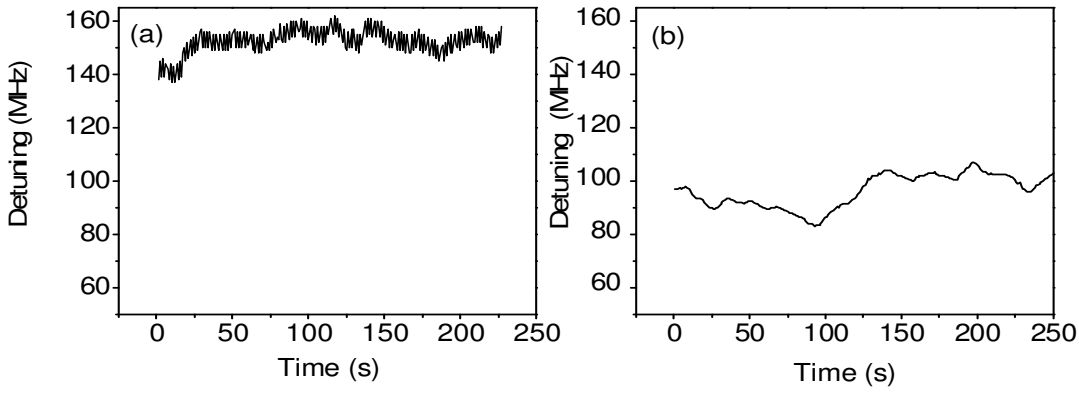

Figure 4.4. The change in the frequency detuning of the two lasers (free- running lasers) with the time , using (a) two pumping sources and (b) one pumping source.

pump the two solid-state lasers rather than two, removes this ripple and proved to be a good refinement in the performance of the OISSL system. Extra refinements are needed to stabilise this system. (Explained in chapter 7 and 8).

4.2.6. Controlling the injected beam using an acousto-optic modulator

The master laser output is directed to the slave laser through an acousto-optic modulator (AOM) with an operating frequency of 80 MHz is used for many purposes:

- To deflect the master laser output using the diffraction action of the acosto-optic modulator, so the first order (with frequency shift of 80 MHz) can be used for injection purpose. With no AOM action, the direct beam from the master laser along with the beam from the slave laser are coupled to generate a beat. The beat is used to determine the frequency detuning between the solid-state lasers. The master laser frequency is decreased by 80 MHz, so the beat detector will show the beat frequency around 80MHz. At the same time, when the AOM switsh on, the frequency of the first order beam will increase by 80 MHz and detuning between the injected field and the slave laser field will be around zero. The shift in the detuning helps distinguish the positive detuning from the negative detuning (explained in section 4.5.1).
- The AOM is used also to control the injection power. By employing a function generator connected to the AOM driver, the AOM can be operated with different types of periodic waves. The AOM output used to inject the slave laser can be controlled with different on-off signal modes. The type of modulation depends on the experiment requirement (explained in 4.3.3, 4.4).

4.3. Operating the system

4.3.1. Using time series analysis

In an optically injected solid state laser system, analysing the time series is a suitable way to obtain the measurement of the detuning and the pulse repetition frequency because the time scale of the generated pulse is in microseconds. With this range there is no need to use a very advanced oscilloscope. While a spectrum analyzer is used in many kinds of lasers where the time scale is in nanoseconds in which a very advanced oscilloscope is required.

4.3.2. The injection parameters

Dimensionless injection parameters, normalized frequency detuning ($\Delta\omega = (\nu_{ML} - \nu_{SL})/\Omega_r$) and normalized injection strength (K = injection strength (κ/Ω_r)) (chapter 3, section 3.2) are commonly used for ease of comparison of the results of different studies. The optimized values of the relaxation oscillation frequencies in most experiments are 4.15 MHz for the slave laser and 3.5MHz for the master laser; the output power of the slave laser is approximately 10 mW (except mentioned otherwise).

4.3.3. Pulse generation, determining the injection parameters and measuring the pulse repetition frequency

The established set up satisfies three basic requirements, which are:

- Generating optical pulses.
- Measuring the injection parameters (K, $\Delta\omega$).
- Measuring the pulse reptition frequency of the generated pulses.

Measuring the injection parameters is important for two reasons: to study the characteristics of the pulses in different regions in the K-$\Delta\omega$ map and to use these parameters as independent parameters to change the PRF of generated pulses. Once the characteristics of a specific OISSL system are known and fixed, it is possible to use the injected power directly instead of the injection strength to control the system.

To generate the pulses, the frequency detuning is chosen to be close to the relaxation oscillation frequency. Within this range and by coupling the master laser beam to the slave laser, different kinds of nonlinear dynamical pulses can be observed, depending on the values of the injection strength and frequency detuning. A square voltage signal with a frequency of 5 kHz and a voltage of approximately 3.8v (Vpp) (within the AOM operating voltage range) is applied to the AOM driver to provide an on-off AOM operation state, causing an on-off injection operation.

In the on state, the AOM will operate and generate the diffracted beams with different orders. The first order-diffracted beam is used to inject the slave laser. When the AOM is operated in the off state no diffracted beam will be generated, and, as a result, no beam will be injected into the slave laser. At the same time, an undiffracted master

laser beam is directed to detecting point PD3 in figure 4.1 to be coupled with the master laser beam. With each on state, the laser beam injects into the slave laser crystal. The intensity time series of the slave laser can then be registered and analysed, and the pulse repetition frequency of the slave laser can be determined.

In the off state, no injection occurs and the frequency detuning between the two free running solid state lasers can be measured. With each trigger, three time series are recorded by the oscilloscope (figures 4.5, 4.6): the square wave voltage is recorded in C1, the slave laser intensity time series (to measure the PRF) is recorded in C2 and the intensity time series of the beat frequency (to find the detuning) is recorded in C3. With an operating frequency of 5 kHz, the oscilloscope will be able to record 50 square waves in 10 ms at every single trigger. The square wave voltage in (C1) is used to find the starting on-off point for each time trace. For each average injection power value, the injection strength is measured. The oscilloscope is triggered by the AOM square wave voltage.

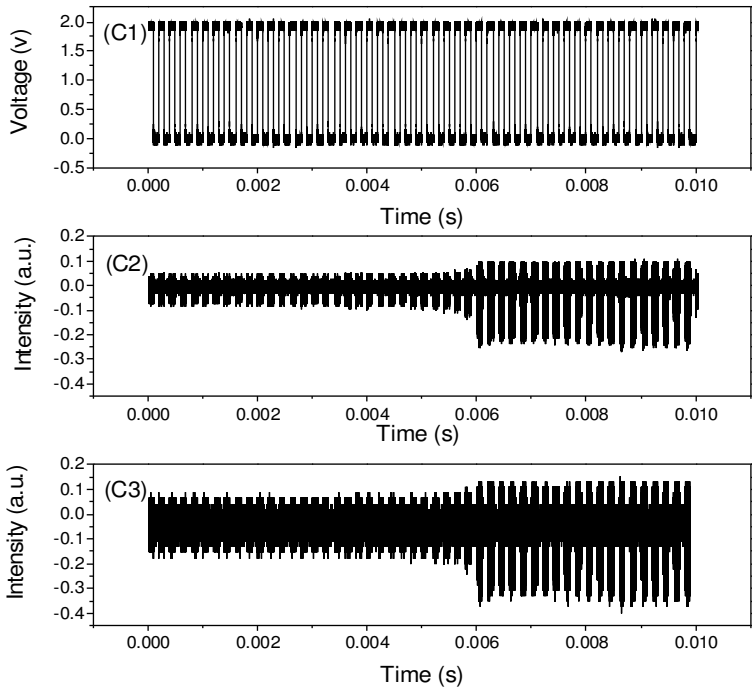

Figure 4.5. Saved data from the three oscilloscope channels: the square wave voltage (C1), the slave laser output (C2) the output from PD3 (the beat) (C3). Each Square contains intensity time series

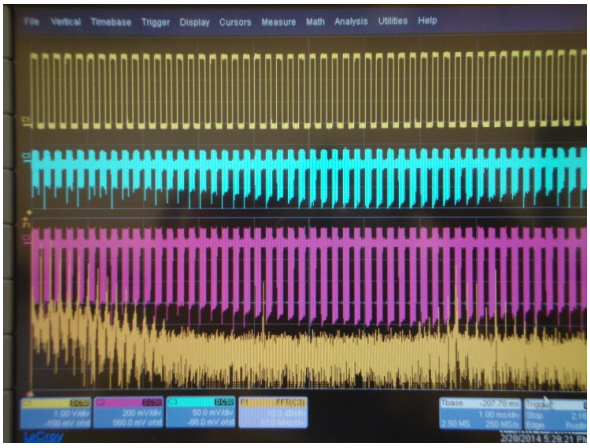

Figure 4.6. The three oscilloscope channels: the square wave voltage (C1) (yellow); the slave laser output in which each square contains the intensity time series (C2) (red); the output of the beat contains the intensity time series (C3) (blue). The yellow bottom trace is used to observe the FFT of the time trace of C3 (the detuning).

4.4. Specifying normalized injection strength values

Measuring the absolute injection power is not possible in this setup because of the unknown coupling rate for the injected field (chapter 3, section 3.2). This is a common difficulty in optically injected systems. The relative injection strength (RIS), which is related to the square root of the relative injection power (the injected power/output power) can be normalized to K by matching the experimental locking range boundary with the corresponding boundary in a simulated K-Δω map generated for this purpose. Fig. 4.7 shows the locking range boundary in the K-Δω plane. Using simulated K-Δω map, two different methods are used to quantify K

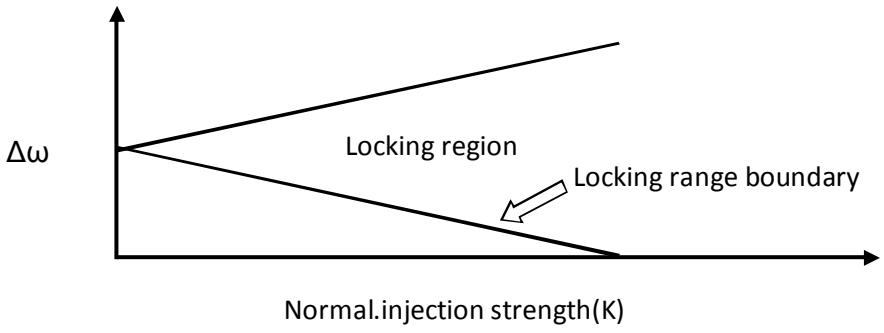

Figure 4.7. Locking range boundary in K- Δω plane

4.4.1. Using saw wave modulation

To find corresponding K values for injection power values, a saw wave modulation with modulation frequency 500 Hz, is used to produce gradual increasing in the injection power, this method is applied as the following:

1. For a fixed frequency detuning, a modulated AOM with a saw wave (figure 4.8, C1) is used to produce a saw wave injected power. The saw modulated voltage is registered in the oscilloscope in channel 1 (C1). Increasing the power injected into the slave laser by increasing the saw wave voltage with the time produces a different dynamics (figure. 4.8, C2). The figures are plotted as a function of the number of samples in order to facilitate finding injunction locking start point in which the injection locking is obtained.
2. The slave laser output data are registered in channel 2 (C2) to find the locking start sample point, the corresponding voltage value at the same sample point can be found from figure 4.8, (C1).
3. The corresponding injected power for this voltage value can be found from a calibrating curve between the voltage and the injected power that is produced separately.
4. The corresponding time trace of the beating between the master and the slave laser are saved in channel 3 (C3) to find the value of the detuning for the corresponding injection power; the detuning value is found by determining the FFT from the time series just before the injection power starts to increase (figure 4.8, C3).
5. These steps are repeated for many values of frequency detuning, and the relationship between the normalized detuning and the square root of relative injection power (RIP) is plotted to represent a locking boundary in a square root of RIP-$\Delta\omega$ plane (the locking boundary is either the saddle-node or Hopf bifurcation line illustrated in chapter 3, section 3.2.)
6. A simulated map with a material parameter of solid state lasers and experimental parameters of the current experiment is plotted. The simulated map was produced by T. Fordell and used in [6,7,8].
7. The intersection of the locking line with the K-axis for an exact value of frequency detuning is found for both the experimental graph and numerical map (figure 4.7).

8. Finally, by comparing these two values, a convert factor can be found to convert the injected power to the normalized injection strength value.

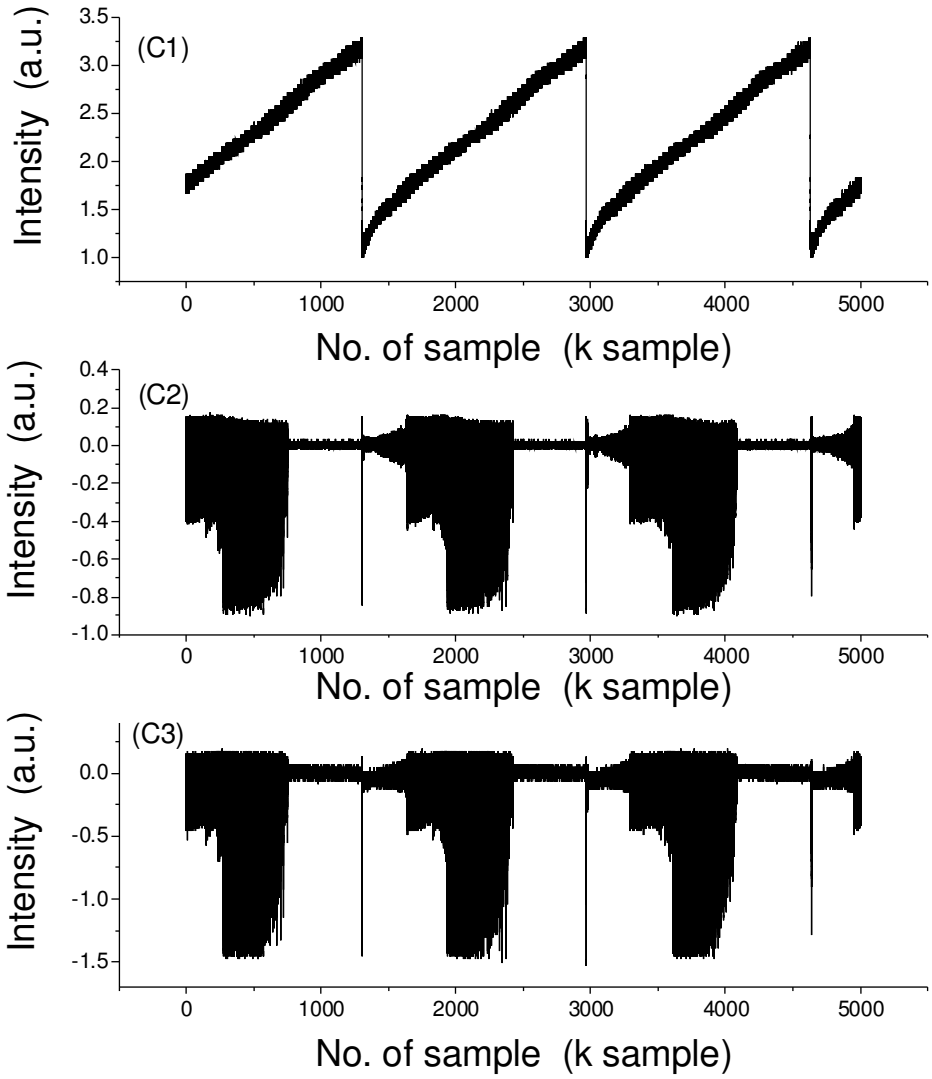

Figure 4.8. The saw wave voltage C1; the slave laser intensity time series C2 ; the intensity time series of the beat frequency C3.

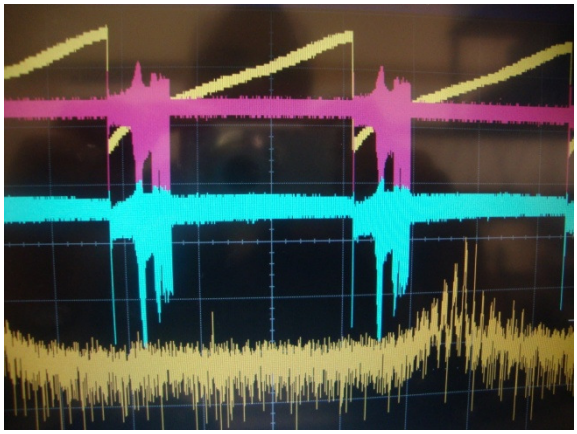

Figure 4.9. The three oscilloscope channels, the saw wave voltage (C1) (yellow top); the slave laser intensity time series (C2) (red); the intensity time series of the beat frequency (C3) (blue). The spectrum at the bottom used to observe the approximate frequency detuning.

4.4.2. Locking line method

The second way to determine the value of the normalized injection strength for exact injection power is by using the locking boundary (locking line) of the simulated map as a reference to determine K. By changing the frequency detuning for a fixed injection power, a different kind of dynamics are generated, at some detuning the locking state attained. The data needed to be saved at this point in order to find the frequency detuning for the specific injection power. Finally, the corresponding K-value can be read for the same frequency detuning on the locking line of the simulated map. Figure 4.10 shows two of the locking data. The square waves are used here is to find a more accurate value for the detuning by analysing the closest data to the locking state only.

This method is more practical than the first method in which many steps and calibrations are needed. In the experiments in the next chapters, most of the normalized injection strength values are found in this way, and a locking data is saved for each group of points that correspond to the same injection strength.

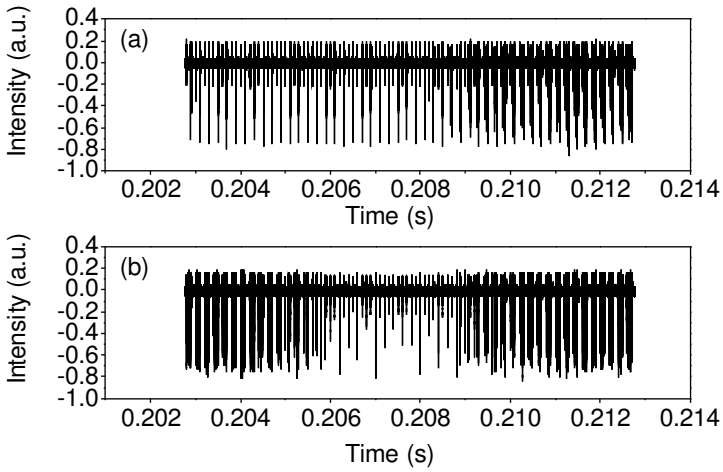

Figure 4.10. A two examples of a locking data where the intensity is suddenly drops to the locking value. The data is for (K ,Δω): (1.3,-1.3) in (a) and (0.72, -0.72) in (b).

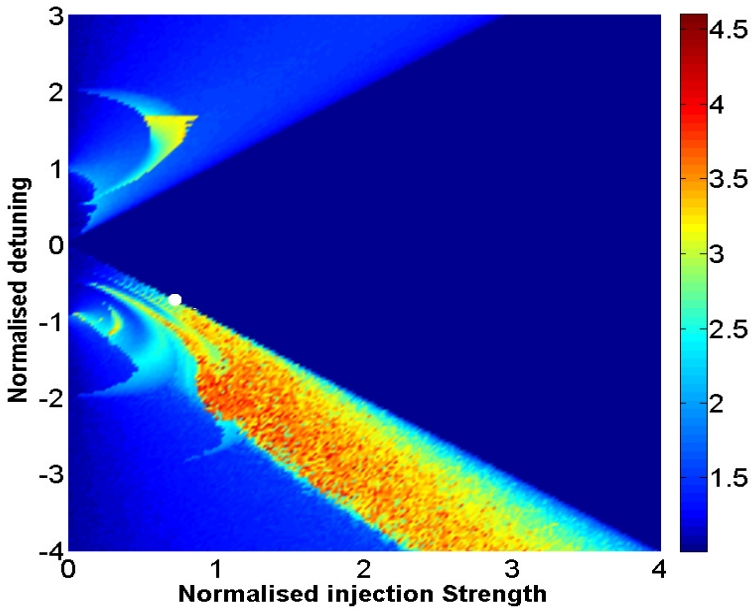

Figure 4.11. The simulated map generated for OISSL current system, using the code developed by T. Fordell [6,7,8] . The map shows a locking point (the white point) on the locking line in which K is found to be =0.72 correspond to Δω= - 0.72,

4.5. Procedures to facilitate OISSL operation

To facilitate the OISSL operation, it was necessary to adopt a number of procedures to resolve practical problems.Three main procedures are discussed here.

4.5.1. Specifying positive and negative detuning

The beat detector PD3 in figure 4.1 shows the beat frequency at around 80MHz depending on which of the two frequencies is higher. If the normalised frequency detuning $((\nu_{ML} - \nu_{SL}) / \Omega_r)$ read is above 80MHz, that means the master laser frequency is higher than the slave laser frequency; practically it is difficult to know which of the two frequencies is higher than the other. The positive and the negative detuning can be specified based on the direction of the change in the detuning with the change in temperature. By increasing the temperature of the master laser, the frequency of the master laser decreases. The detuning indicator moves from high to low values until it reaches 80MHz, which actually represents the zero point at which the frequency of the master and the slave laser are equal. With a further increase in the master laser temperature, the slave laser output becomes higher, and the detuning indicator moves towards the 70s; therefore, the values of the detuning less than 80 MHz (the 70s) represent the negative detuning, and the values higher than 80 MHz (the 80s) represent the positive detuning. This scenario is used in all experiments in the thesis.

It is worth mentioning that negative and the positive frequency detuning can be distinguished also depending on the theoretical maps [6]: the negative detuning range includes dynamics that extend over a wide K range, while the positive detuning includes dynamics that extend within small K range. This difference can be distinguished practically easily in OISSL.

4.5.2. Injection laser beam alignment

The system output is very sensitive to the alignment of the injection beam. The beams in the common paths should coincide, but this is not enough to ensure the best injection direction. For best alignment, the output of the slave laser has to be examined to give the maximum output intensity at some reference point for a specified injection power. This reference point could be chosen at any frequency detuning far away from the dynamical pulses. Optimizing the intensity can be done by any of the reflecting apparatus that used to direct the injection beam to the slave laser.

4.5.3. Single mode operation

To ensure single mode operation of the master and slave laser during the experiment, a Fabry-Perot interferometer was occasionally used in points A and B (figure 4.1). This meant removing some of the apparatus and aligning the interferometer every time; this process was replaced by checking the spectrum of the time series (the FFT) of each of the lasers by detector PD3. The growing of an additional longitudinal mode is accompanied by the appearance of a second relaxation oscillation frequency peak. This feature can be employed to observe and eliminate any additional longitudinal mode that could appear, to ensure the single mode operation.

4.6. Conclusion

This chapter explained the optically injected solid state laser system. The system is used to study the characteristics of the optically injected solid state laser (chapter 5) and to generate optical pulses with controllable pulse repetition frequency (chapter 6). This chapter discussed many experimental issues related to the experimental setup like obtaining single mode operation, the effect of the pumping beam alignment on the OISSL system, controlling the optical frequency offset between the crystals. Controlling the injected beam using an acousto-optic modulator is discussed also. Operating the system using a single optical pumping beam to pump the two solid-state lasers and determining the injection parameters is explained. Procedures to facilitate OISSL operation are presented also.

References

1. Koechner, Walter. Solid-state laser engineering. Vol. 1. Springer, 2006.
2. Scheps, Richard. Introduction to laser diode-pumped solid state lasers. SPIE Press, 2002**.**
3. Laporta, Paolo, and Marcello Brussard. "Design criteria for mode size optimization in diode-pumped solid-state lasers." IEEE Journal of Quantum Electronics, vol. 27, no. 10, pp. 2319-2326, 1991.
4. Taira, Takunori, Akira Mukai, Yukihiro Nozawa, and Takao Kobayashi. "Single-mode oscillation of laser-diode-pumped Nd:YVO_4 microchip lasers." Optics Letters, vol. 16, no. 24, pp. 1955-1957, 1991.

5. Day, Timothy, Eric K. Gustafson, and Robert L. Byer. "Sub-hertz relative frequency stabilization of two-diode laser-pumped Nd: YAG lasers locked to a Fabry-Perot interferometer." IEEE Journal of Quantum Electronics, vol. 28, no. 4, pp. 1106-1117, 1992.
6. Fordell, T. and Å. M. Lindberg. "Numerical stability maps of an optically injected semiconductor laser." Optics Communications, vol. 242, no. 4,pp.613-622, 2004.
7. Valling, Simo, Thomas Fordell, and Åsa Marie Lindberg. "Maps of the dynamics of an optically injected solid-state laser." Physical Review A, pp. 72, no. 3, pp. (033810)1-7, 2005.
8. Fordell, Thomas. "Dynamics of free-running, pump-modulated and coupled semiconductor and solid-state lasers.", PhD Thesis, University of Helsinki, 2007.

Chapter 5

The response of pulse repetition frequency to change in detuning

5.1. Introduction

An important feature of optically injected solid state laser (OISSL) is the ability of the system to generate a continuous range of pulse repetition frequencies (PRFs), either by controlling the injected field strength (K), or controlling the frequency detuning between the slave laser and the master lasers ($\Delta\omega$) or both.

This chapter provides an experimental demonstration of the dynamics of different regions of the dynamical map of this system (chapter 4, section 4.4, figure 4.11). In this regards, the relative intensity level of the pulses, the waveform, the values of the pulse repetition frequency and the stability of the dynamics are important factors.

The chapter is also devoted to study the response of the pulse repetition frequency (PRF) to the changes in the frequency detuning between the master and the slave lasers for a fixed value of normalised injection strength (K). This study is important in identifying the regions of the dynamical map that are appropriate for generating a variable pulse repetition frequency. The existence of an unexplained large pulse timing jitter from the mean period in a specific region on the map is studied also, by measuring the standard deviation of PRF in this region (explained in chapter 2, subsection 2.3.2, figure 2.7) [1,2].

To accomplish this, specific points on the ($K,\Delta\omega$)-plane of OISSL are chosen to represent different regions on the map of the dynamics. At each specific point, the frequency detuning was forced to change at approximately the same rate by altering the temperature of the master laser. The details are explained in the next section.

5.2. Experimental arrangement

The experimental setup explained in chapter 4, subsection 4.2.1 is used. The setup is shown in Figure 5.1. The injection beam from the master laser was directed to the cavity of the slave laser through the acousto-optic modulator (AOM).

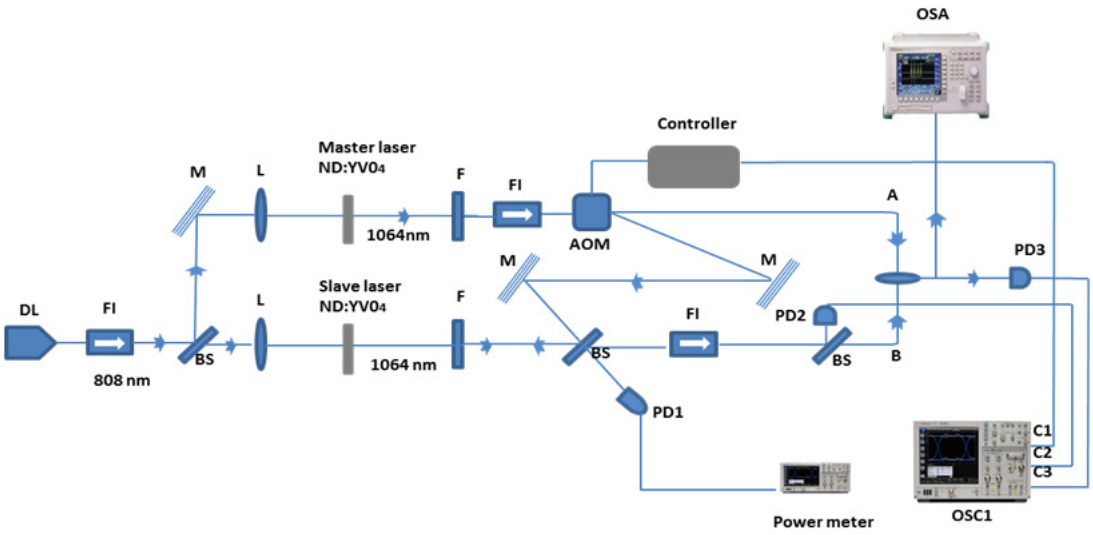

Figure 5.1. Schematic diagram of the pulse generation system showing the basic apparatus: DL, Diode laser; BS, beam splitter; F, filtter; FI, Faraday isolator; L, lense; M, mirror; AOM, acousto-optic modulator; OSC, oscilloscope; OSA, Optical spectrum analyzer; A, B fiber heads; C1, C2, C3 are oscilloscope chanels, PD1, PD2, PD3 photo detectors.

The AOM was modulated via a square wave with a frequency of 5 kHz. The voltage signal was offset from the zero level by V/2 volts to ensure oscillations with a positive voltage (figure 5.2). The zero level represented the off state, in which no injection occurred. In this state, the two lasers operated as a free-running laser, and the detuning could be measured. The AOM produced many orders of diffraction beams. The zero order (point A) was coupled with the slave laser beam (point B) by a fiber coupler to measure the detuning. The first-order-diffracted beam was used to inject the slave laser, representing the on state, while the other higher orders of diffraction beams were blocked.

The temperature controller controlled the master laser temperature through a DC supply to increase the resolution. By changing the voltage by 3 x 10^{-4} volts each time, the rate of change of the frequency detuning was approximately 2.5 MHz/s. To study the behaviour of the dynamical pulses following the change in the detuning and to study the level of correlation between the PRF and the detuning, the data were collected for 10 msec.

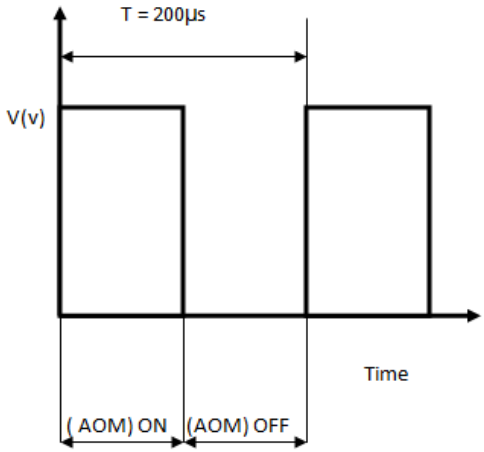

Figure 5.2. The square wave used to modulate the AOM

The output of the system had the same square modulation as the injected beam. To record these pulses in the oscilloscope, a sample rate of 250 MSample/s was used. In 10 ms, 25,000 sample points were recorded for each square pulse (100 µs). With an oscilloscope time base 1 ms/div and using single-trigger mode, the screen showed a 50 on-off square period to record at the same time(chapter 4, figure 4.6).

As explained in Chapter 4 section 4.2.1, the output of the system is detected by PD2. The detected intensity time series (fifty squares of intensity time series are recorded in channels 2 (C2) (figure 5.1), while the detuning is changed. The recorded data in C2 are analysed for each square to measure the PRF (based on finding the fast Fourier transformation (FTT) of the time series). All the squares are analysed to obtain the change of the PRF within a given time period (10 ms). At the same time, fifty intensity time series of the beating of the intensities of the master and slave lasers, is detected by PD3 and recorded in channels 3 (C3) (It is important to mention that the photo detectors used in the experiment shows the intensity inversely). The data registered in C3 are analysed to measure the change in the normalised detuning within the same time period by finding the FFT also. For every point chosen on the (K, ω)-plane of the

dynamical map, data is registered by varying the frequency detuning with a fixed injection strength. Figure 5.3 shows the location of these points on the map of the dynamics generated for the system with normalised pump power (J) = 1.68 and linewidth enhanisment factor (α) = 0.12.

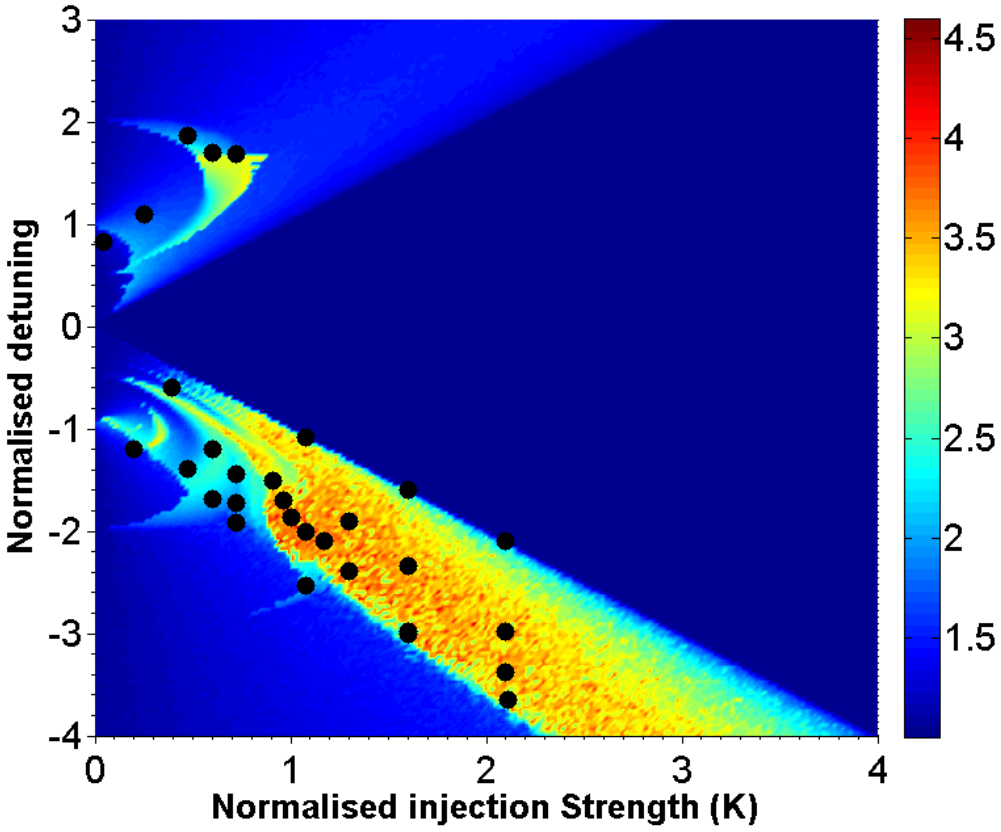

Figure 5.3. The map genrated for this system showing the studied data points on the K-Δω map.

The basic dynamics of the optically injected laser can be summarized by three regions of operation: the stable locking region (dark blue on the map), the nonlocking region (light blue on the map) and the destabilized locking region (sky blue (very light), yellow, orange colour). The colour bar is explained in chapter 4, section4.4. This study is concerned with the destabilized locking region only because the aim of this system is to generate variable PRF pulses with good performance.

5.3. Intensities and PRF characteristics in various map regions

To study the main characteristics of the various dynamical regions and the response of the pulse repetition frequency to the changes in the frequency detuning, points from various dynamical regions of the map (figure 5.3) are chosen. The regions was specified according to [1-3]. For each point on the dynamical map the results will be organized in four rows. The change in the intensity of the pulses with time will be shown in row (a). Row (b), is an enlargement of the intensity time series to show the waveform at the specified point. The change in the normalised detuning with the number of the square wave (and, consequently, with time) will be shown in row (c). The change in PRF with the number of the square wave will be shown in row (d). The graphs of rows (c) and (d) will be used to find the correlation coefficient between the frequency detuning and the PRF at each point on the map.

5.3.1 Period-doubling regime pulses

This group of dynamical points includes the data in the (K,Δω)-plane with positive and negative detunings as shown in figure 5.4

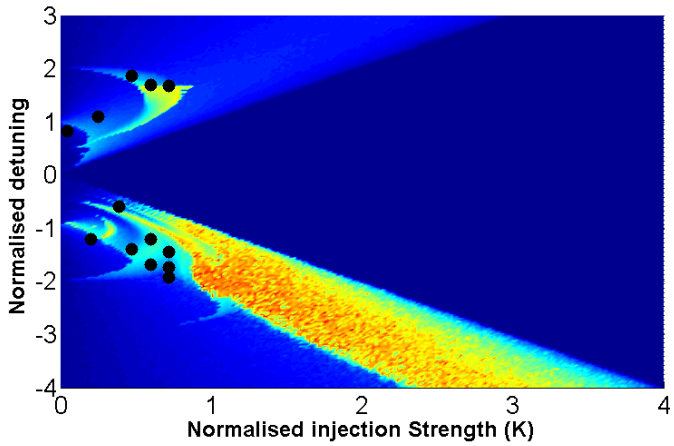

Figure 5.4. The location of the points in period-doubling regime pulses where K, Δω ; (0.043, 0.83), (0.25, 1.1), (0.47, 1.87), (0.6, 1.7), (0.6, 1.4), (0.72, 1.6), from positive detuning region. And; (0.2, -1.2), (0.39 , - 0.6), (0.47 , - 1.39), (0.6, - 1.27) , (0.6, - 1.68), (0.72 , - 1.44) , (0.72 , - 1.73), (0.72 , - 1.92) from the negative detuning region.

5.3.1.1. Positive detuning region

The intensity oscillations in the positive detuning region above the Hopf bifurcation curve (chapter 2, figure 2.3), are almost periodic waveform (limit cycle), which

represents period 1 (P1), created by Hopf bifurcation [1,2]. The shape of the pulse is (roughly) Gaussian [3]. Another periodic oscillation is the oscillation generated by period-doubling bifurcation. This periodic oscillation represented by period 2 (P2) and period 3 (P3). Figures 5.5 and 5.6 are examples from each kind of the two regimes. Figure 5.5 (a) shows the fifty squares of the intensity time series, contain pulses operating with a limit cycle regime that appears with injection parameters (K, $\Delta\omega$) = (0.25, 1.1). The second row (b) is the enlargement of a part of one of the fifty intensity time series, showing the waveform of this regime. Row (a) shows lower intensity levels as compared with the level of intensity in figure 5.6 (a), where the system operates in period-doubling regime. In figure 5.5 (c), the value of the detuning is determined for every square of the intensity time series as mentioned in the previous section. The row represents the change of detuning with the number of the square wave. Row (d) represents the change in the PRF with the number of the square wave that results from the change in the detuning. The change in the number of the square wave represents the change in the time, since the fifty squares of the intensity time series are recorded in 10 ms.

In figure 5.6, where the injection parameters (K, $\Delta\omega$) = (0.6,1.7), the pulses operate with period doubling regime [1,2]. Row (b) demonstrates a Gaussian waveform. The pulse train is with two intensity peaks. Rows (c) and (d) represent the same parameters as in figure 5.5 (c) and (d).

To determine the response of the PRF to the detuning change, the correlation coefficient has been found between the PRF (row d) and the detuning (row c) for both figure 5.5, and 5.6. High correlation coefficients between the PRF and the detuning have been found (0.99) for these points.

In general, the intensity level and the PRF in 5.5 and 5.6 are stable (no fluctuations in the intensity and PRF with the time). The stable performance in these points is attributed to the nature of the limit cycles to oscillate with an exact period, waveform and amplitude such that if the system is perturbed slightly for any reason, it always returns to the standard cycle. This feature encourages the use of limit cycle regime (regardless of the low intensity level of this regime) and period doubling regime as a source of pulses.

The same behaviour is found for the rest studied points where (K, Δω) = (0.04, 0.84), (0.47, 1.87), (0.72, 1.6). High correlation coefficients between the PRF and the detuning have been found (0.99) for all points in this region, which indicates the possibility of using this region to control the PRF by varying the frequency detuning . All the results are shown in table 5.1.) (Figures A1, A2 are in appendix A).

Figure	K	Δω	PRF (MHz)	Correlation Coefficient
A1	0.04	0.84	4.3	0.99
5.5	0.25	1.1	4.8	0.99
A2	0.47	1.87	3.9	0.98
5.6	0.6	1.7	3.6	0.99
5.7*	0.72	1.6	2.5	0.69
			3.44	0.82
			7.1	0.98

Table 5.1. The PRF and correlation coefficient for the pulses operate with limit cycle and period doubling regime in the positive detuning region. (*); figure 5.7 belong to a point where three dynamical regimes existed and changed sequently (explained later in the section).

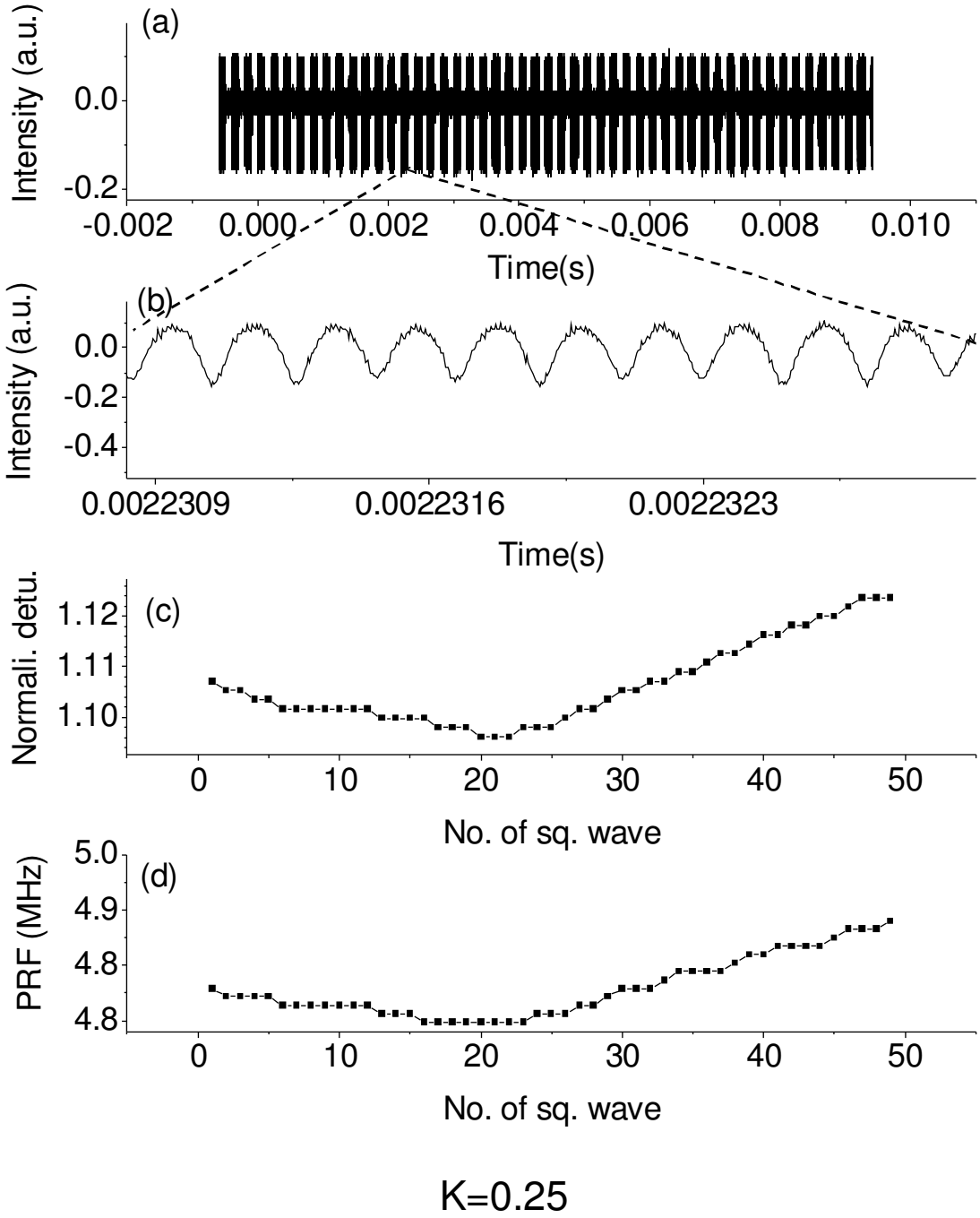

Figure 5.5. (a) The intensity level for 50 squares of pulses; (b) pulses waveform; (c) the change in frequency detuning in 10ms; (d) the change in PRF in 10ms. The relations for the injection parameters, (K, Δω)= (0.25, 1.1).

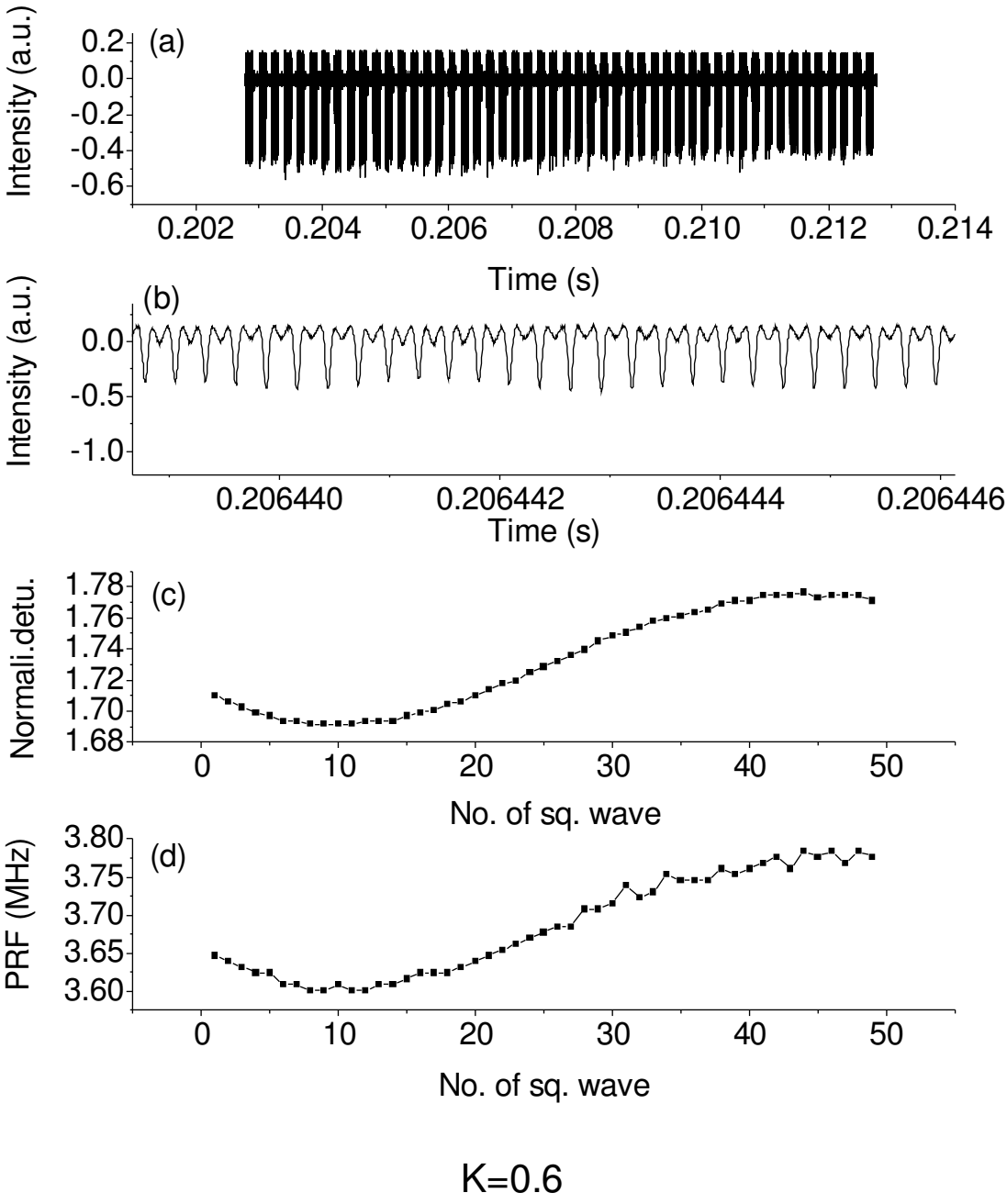

Figure 5.6. (a) The intensity level for 50 squares of pulses; (b) pulse waveforme; (c) the change in frequency detuning in 10ms; (d) the change in PRF in 10ms. The relations for the injection parameters (K, Δω)= (0.6, 1.7).

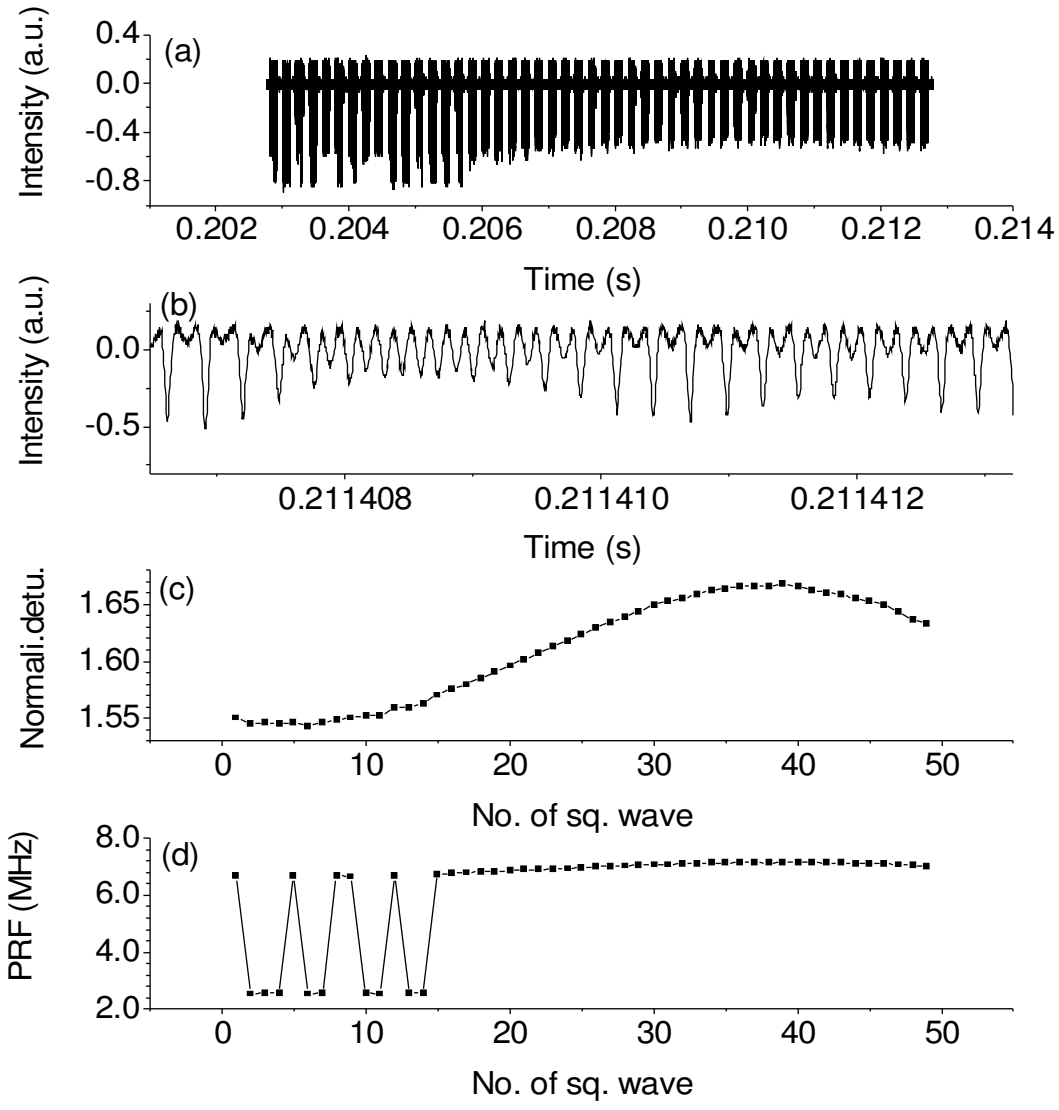

Figure 5.7. (a) The intensity level for 50 squares of pulses; (b) pulses waveform; (c) the change in frequency detuning in 10ms; (d) the change in PRF in 10ms. The relations for the injection parameters (K, Δω)= (0.72 , 1.6).

Figure 5.7 in which (K, Δω) = (0.72,1.6), is drawn to attention. At this point three dynamical regimes existed and changed sequently. The oscillating waveforms which shown in figure 5.8 a, b and c are from the time series of squares 4, 15 and 38 in figure 5.7 (a). These figures represent the evolution of P3 dynamic, which is expected in this region.

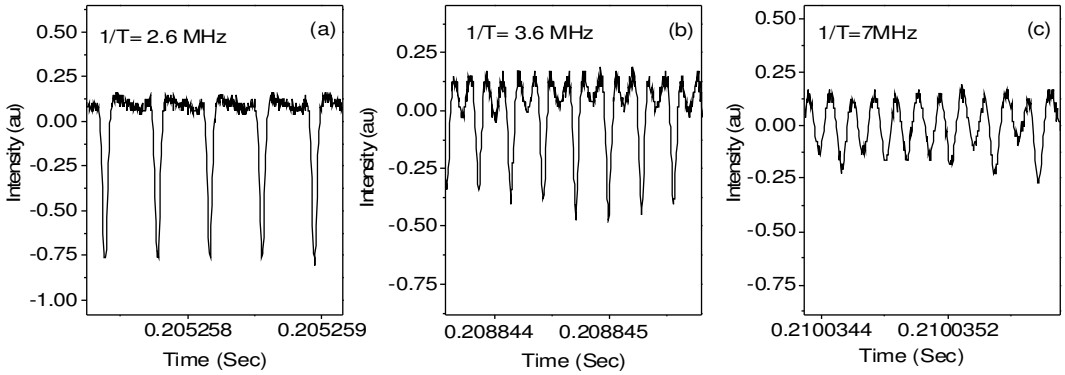

Figure 5.8. Three kinds of dynamics exist in time series of Figure 5.7

The spectrums of the time series belong to these squares are shown in figure 5.9 a, b and c. Figures 5.8 (b) and 5.9 (b) show that the frequency (2.6 MHz) is shifted to a new frequency (3.6 MHz) which is, in turn, converted by a period-halving mechanism (or period doubling depending on the change direction) to another waveform with frequency =7.1 MHz (figure 5.8, 5.9 (c)). Such mechanism hasn't shown in the bifurcation analysis in [1,2]

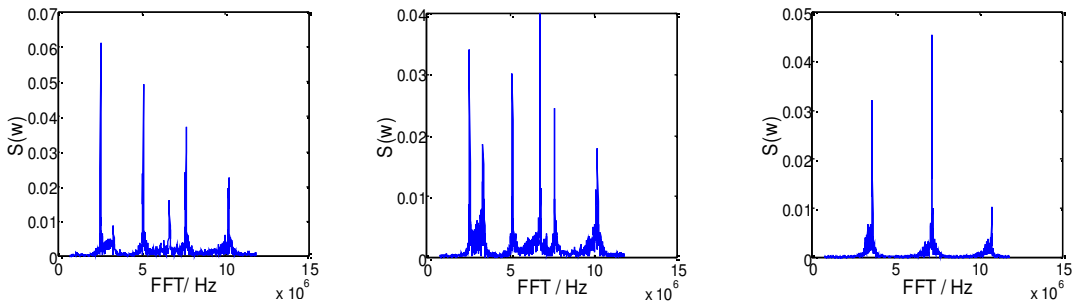

(a) (b) (c)

Figure 5.9. The spectrum of the time series belong to pulses squares 4, 15 and 38 in Figure 5.7, (K, Δω)=(0.72,1. 6)

5.3.1.2. Negative detuning region of period-doubling regime pulses

A periodic orbits related to the period-doubling regime (P2, P3) are coexisted between the torus curve and the saddle-node curve (chapter 2, figure 2.3). The same way of analysis explained in the positive region is applied in this region (and the other regions in the rest of the chapter). Table 5.2 shows the values of the correlation coefficients for all the tested points in the negative detuning region of period-doubling regime for (K, Δω) = (0.2, -1.2), (0.39, - 0.6), (0.47, - 1.39), (0.6, - 1.27), (0.6, - 1.68), (0.72, - 1.44), (0.72, - 1.73), (0.72, - 1.92) (points A3, A4, A5, A6, A7, A8 are in appendix A).

Figure	K	Δω	PRF (MHz)	Correlation Coefficient
A3*	0.2	-1.2	4.4	0.17
A4	0.39	-0.6	3.7	0.94
A5	0.47	-1.39	5.7	0.99
A6	0.6	-1.27	2.7	0.97
A7	0.6	-1.68	3.6	0.97
5.10	0.72	-1.44	3	0.98
A8*	0.72	-1.73	7.3	0.99
			3.69	0.86
5.11*	0.72	-1.92	8.1	0.98
			3.6	0.3
			0.9	0.3

Table 5.2. The PRF and correlation coefficient for period-doubling regime pulses for the negative detuning.(*) These points represent transitions between two regimes or pulses with more than one frequency. (points A3, A4, A5, A6, A7, A8 are in appendix A).

Figure 5.10, in which (K, Δω) = (0.72 , -1.44), shows the characteristics of the periodic oscillations in this region. Figure 5.10 (a) shows a typical example of the relative intensity level in this region.

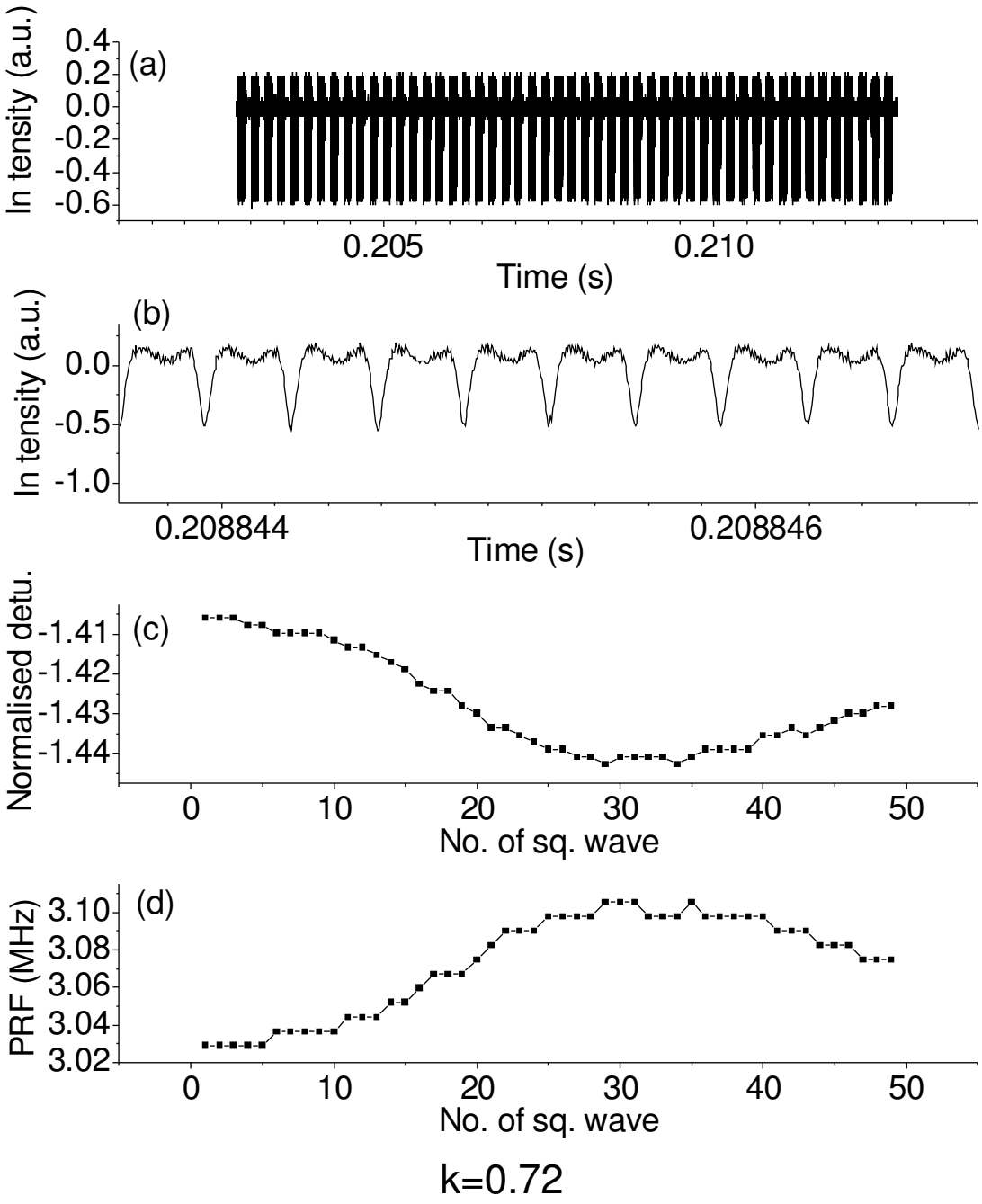

Figure 5.10 (a) The intensity level for 50 squares of pulses; (b) pulses waveform; (c) the change in frequency detuning in 10ms; (d) the change in PRF in 10ms. (The relations for the injection parameters (K ,$\Delta\omega$)=(0.72, - 1.44)

The waveform is shown in (b). The PRF (row c) is inversely proportional to the change in detuning (row d) which is opposite to the behaviour in the positive detuning region.

All the points show a high degree of correlation between the PRF and the detuning except the points on the boundaries which are closed to the torus curve (table 5.2).

As an example, figure 5.11, which represents the point (K, $\Delta\omega$) = (0. 7 , -1.92), is on the boundary where the transition between two regime occures. Figure 5.11 a, b provides a closer look at the behavior of the system when a periodic oscillation evolves to a quasi-periodic oscillation in which three frequencies oscillate. Table 5.2 shows that the two main frequencies have low correlation coefficients which means that the boundaries are not suitable for use to generate pulses. Figure 5.11 shows also, that the boundary between the two dynamics is not sharp, because the existence of the two dynamics, continues to alternate, even when the detuning is continuously increasing. This behavior can be attributed to the influence of different kinds of noise.

The high correlation coefficients between the PRF and the detuning for most of the points in this region indicates the possibility of using this region to control the PRF by varying the frequency detuning.

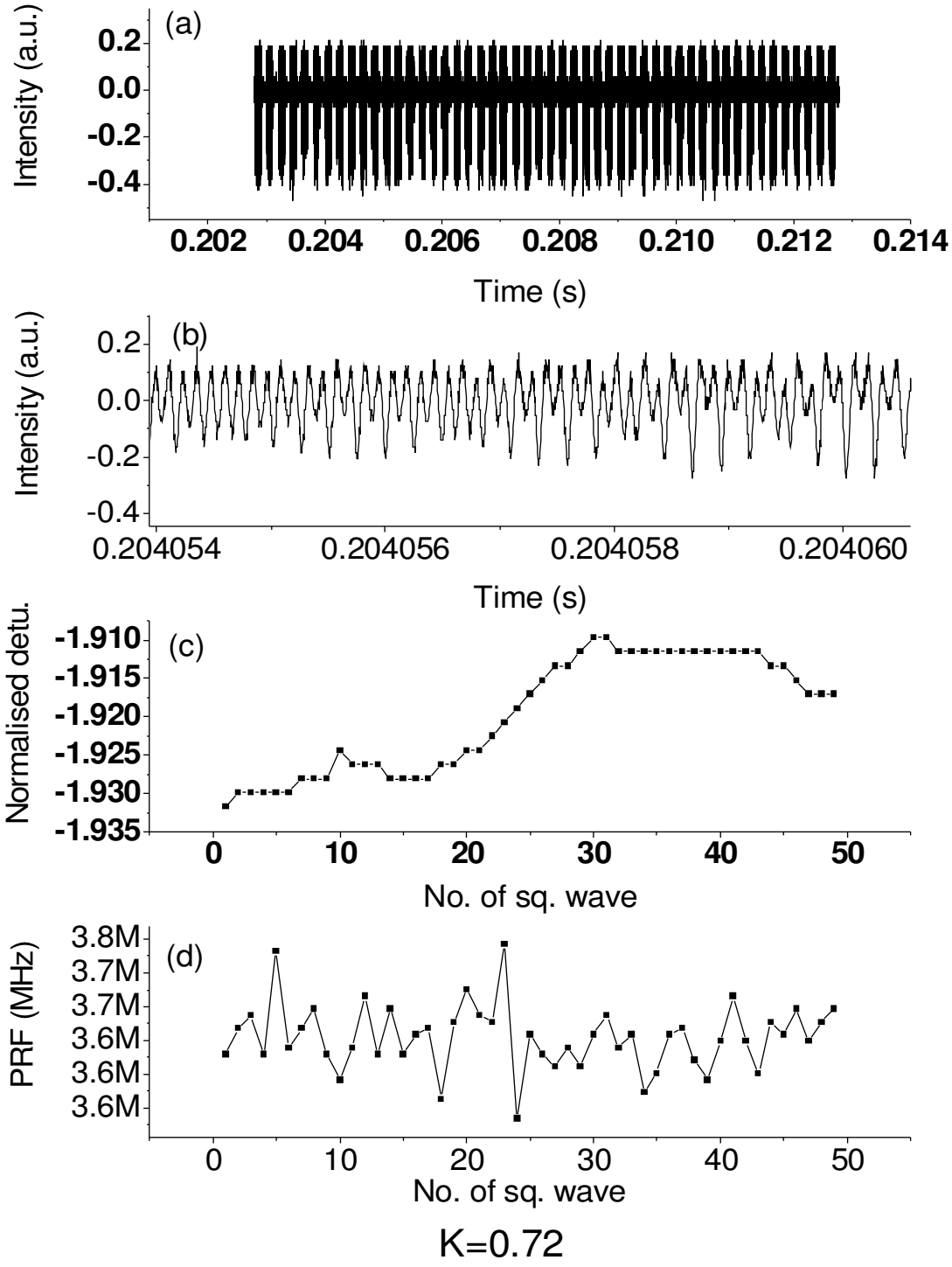

Figure. 5.11. (a) The intensity level for 50 squares of pulses; (b) pulses waveform; (c) the change in frequency detuning in 10ms; (d) the change in PRF in 10ms. The relations for the (injection parameters (K ,Δω)=(0.7,-1.92).

5.3.2. Spiky regime pulses

This region lies between the saddle-node curve and the torus curve, beyond the period-doubling region (chapter 2, figure 2.1B, c and chapter 2, figure 2.3). The studied points are: (K, Δω) = (0.91- 1.56), (0.96,-1.7), (1,- 1.87), (1.08,-2.0), (1.17,-2.1), (1.3 ,- 1.91), (1.3 ,- 2.39), (1.6 ,- 2.34), (1.6 ,- 2.99), (2.1, - 2.98), (2.1, - 3.38).

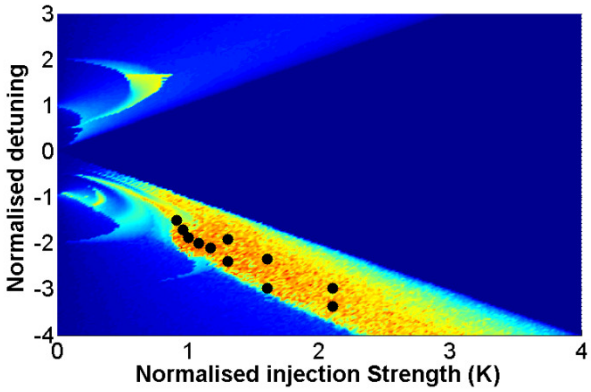

Figure 5.12. The studied points in the spiky regime, where (K, Δω) = (0.91- 1.56), (0.96,-1.7), (1,- 1.87), (1.08,-2.0), (1.17,-2.1), (1.3 ,- 1.91), (1.3 ,- 2.39), (1.6 ,- 2.34), (1.6 ,- 2.99), (2.1 ,- 2.98), (2.1 ,- 3.38).

The location of the points is demonstrated in figure 5.12. The oscillations represent a range of oscillations of two types of waveforms combining with each other and having two close frequencies. The first waveform pattern is spiky periodic contains long phases with unchanged amplitude, separated by short phases of sudden change and the second pattern is a quasi-periodic waveform. Figure 5.13 is a typical example of the relative intensity level (row a), the waveform (row b) and the change in the PRF (row c) due to the change in the detuning (row d).

The first row in figure 5.13 shows the fifty intervals of intensity time series collected near this point. The figure demonstrates the high intensity level compared to the level of the intensity time series of all other regimes.

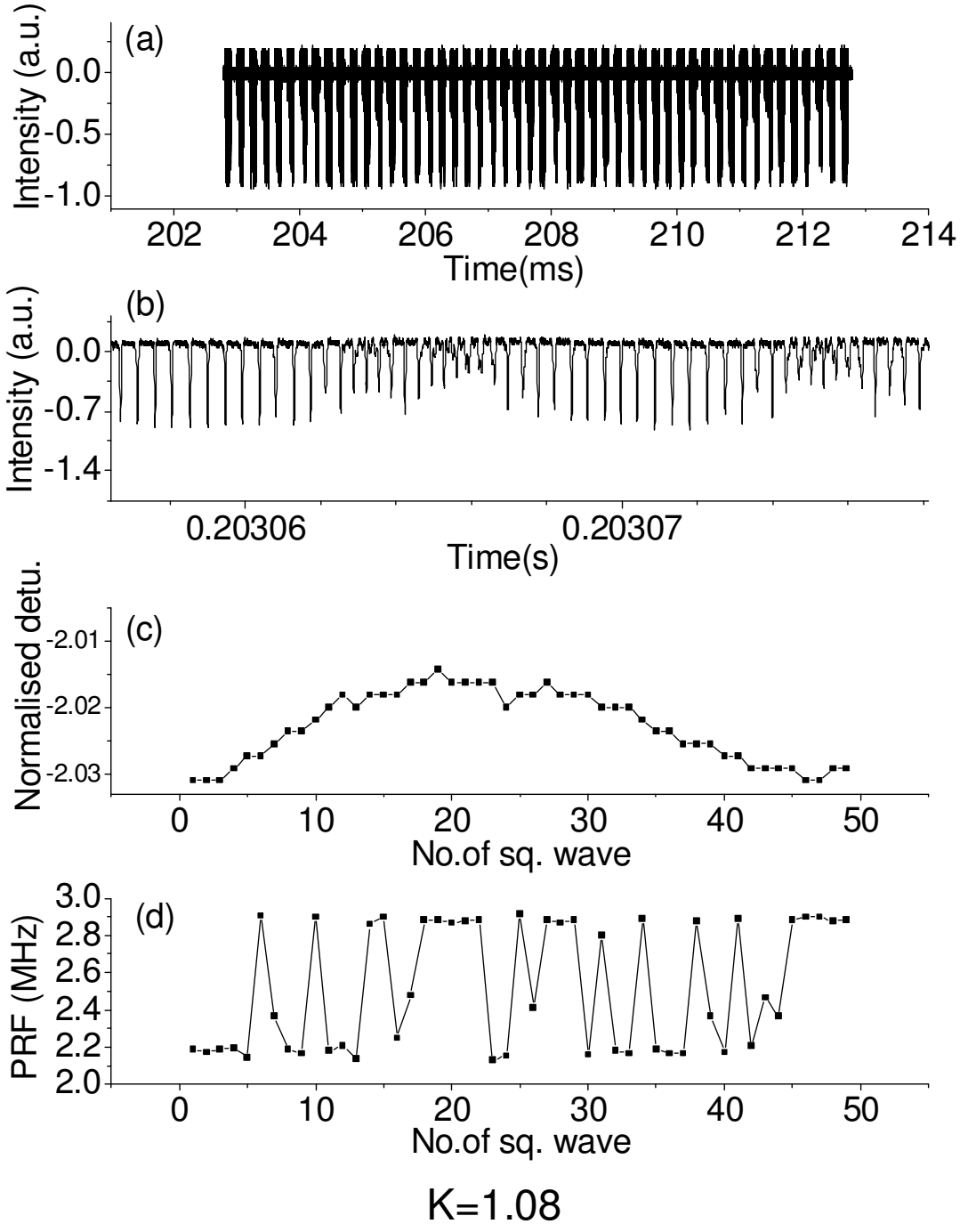

Figure 5.13. (a) The intensity level for 50 squares of pulses; (b) pulses wavform; (c) the change in frequency detuning in 10 ms; and (d) the change in PRF in 10 ms The relations for the injection parameters are K= 1.08, Δω= -2 (Point e).

All the points in this region showed very low correlation coefficient values as shown in table 5.3. (Figures A9-A17 are in appendix A).

The weak responses to the change in the PRF with the change in the detuning do not allow to use the region as a source for changeable PRF pulses.

Figure	K	Δω	PRF (MHz)	Correlation coefficient
A9	0.91	-1.56	2.07	0.06
A10	0.96	-1.7	2.03	0.12
A11	1	-1.87	2	0.04
5.13	1.08	-2.0	2.26	0.04
A12	1.17	-2.1	2.2	0.2
A13	1.3	-1.91	1.6	0.2
5.19	1.3	-2.39	2.43	0.09
A14	1.6	-2.34	1.6	0.1
A15	1.6	-2.99	1.2	0.1
A16	2.1	-2.98	1.8	0.34
A17	2.1	-3.38	2.6	0.08

Table 5.3. *The PRF and correlation coefficient for spiky regime pulses for negative detuning. (Figures A9-A17 are in appendix A).*

The correlation coefficients between the detuning and PRF for the two frequencies of the quasi-periodic waveform are tested also. Figure 5.14 is an example of the behivour of the two frequencies with detuning change. The correlation coefficient of the low frequency (a) was 0.1 while the correlation coefficient of the high frequency (b) was 0.9.

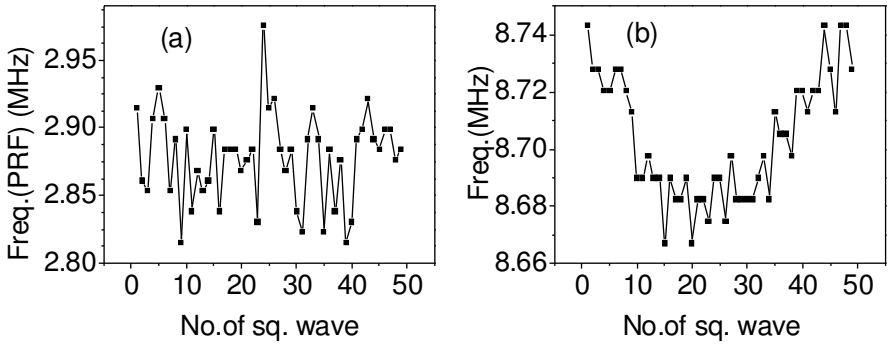

Figure 5.14. The change in the PRF while changing the detuning through 10 ms shows (a) a weak correlation for the first frequency (b) high correlation for the second frequency of the waveform.

5.3.2.1. Instability of the time periods in spiky region

As discussed in chapter 2, section 2.3.2, the region just above the period doubling bifurcation boundary for negative detunings (spiky region) showed high standard deviation values of the time period between pulses. This kind of instability is shown in figure 2.6 in chapter 2. This section investigates the fluctuation of the time period in this region as illustrated in [4].

The short intensity time series in figure 5.13 (b) (and all the specified K, Δω points in this region in appendix A) reveal the existence of sequences of a two waveforms and two main frequencies, mentioned above in the previous section.

The enlargement of the intensity time series of one of the square waves of figure 5.13 (a) is shown in figure 5.15. The figure demonstrates a quasi-periodic waveform with two frequencies. The first frequency (PRF) is equal to 2.88 MHz and the second frequency equal 8.5 MHz, in addition to the periodic spiky waveform oscillate with frequency 2.4 MHz.

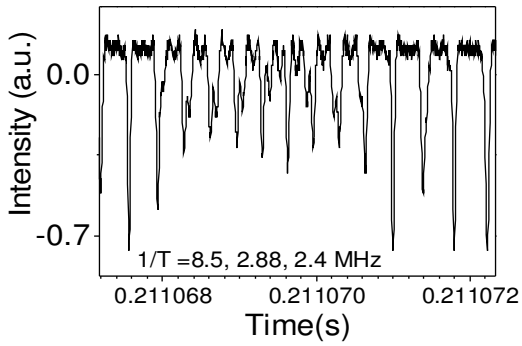

Figure 5.15. The enlargement of the intensity time series from the square waves no. 5 in figure 5.13, demonstrates a waveform of the a quasi-periodic with two frequencies and a spiky waveform.

The spectrum of the intensity time series of the same square waves of figure 5.15 is shown in figure 5.16 as an example of the spectrum in this region in which two main frequencies dominate: 2.2 and 2.88 MHz. (the peak with 8.5 MHz is not shown in the figure).

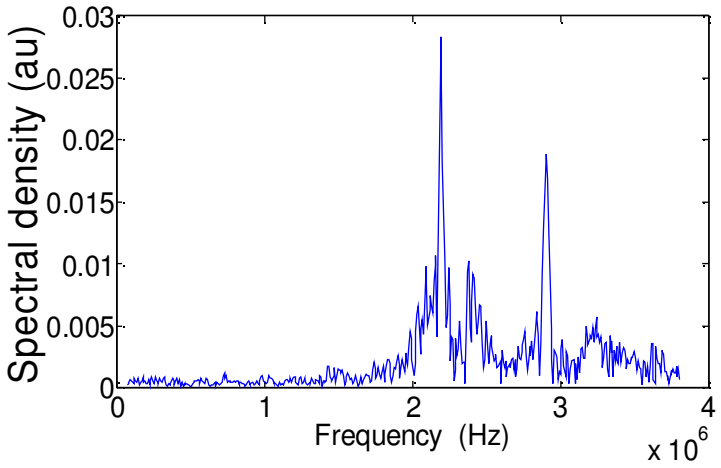

Figure 5.16. The spectral density of the square waves no. 5 of figure 5.13a with injection parameters (K,Δω =1.08, -2), showing the presence of two main frequencies with wide distribution. A third higher frequency is not shown here.

The quasi-periodic pulse can be described as an envelope superimposed on a carrier wave. Figure 5.17 shows this kind of pulses.

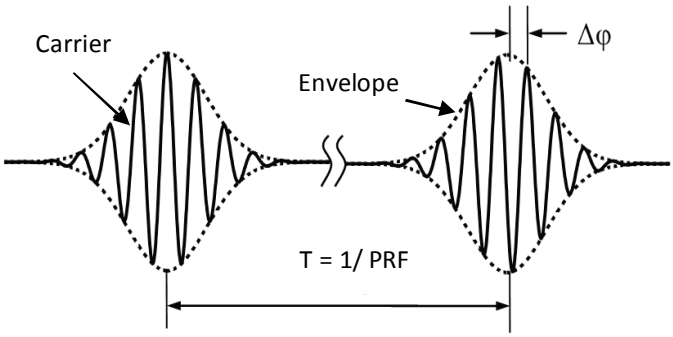

Figure 5.17. A typical quasi-periodic pulses, where the PRF is the envelope frequency,Δφ, is the offset phase between the successive pulses producing after one round trip.

For more investigation, the standard deviation of the PRF from the mean is studied for some of the examined points, in figure 5.18. The difference in the values of the standard deviation is shown in Figure 5.19. In this figure, the standard deviation values for points e, f, g and h which are closer to the torus curve, are higher than the standard deviation for points a, b, c and d which are farther away from the torus curve.

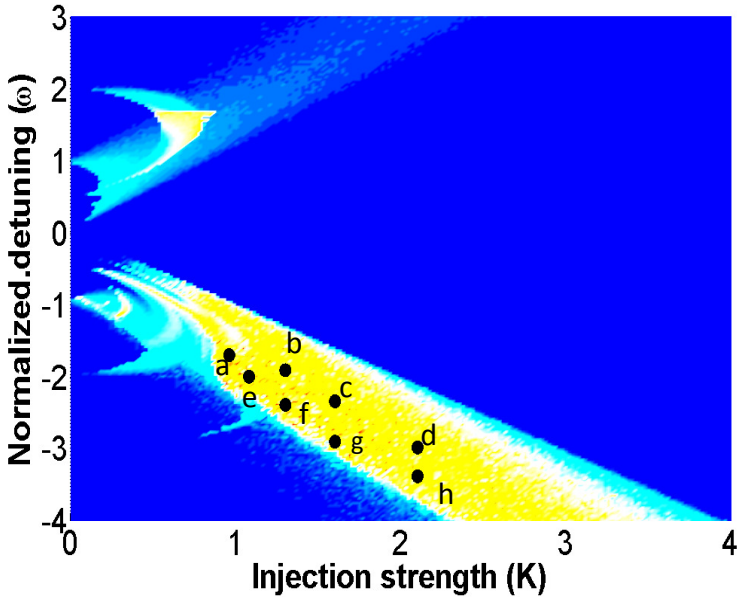

Figure 5.18. The location of the studied points on K, Δω-plane: Point a (0.96,-1.7); Point b (1.3,-1.9); Point c (1.6, -2.34); Point d (2.1,-2.98); Point e (1.08, -2.0); Point f (1.3, -2.39); Point g (1.6,-2.99); Point h (2.1,-3.38).

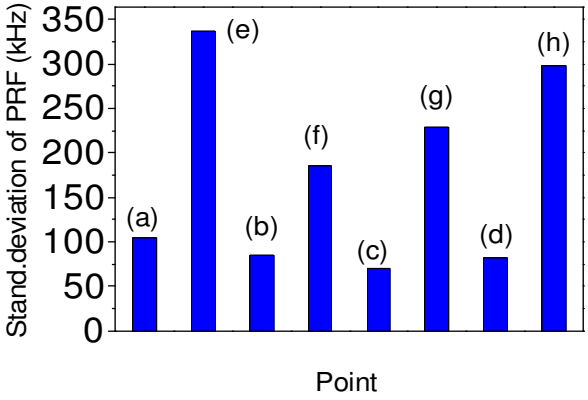

Figure 5.19. The standard deviation values of the points illustrated in figure 5.16 Point e, f, g and h, have high standard deviation. Points a, b, c and d, have low standard deviation.

The difference in the values of the standard deviation between the points which are close to the torus curve and the points which are far from the torus curve indicates that the torus curve play a role in the appearance of the two waveforms.

Furthermore, following the changes in the pulse repetition frequency in most figures in this region (where K is constant), is showing that even if there is no change in the detuning (which means that all the dynamical parameters are constant), the PRF continue to fluctuate between the two waveforms with the time. As an example, figure 5.20 c includes a fixed detuning interval from square point number 18 to square point no 24, while the PRF fluctuates continuously between the two main frequencies.

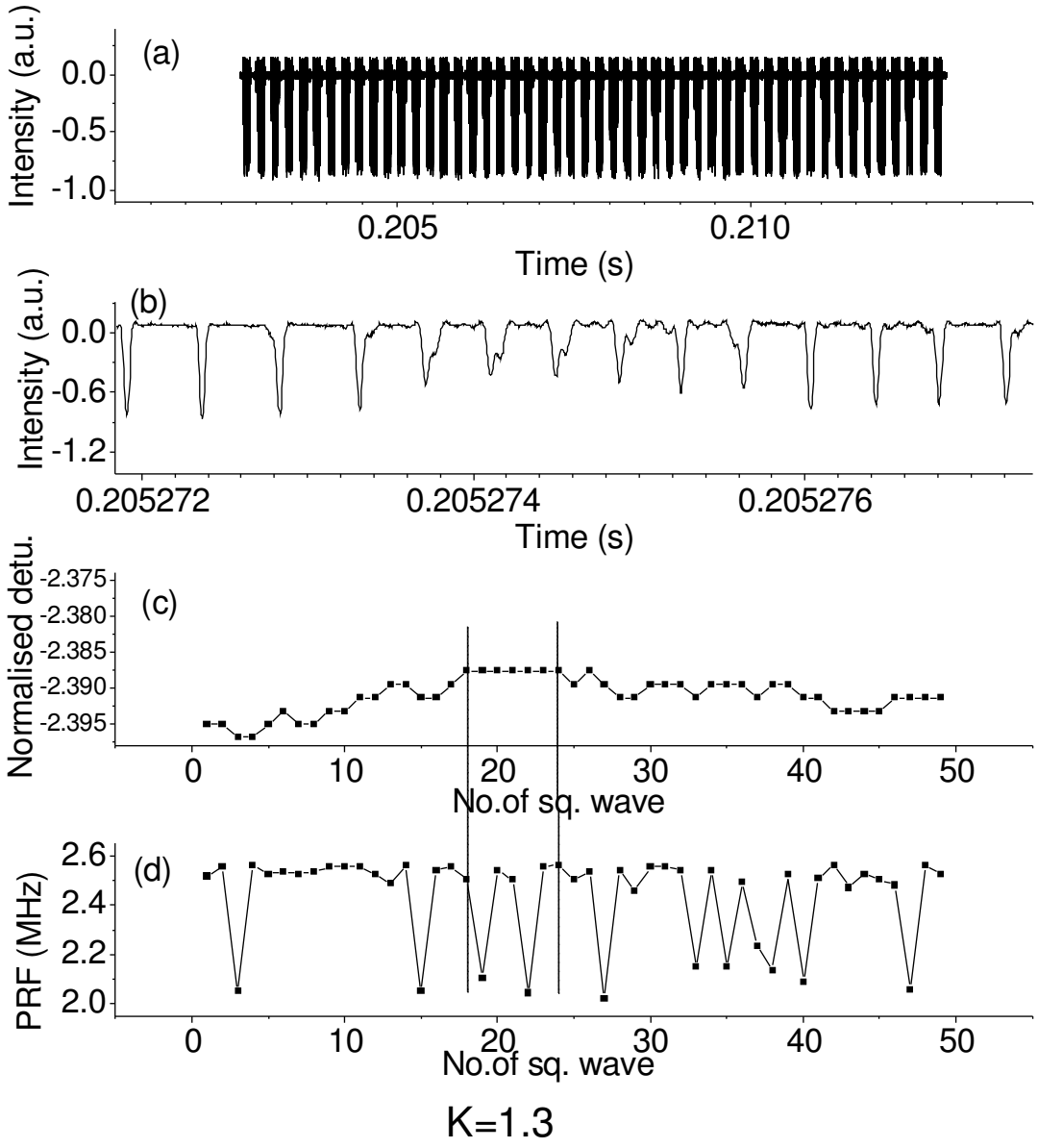

Figure 5.20 (a) The intensity level for 50 squares of pulses; (b) pulses waveform; (c) the change in frequency detuning in 10ms; (d) the change in PRF in 10ms. (The relations for the injection parameters K=1.3 ,$\Delta\omega$=- 2.39).

To explain the coexistence of the two waveforms, the periodic (spiky) and the quasi-periodic in the slave laser output in this region, the bifurcation diagram showed in chapter 2, figure 2.1c [6] is adopted. Although this study is concerned with the optical injection of semiconductor lasers and used semiconductor material parameters, it can be used to explain the dynamical characteristics of an optically injected solid state laser to a large extent.

The studies of the dependence of the dynamical characteristics of an optically injected laser on the material parameters [7] is presented that the effect of the nonlinear gain relaxation rate (γ_p) is opposite to the effect of the differential gain relaxation rate (γ_n). In the sense that decreasing the first, causes to enlarge the instability regions, while decreasing the second, causes to shrink the instability regions. In solid state laser both of these parameters are less than its values for semiconductor laser in approximately the same order [2,6]. Because the decay rate of upper state level (γ_s) has a little effect and the cavity decay rate (γ_c) has approximately a close value, it is possible to consider the linewidth enhancement factor (α) the most important factor to determine the dynamical characteristics of the injected system.

The study in [6] states that the complicated interplay between the saddle-node of limit-cycle bifurcation and the torus bifurcation gives rise to bistability in this region. In other words, when the torus bifurcation curve T crosses the saddle-node of limit-cycles orbits, a bistability occurs, causing the switching between the two oscillating dynamics. This can explain the coexistence of the two waveforms, the periodic (spiky) and the quasi-periodic waveform in the slave laser output in this regime.

5.3.2.2. The difference between the values of frequency of quasi-periodic and spiky waveforms

The difference between the frequency values of quasi-periodic and spiky waveforms (f_2-f_1) can be used as an indicator to specify the value of the injection strength where the fluctuation between the two waveforms is eliminated, in which the rest region could be used to generate pulses. Using (f_2-f_1) as an indicator is possible due to the direct relation between the standard deviation of the PRF and the frequency difference between the two waveforms as shown in figure 5.21.

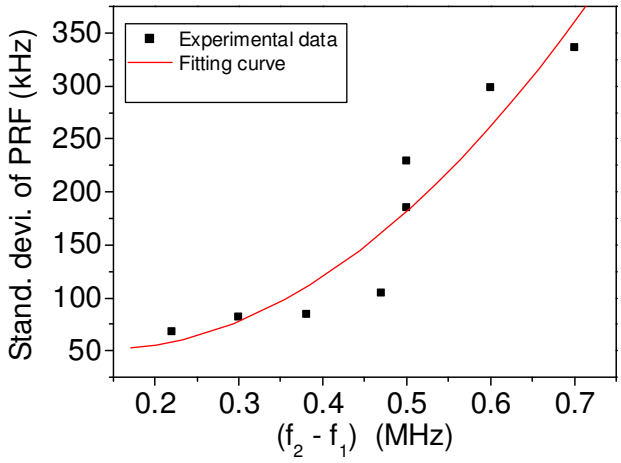

Figure 5.21. The relation between the standard deviation of the PRF and the frequency difference between the two waveforms.

Figure 5.22 shows that the frequency difference between the two waveforms drops rapidly to a low value at an injection strength of approximately = 2.8 and

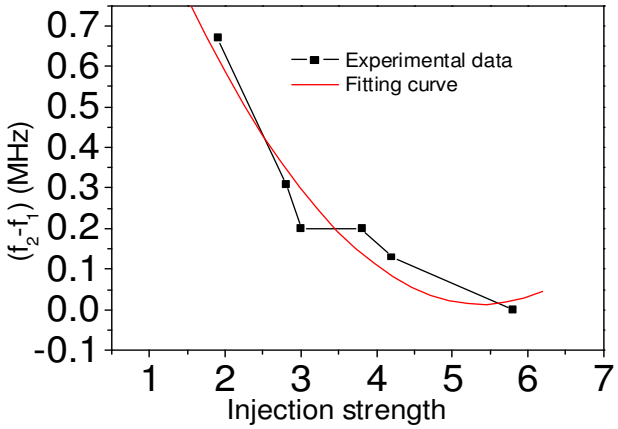

Figure 5.22. The dependence of the frequency difference between the two waveforms on the injection strength.

drops slowly after this value. This means the possibility of using this region with the high injection strength value to generate regular pulses.

5.3.3 Quasi-periodic regime close to saddle-node curve

The three points, in which (K,Δω) = (1.08,-1.08), (1.6,-1.6) and (2.1,-2.1), in figure 5. 23 are the location of the specified points which belong to quasi-periodic regime in the boundary just before the injection locking regime, in the (K, Δω)-plane.

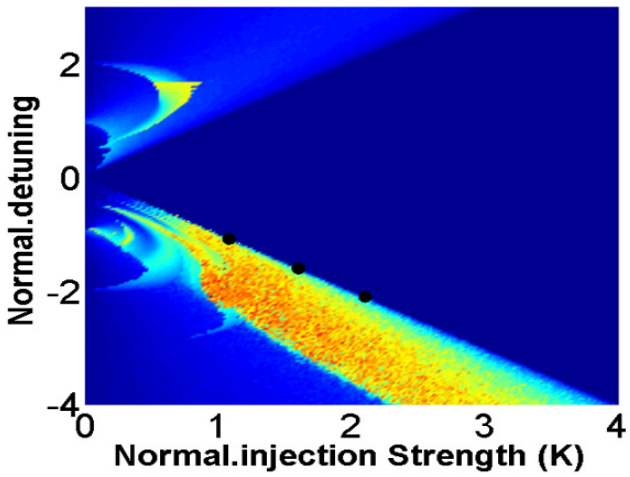

Figure 5.23. The location of the points (K-Δω)= (1.08,-1.08), (1.6,-1.6) and (2.1,-2.1) of quasi-periodic regime on the K-Δω map

Figure 5.24 is a typical example of the characteristics of the dynamics in this region. Row (a) shows an unstable intensity level. A sharp quasi-periodic waveform with two frequencies, the envelope frequency and the carrier frequency, is shown in row (b). The interval between the pulses represents the locking regime since the points are very close to the locking regime.

The envelope frequency was taken to be the PRF of the pulses. The change of the PRF in the row (d) due to the change of detuning in row (c) shows a moderate dependence on the detuning.

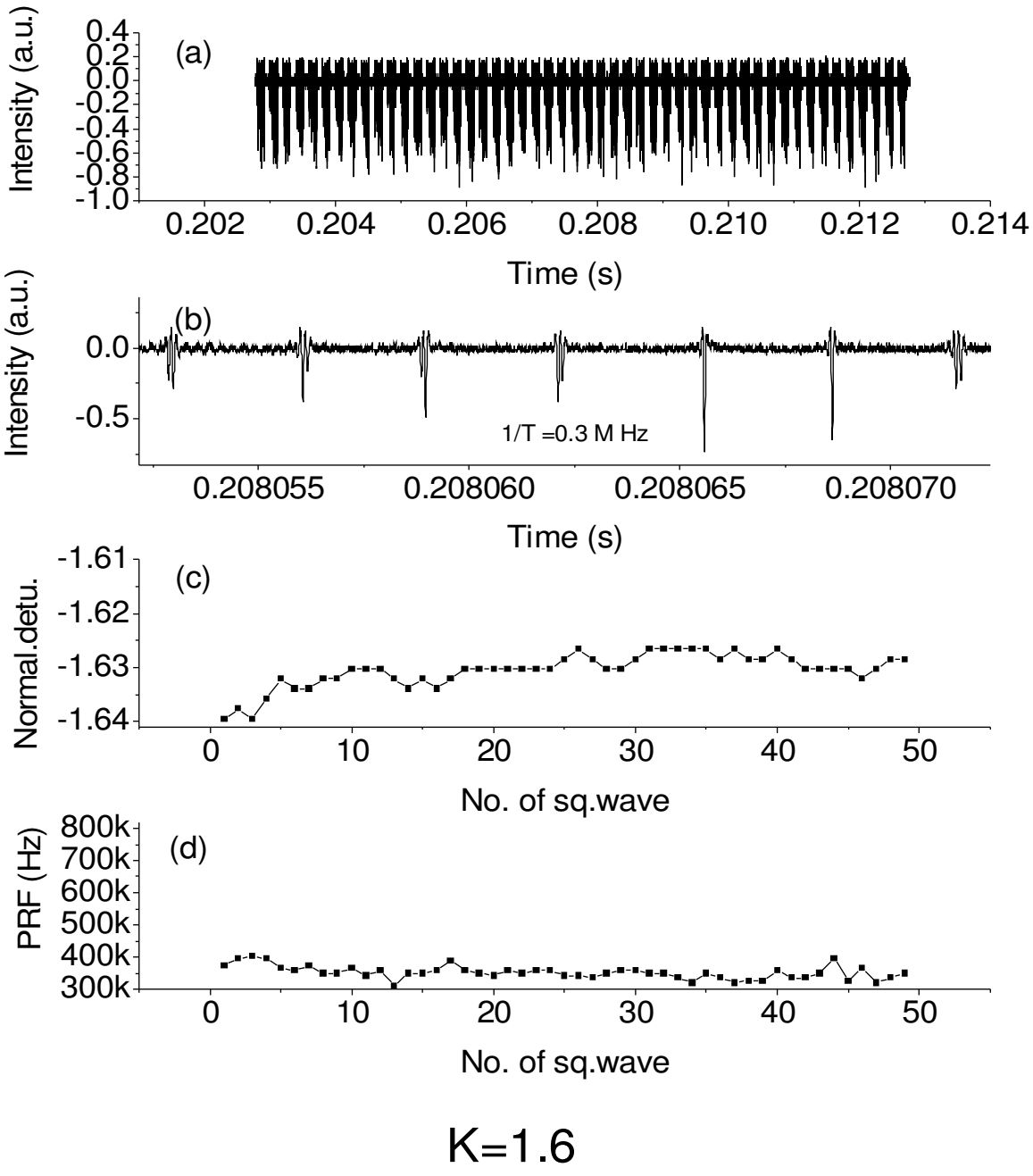

Figure 5.24 (a) The intensity level for 50 squares of pulses; (b) pulses waveform; (c) the change in frequency detuning in 10ms; (d) the change in PRF in 10ms. The relations for the injection parameters (K ,Δω) =(1. 6, - 1.6).

The correlation coefficients of PRF with Δω (table 5. 4), show moderate values with the coefficient decreasing as K, Δω increases.

Figure	K	Δω	PRF (MHz)	Correlation coefficient
A18	1.08	-1.08	0.9	0.95
5.21	1.6	-1.6	0.35	0.63
			7.8	0.33
A19	2.1	-2.1	0.34	0.45
			9.7	0.15

Table 5.4. The PRF and correlation coefficient for pulses just before the injection locking regime.Figures A18 and A19 are in the appendix A.

Figure 5.25 shows the different behaviours of envelope and carrier frequencies with changing the detaining for injection parameters (K, Δω) = (1.6, -1.6).

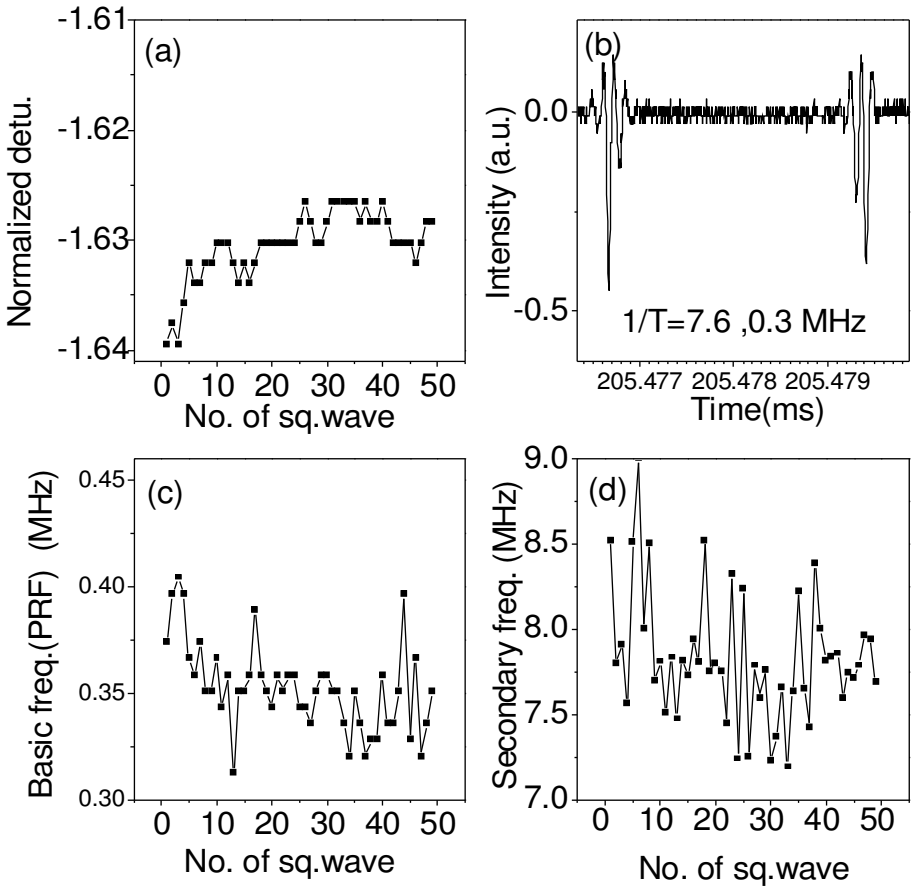

Figure 5.25. the different behaviours of envelope and carrier frequencies with the change in the detuning for the data point $K = 1.6$ and $\Delta\omega = -1.6$

5.3.4 Quasi-periodic regime close to torus curve

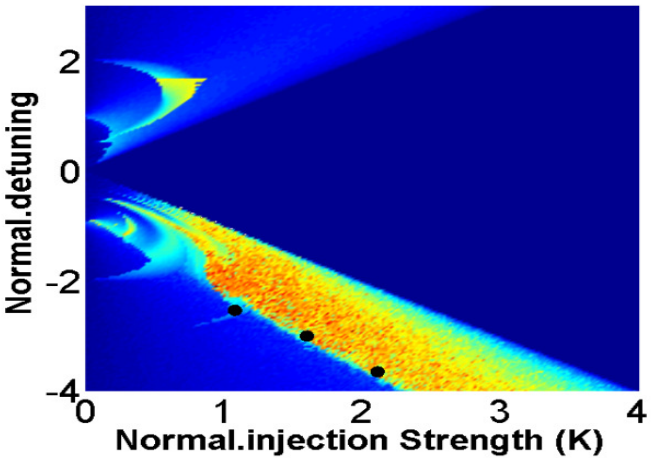

Figure 5.26. Location of points (1.08,-2.53), (1.6,-3) and (2.11,- 3.63) in (K,Δω)- plane

Figure 5.26 represents the locations of three points close to the torus curve, in which the waveform is quasi-periodic. The points are (K, Δω) = (1.08,-2.53), (1.6,-3), and (2.11,-3.63).

Figure 5.27 is an example of the points in this region. The figure shows the behaviour in point (1.6,-3). Rows (a) and (b) represent an example of the relative intensity level and the waveform in this region. Row (c) represents, the change in the detuning within a time period of 10 ms. finally, row (d) shows the change in the PRF (the envelope frequency) due to the change in the detuning in which low correlation level is found.

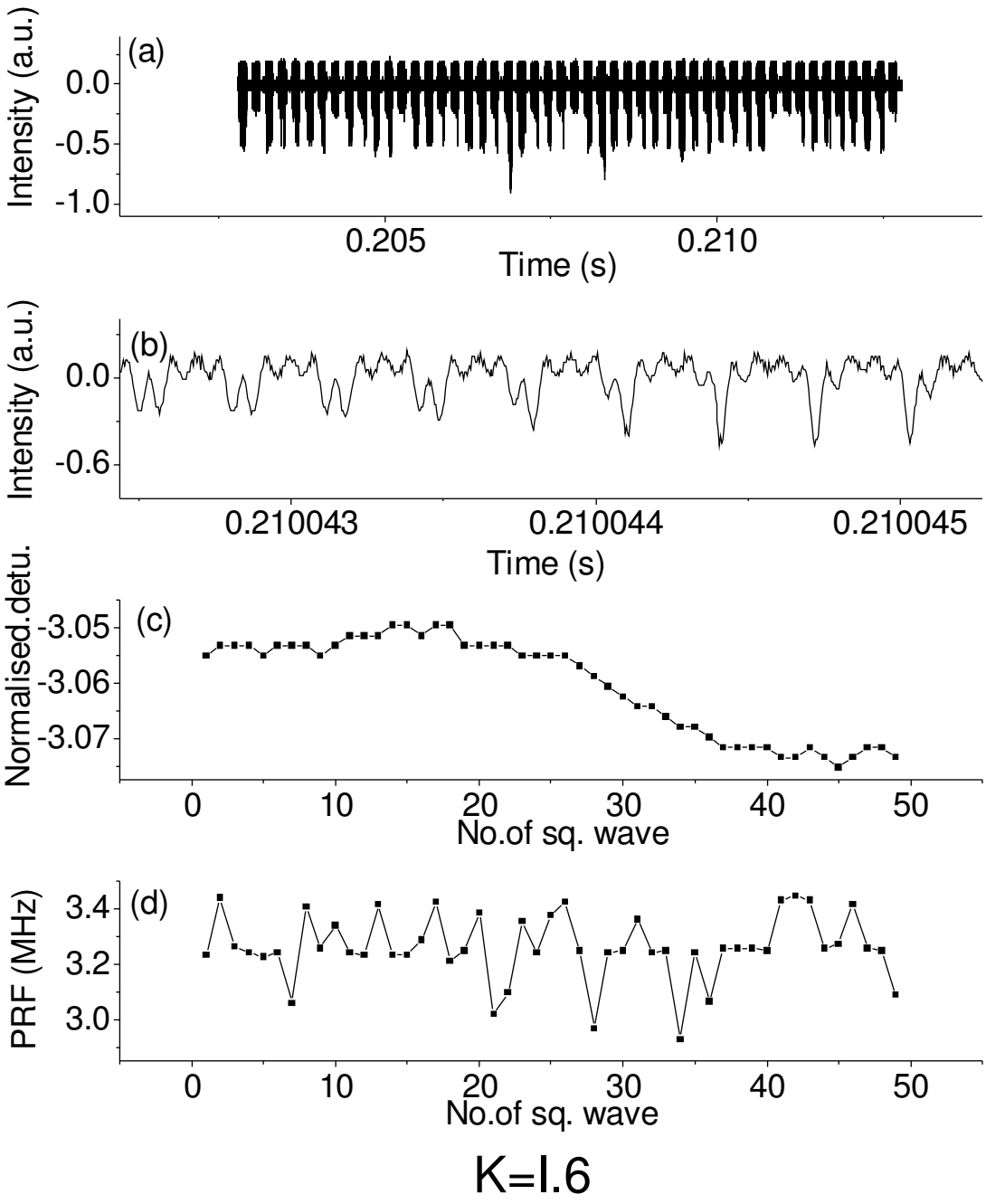

Figure 5.27. (a) The intensity level for 50 squares of pulses; (b) pulses waveform; (c) the change in frequency detuning in 10ms; (d) the change in PRF in 10ms. The relations for the injection parameters (K, Δω) =1.6 ,- 3).

Table 5.5 shows the values of the correlation coefficient that related to these points which show different behaviours.

Figure	K	Δω	PRF (MHz)	Correlation coefficient
A20	1.08	-2.5	3.5	0.98
			10.6	0.99
5.24	1.6	-3	3.2	0.04
			12.3	0.99
A21	2.1	-3.65	2.45	0.11
			15.5	-0.08

Table 5.5. The PRF and correlation coefficient for pulses closed to torus bifurcation curve. Figures A20 and A21are in appendix A.

The results showed a high level of correlation coefficient of both frequencies in the regions close to the torus curve for low injection strength. For high injection strength, the correlation coefficient of both frequencies drops very fast compared with the values of the correlation coefficient close to CN curve.

5.4. Conclusion

In this chapter, the characteristics of various dynamical regimes of an optically injected solid state laser are investigated. An experimental demonstration of the dynamics at specific points on the dynamical map, belonging to various dynamical states has been introduced. The response of the pulse repetition frequency to changes in the detuning at these points is evaluated. The results showed a high level of response of PRF to changes in detuning for the period-doubling regime (P2, P3) and for the limit cycle regime (P1) in both the positive and negative detuning regions. Although limit cycle regime shows a low intensity as compared with period-doubling regime, the regime operates without noise which encourages the use of this regime as a source of regular pulses in addition to P2 and P3. The PRFs of the two regimes complement each other.

In the spiky region, we demonstrate a kind of bistability in which two dynamics can oscillate for the same injection parameters. The coexistence of the dynamic in this region was suggested theoretically in [6], and it is attributed to the intersection of the SL curves with the torus curve. However, this dynamics which has the highest intensity among the dynamics in this system, shows a very low correlation between the PRF and the detuning, and could not be used to generate pulses with variable PRF. Nevertheless, switching between outputs with different intensities and frequencies may reveal applications in other fields, such as logic gates or optical communication.

The difference between the values of frequency of quasi-periodic and spiky waveforms (f_2-f_1) is used as an indicator to specify the value of the injection strength where the fluctuation between the two waveforms is eliminated, in which the rest region could be used to generate pulses. The results show that the frequency difference between the two waveforms drops rapidly to a low value at injection strength approximately = 2.8 and drops slowly after this value. This means the possibility of using this region with the high injection strength value to generate regular pulses.

Different correlation coefficients of PRF and detuning were obtained in the quasi-periodic regime in the regions close to SN and T curves, showing the different responses of the PRF to changes in detuning. In general the carrier frequency shows high correlation, while the envelope frequency shows lower correlation. A high level of correlation has been seen in the regions close to the SN and T curves for low injection strength. For high injection strength, the correlation coefficient shows modurate values in the regions closed to the SN curve while the correlation coefficient of both frequencies drops very fast with increasing K in the region close to the torus curve.

More investigation is needed to determine the full continuous range of the change in PRF by changing the frequency detuning that the OISSL can offer. This will be investigated in Chapter 6. The investigation will focus on the regions in the (K,Δω)-plane that showed positive response to the change in detuning.

References

1. Valling, S., T. Fordell, and Å. M. Lindberg. "Experimental and numerical intensity time series of an optically injected solid state laser." Optics Communications, vol. 254, no.4, pp. 282-289, (2005).
2. Valling, Simo, Thomas Fordell, and Åsa Marie Lindberg. "Maps of the dynamics of an optically injected solid-state laser." Physical Review A, vol 72, no. 3, pp. 033810(1-7), 2005
3. Webb, Colin E., and Julian DC Jones, eds. "Handbook of Laser Technology and Applications: Laser design and laser systems". Vol. 2. CRC Press, 2004.
4. Toomey, J. P., C. Nichkawde, and D. M. Kane. "Uncertainty in interpulse time interval evaluated as a new measure of nonlinear laser dynamics." Conference on Lasers and Electro-Optics/Pacific Rim. Optical Society of America, 2011.
5. Krauskopf, Bernd, and Sebastian Wieczorek. "Accumulating regions of winding periodic orbits in optically driven lasers." Physica D: Nonlinear Phenomena, vol. 173, no. 1, pp. 97-113, (2002).
6. Wieczorek, Sebastian, et al. "The dynamical complexity of optically injected semiconductor lasers." Physics Reports, vol. 416, no. 1, pp.1-128, 2005.
7. Hwang, S. K., and J. M. Liu. "Dynamical characteristics of an optically injected semiconductor laser." Optics Communications, vol. 183, no. 1, pp. 195-205, 2000.

Chapter 6

OISSL system as a laser pulse generator

6.1. Introduction

An optically injected solid-state laser system can be used to generate pulses with a continuously variable pulse repetition frequency. The most important feature of the OISSL is its ability to generate on-demand pulses with different pulse repetition frequency (PRF) values using a single variable parameter. By adjusting the injection strength, different ranges of PRF and different rates of change of PRF can be covered. This has been studied in [1,2]. Another approach involves varying the frequency detuning between the free-running optical frequencies of the master and slave lasers. In this chapter, the characteristics of laser pulse generation, by adjusting the injection strength of OISSL, are demonstrated and, the characteristics of laser pulse generation by adjusting the frequency detuning of OISSL, are investigated as an alternative approach with different properties.

6.2. Characteristics of continuously variable PRF pulsed systems

Characteristics of continuously variable PRF pulsed laser systems are the same as the characteristics of single valued pulsed laser systems In addition to characteristics specific to the a continuously variable PRF pulsed laser. The characteristics of single valued pulsed laser systems include pulse power, pulse energy, pulse repetition frequency, pulse duration and timing jitter. For continuously variable PRF pulsed laser systems, the range and the rate of change of these characteristics should be considered. In an optically injected solid state laser system many pulse waveforms are obtainable in the output of the system. This feature is not available in other laser pulsed systems. Many applications require a particular kind of pulse. In this investigation attention is focused on:

- The pulse repetition frequency range that can be attained continuously.
- The rate of change of the pulse repetition frequency with the frequency detuning. The smaller rate of change, for example, means it is possible to obtain more accurate values of PRF.

- The change in the pulse intensity and pulse waveforms that are associated with the change in the pulse repetition frequency.

The average power of the used Nd:YVO_4 OISSL system is 10 mW (slave laser output). It is not expected that the average output power can greatly exceed this value in this setup, this is due to the difficulty in obtaining a single longitudinal mode high power diode laser, to pump the solid-state laser and also due to the single longitudinal mode operation considerations. Therefore, it is preferred to use optical power amplification methods to produce high power pulses for different applications. These methods can amplify the output power by a factor of 100 [3]. However, it is preferable for the base system to provide as high an output power as possible. A base system with clean, high power pulses is expected to be more efficient.

The value of pulse duration (τ_d) in this system is between 6 ns and 77 ns with no systematic variations related to changes in either of the injection parameters, K or $\Delta\omega$. The arbitrary fluctuations in the pulse duration indicate that the pulse duration is very sensitive to noise effects. For this reason this study is not concerned with the pulse duration.

The complex configuration of the (K,Δω) map (chapter 5, figure 5.3) with different dynamical characteristics implies that different paths of pulse repetition frequency, either by varying injection strength or by varying detuning frequency between the master and slave laser, can have different characteristics.

6.3. Controlling PRF in OISSL by adjusting the injection strength

Controlling the PRF by changing the normalized injection strength (K) for fixed frequency detuning values has been studied experimentally [1, 2]. Figure 6.1 showed the results for the negative detuning region. The results showed a good response to the change in the injection strength in many parts of the figure, but a weak response in other parts. Consequently, to cover a wide range of PRF many frequency detuning values should be employed. In other words, to obtain a wide range of PRF, two injection parameters should be used instead of one. The accessible range of pulse repetition frequency is from approximately 200 kHz up to 4.2 MHz, using several piecewise regions. Discontinuous curves of PRF versus k are seen in figure 6.1.

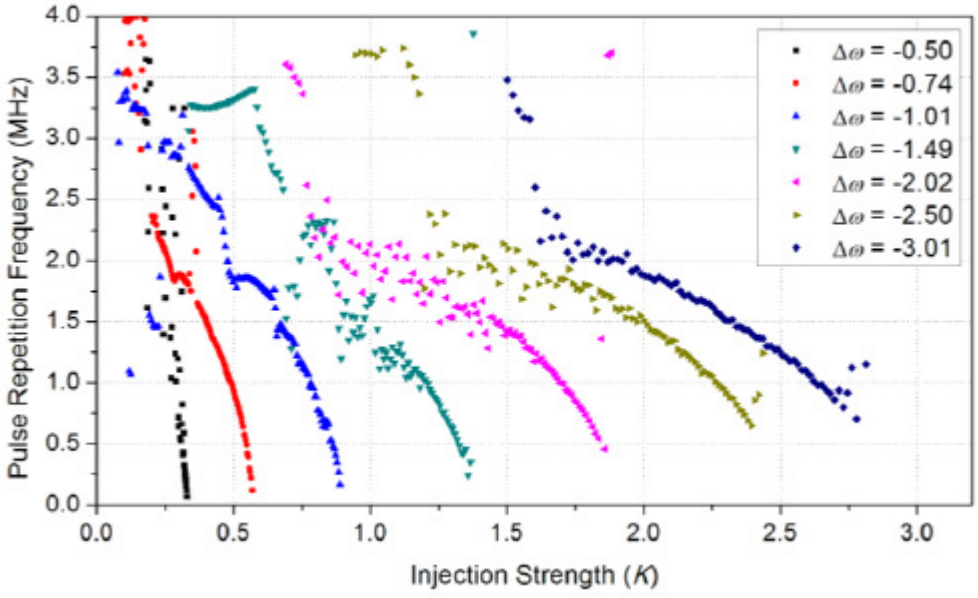

Figure 6.1. Dominant frequency as a function of injection strength for detuning Δω = -0.50, -0.74, -1.01, -1.49, -2.02, -2.50 and -3.01 [1, 2]

For example, in the case of $\Delta\omega$ = -0.74 the PRF can be varied between 200 kHz and approximately 2.3 MHz by changing the injection strength from 0.55 to 0.2. For lower injection strength, the PRF varies erratically, then for higher PRF values, the curve with $\Delta\omega$ = - 1.01 MHz can used, for the PRF from 2.3 MHz to 2.7 MHz for injection strength between 0.45 and 0.3.

In the following experimental work we will refer to a region in which continuous change in PRF can be obtained as a one path.

6.4. Controlling PRF in OISSL by adjusting the frequency detuning

6.4.1 Experimental arrangement

To generate a continuous range of PRF by varying frequency detuning for fixed values of injection strength, and to study the properties of this system, a similar setup explained in Chapter 5 is utilised (as shown in figure 6.2). In this experiment, an unmodulated injection beam from the master laser is injected into the slave laser to produce dynamical pulses. To obtain the curves between the PRF and the detuning for fixed values of injection strength, the frequency detuning is changed by controlling the temperature of the master laser.

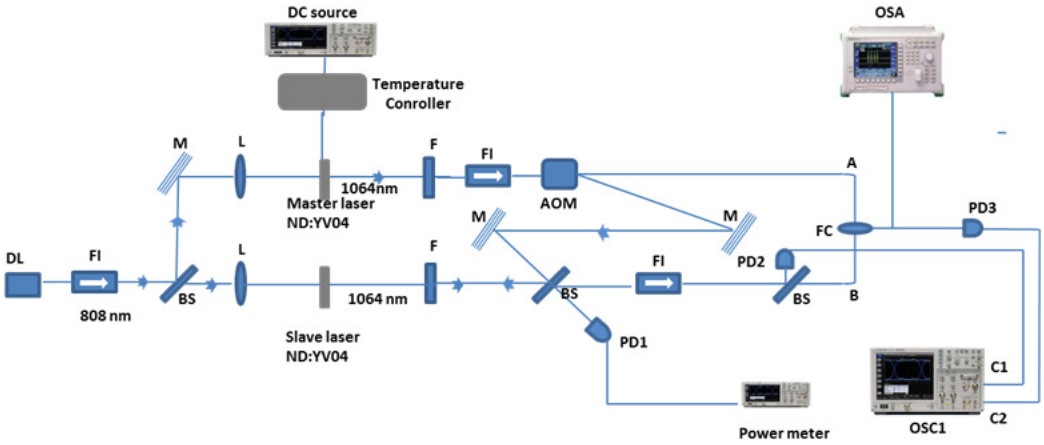

Figure 6.2. The experimental set-up showing the OISSL system as a laser pulse generator: DL, Diode laser. BS, beam splitter. F, filter. FI, Faraday isolator. L, lens. M, mirror. OSC, oscilloscope. OSA, Optical spectrum analyzer, PD detectors. FC, fibercoupler.

The values of the frequency detuning between the free running optical frequencies of the master and slave lasers are measured by beating the outputs of the two lasers and monitored at C1 by a LeCroy LC564A oscilloscope (FFT spectrum). The temperature controller of the master laser is coupled to a DC voltage source for fine temperature controlling, and to obtain a suitable rate of change in the frequency detuning. An exact change in frequency detuning is produced over a specific time. A calibration curve between $\Delta\omega$ and the time (figure 6.3 (a)) is first obtained without injection to determine how the frequency detuning changes with the time for a specific change in temperature. Recording of data is started from the first value of the specified detuning and stopped at the last detuning value. The time when each data is recorded is read from the properties window of the file used to record the data.

In the second stage, optical injection is applied. The same frequency detuning change is stimulated by the same change in temperature. Intensity time series of the slave laser output contain nonlinear dynamics, are recorded sequentially at C2 while the detuning is changed. In this way, a large amount of data is recorded (100 files) for each value of K.

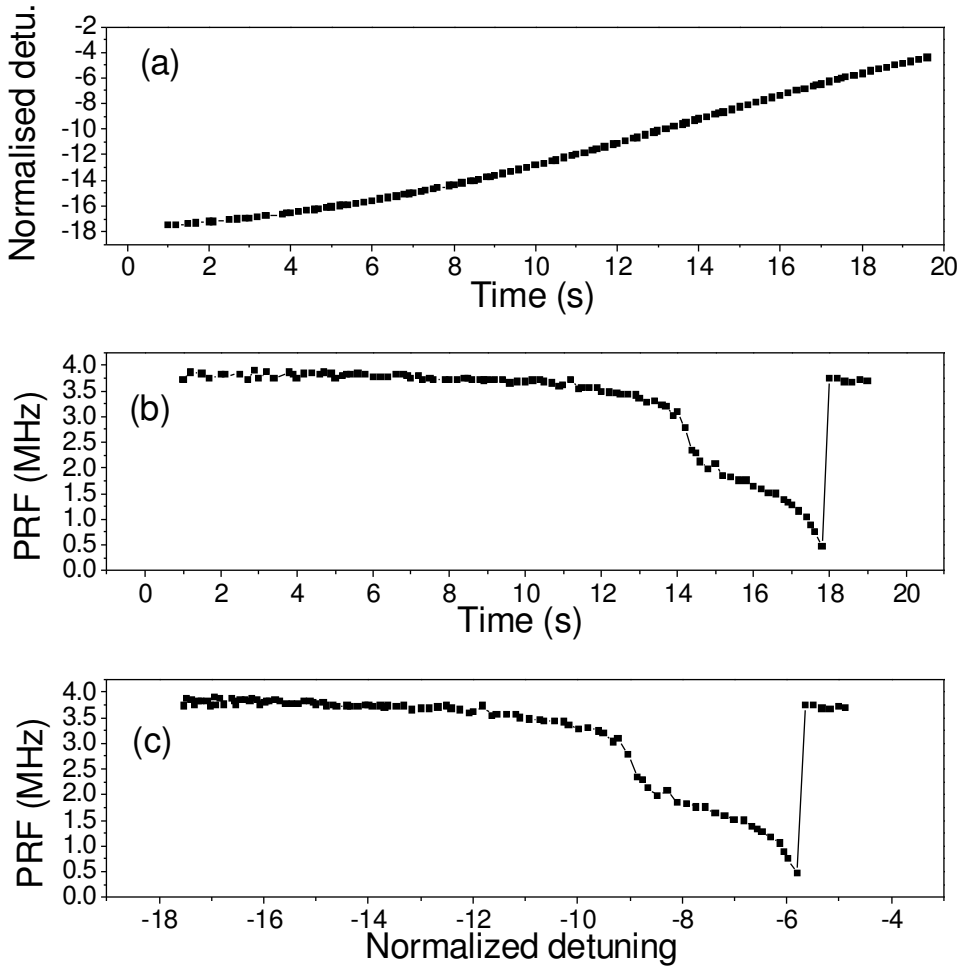

Figure 6.3. The steps followed to obtain the relation between the PRF and the detuning for one of injection strength values.

The relation between the PRF and the time (and between the intensity and the time) are determined from the recorded data (figure 6.3 (b)).

The magnitude of the voltage change to control the temperature controller is chosen carefully to ensure that the rate of change of the detuning is suitable for recording the same number of intensity time series (or FFT spectrums) each time. In the last stage, PRF-Time (and Intensity- Time) curves are calibrated using a $\Delta\omega$-Time fitting curve (figure 6.3 (c)).

The values of the injection strength are determined by calibrating the frequency detuning at the injection locking to the values obtained from the simulated data generated for this system. This calibration is possible because all swept data include a

point where the injection locking starts. This method has been explained in details in Chapter 4, section 4.4.

6.4.2 PRF-Detuning curves

To study the characteristics of generating laser pulses by changing the frequency detuning, two different regions of the dynamical map of the current solid state laser system are highlighted. The relation of the PRF with the normalised frequency detuning (and maximum intensity with the same parameter), is found for many injection strength values. Injection strength in the range between 0.65 and 1.9, is avoided in this study due to the low response of the PRF to the injection parameters in this region, which was discussed in chapter 5, section 5.3.2. The small chaos region specified in figure 2.4 in chapter 2, is avoided also. Regarding the range of injection strength from 0-0.65, the normalized frequency detuning changes from -5.5 to +5.5 to cover both the positive and the negative nonlinear dynamical regions (figure 5.4, section 5.3.1). For K greater than than 1.9, the normalized frequency detuning changes from -17.5 to approximately -1.5, since there are no dynamical pulses for the positive detuning side. Figure 6.4 shows these two regions. The dependence of the pulse repetition frequency on the frequency detuning for a fixed value of injection strength in an optically injected solid state laser is shown in Figures 6.5 - 6.7.

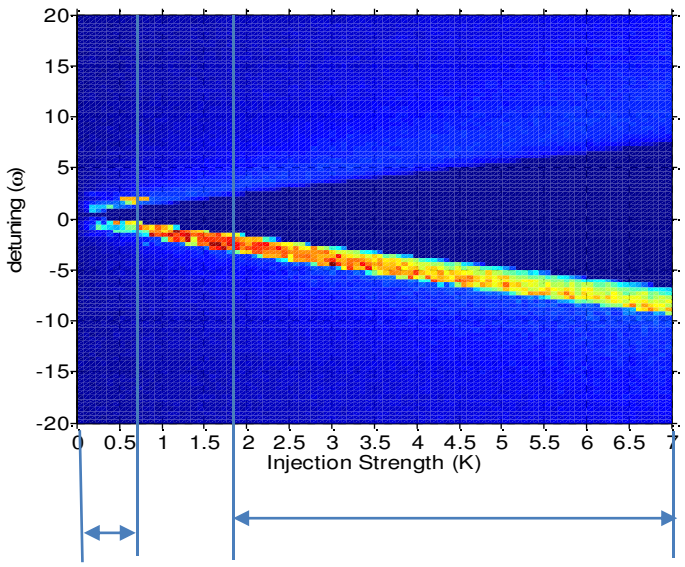

Figure 6.4. Diagram shows the two tested regions where the dependence of pulse repetition frequency on the frequency detuning for a specific values of injection strength is tested

6.4.2.1. The first range of injection strength values

Figure 6.5 and 6.6 shows the values of pulse repetition frequency, as a function of the detuning (Δω) that were attained from this system for fixed levels of injection strength: 0.21, 0.38, 0.52, and 0.65. The diagram for each specific injection strength value, is a piecewise curve, which represents an evolution of the dynamical states. The path, defined as all the parts of the piecewise curve for a specific value of the injection strength, included approximately 8 distinguishable dynamical stages, including nonlinear dynamical pulses and the surrounding noisy regions. The stages for K = 0.21 are denoted by numbers and are shown in Figure 6.5. These stages are:

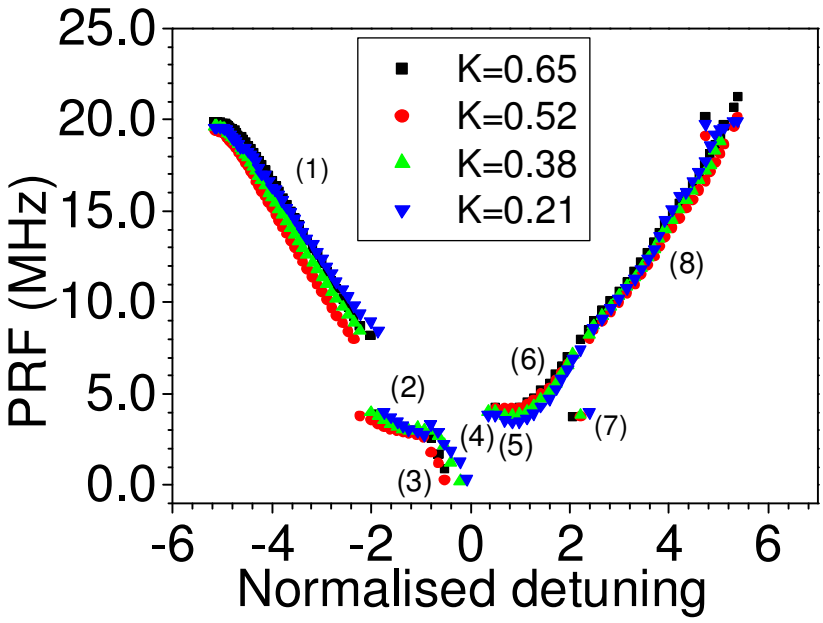

Figure 6.5. The dependence of PRF on the detuning for different values of injection strength (K).

(1) For detuning values from -1.7 and less, the stage represents the noisy region. For large detuning values, the pulses approach free running laser pulses, in which the output of a continuously pumped laser consists of irregular oscillations. These oscillations are attributed to the relaxation oscillation of the slave laser (4MHz), excited by various noises.

(2) For the detuning between -1.7 and -0.94, the detuning-PRF curve starts with quasi-periodic pulses (explained in chapter 5, section 5.3.4) where a two frequencies exist (the envelope and the carrier frequency). The measured frequency is the envelope frequency since this frequency is the one which will improve to the next dynamical state. By moving more, at approximately -1.58, the quasi-periodic pulses quickly change to periodic pulses, and the system operates with periodic pulses of P1 state with (roughly) Gaussian shape.

(3) For the detuning change from -0.94 to -0.20, the system continues to operate with periodic pulses; in the last stage, the pulses change gradually to sharp quasi-periodic pulses.

(4) Frequency detuning from -0.2 to +0.2 represents the injection locking region, the slave laser is locked to the master laser and operate with the relaxation oscillation frequency of the master laser (3.6MHz).

(5) For frequency detuning from +0.2 to +0.96, the system operates with periodic pulses related to the limit cycle oscillation; periodic pulses of the limit cycle are sharp.

(6) For frequency detuning from +0.96 to 2.23, the system operates with periodic pulses (period-one region).

(7) For frequency detuning from +2.23 to +2.39, the system operates with periodic pulses (period-two state region).

(8) For frequency detuning from +2.39 and over, the system operates with periodic pulses (noisy limit cycle) which changed gradually to noisy pulses similar to stage 1.

Most of these oscillation types have been discussed in Chapter 5, section 5.3. In general, the stages are the same for the different values of K. Figure 6.5 shows that the ranges of PRF that can be attained with different values of K is approximately similar for each other. Figure 6.6 is the enlargement of the main two regions of the varaies dynamics in figure 6.5, for injection strength less than approximately 0.65 for the negative detuning (a) and for the positive detuning (b).

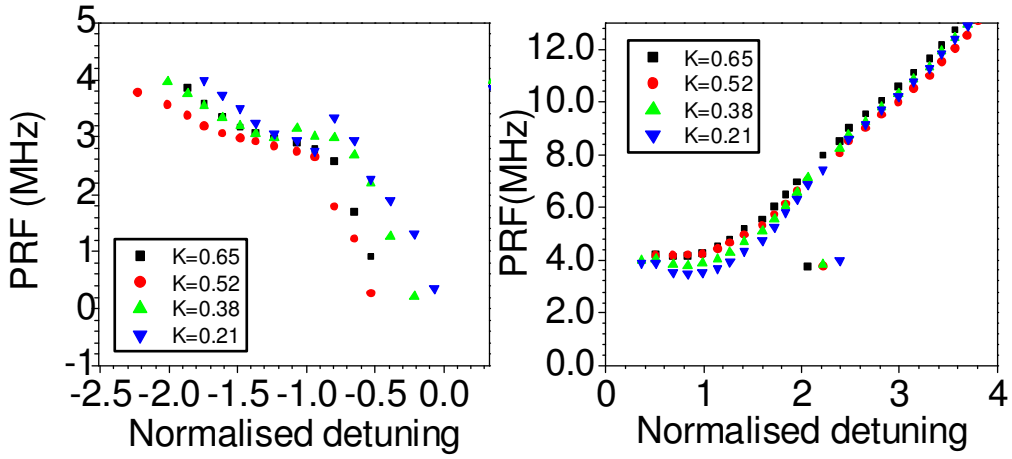

(a) *(b)*

Figure 6.6. Enlargement of the regions in figure 6.4. (a) the change in PRF with the detuning for different values of injection strength for negative detuning, (b) for posative detuning.

Regardless of the differences in the type of oscillating , changing the detuning in this system offers a range of pulse repetition frequencies, from approximately 200 KHz to 7.5 MHz. Figure 6.6 (a) shows that the path with an injection strength of 0.38 offers the longest range of PRF for the negative detuning (from 200 KHz to 4MHz). However, the path with K = 0.52 also offers a long range of PRF, with a continuous decrease rather than the irregular change in the PRF with K = 0.38. For positive detuning, Figure 6.6 (b) shows that a continuous range of pulses clear from any noise from 4 MHz to 7.5 MHz is possible, irrespective of the low intensity in some parts. This range can be attained by any of the PRF-detuning curves of different injection strengths, starting from the stage (6) and ending before stage (7), where the frequency is reduced by half when period one (P1) state bifurcates to period two (P2) state. For the detuning higher than P2 state , a noisy region starts. Therefore, its convenient to consider the end of the periodic region of stage 6, the end of the useful pulses. In genral, the rate of change of all stages is similar except for stage 3 in which the PRF drops down fast where the system at this stage operates in torus regime and offers sharp, quasi-periodic pulses in the kHz range.

It is worth mentioning that the similar paths of all injection strength values indicate that the positive detuning regions have a spot shape rather than a crescent shape, as

shown in [2]. This can be concluded from the same continuous gradual change in PRF - detuning diagram for all values of K.

6.4.2.2. The second range of injection strength values

In the second range of K values, where K is 1.9, 3, 3.8, 4.2, 5.8, a continues range of pulse repetition frequency from 200 kHz to 4 MHz can be attained by changing the detuning. Figure 6.7 shows how the pulse repetition frequency varies with the detuning for every injection strength value. Each path for each specific injection

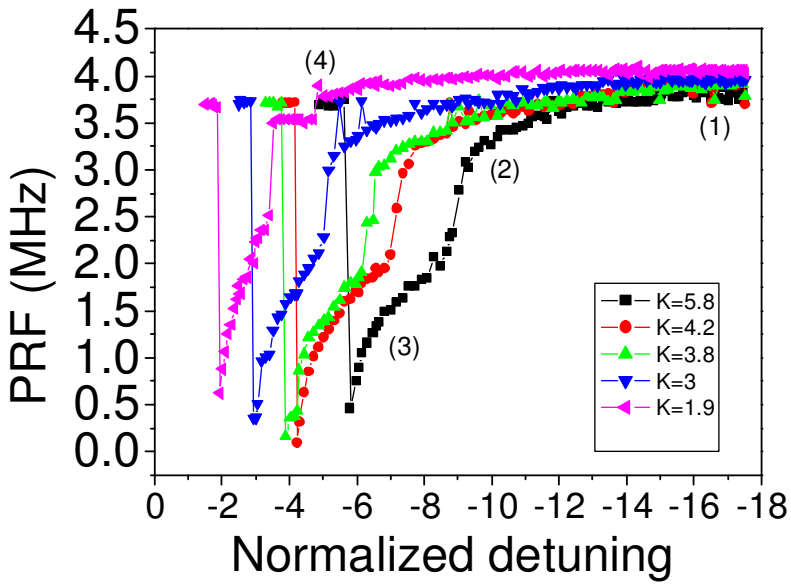

Figure 6.7. PRF versus detuning for large values of injection strength(K), for the negative detuning.

strength includes 2 stages of nonlinear dynamical pulses in addition to the surrounding noisy region. These stages form different paths from that seen in the first range of K values. The stages for injection strength 5.8 are denoted by numbers and shown in figure 6.7, are:

(1) For the negative detuning values -13.5 and less, the stage represents noisy region. The properties of this region are the same as stage (1) in figure 6.5.

(2) For detuning change in the range -13 to - 8.5, the system operates with quasi-periodic pulses.

(3) For detuning between approximately - 8.5 and - 5.8, the system operates with mixed pulses. These pulses have been discussed in chapter 5. Section 5.3.2. Operation includes sequences of spiky and quasi-periodic pulses having slightly different frequencies. In the last part before of the injection locking the pulses changed to sharp locked quasi-periodic pulses.

(4) At a frequency detuning of - 5.8, the slave laser is locked to the master laser and operates with the relaxation oscillation frequency of the master laser (3.6MHz).

These stages which represent a route to locking for a fixed value of K are similar for all other PRF-detuning paths of other injection strength values.

The second range of injection strength values lies between the saddle-node curve and the torus curve, beyond the period-doubling region (chapter 2, figure 2.1B, c and chapter 2, figure 2.3). The range of injection strength values has been selected according to the results of chapter 5, section 5.3.2. The result showed that for this region, for smaller values of injection strength, the PRF weakly responds to the change in detuning. Figure 6.7, K =1.9 shows that this effect is still there and stage 3 is weakly responded to the detuning change in the last part of this stage, therefore the path for K=1.9 should be excluded from the range.

Figure 6.7 shows that the range of PRF is shifted slightly towards lower values PRF with increasing injection strength, until the injection strength reaches 4.2. After this value the range shifts to higher values of the PRF. The rate of change of PRF for both stages 2 and 3 is generally higher for low injection strength.

As the injection strength increases, the rate of change of PRF became low which allows for more accuracy in choosing PRF values. However the path for K = 4.2 offers the longest continuous range of PRF (from 200 kHz to 4 MHz) and represents the most suitable path .

6.4.3. The change of intensity associated with the PRF change

To get additional insights into the performance of the OISSL system, the peak intensity amplitudes of the intensity time series, are found, for all registered data in figures 6.5 and 6.7, as a function of detuning. Figure 6.8 shows the relation between Δω and PRF and the associated relation between Δω and Intensity for each value of the injection strength separately for the first range of K values (0.21-0.65). Figure 6.9 shows the same relations for the second range of K values (1.9 - 5.8).

An arbitrary unit is given to the intensity values and used for a comparison purpose since the photodiodes convert the optical power to an instantaneous voltage.

Both figures 6.8 and 6.9 show that the pulse intensity in this system is not fixed and that there is a correlation between the PRF and the intensity of the dynamical pulses. If a fixed intensity is a basic requirement in an application, optical power amplification methods can be used to modify and amplify the power at the same time. On the other hand, the correlation between the PRF and the intensity of the pulses could be of major benefit and can be used to stabilize the PRF of the system by using the intensity as a sensor for the PRF fluctuations. In this case a suitable comparative circuit could be used to modify the temperature of the laser crystal.

In figure 6.8 a, for injection strength values less than 0.65, most of the Δω-Intensity graphs include 4 peaks except for K 0.38, where the intensity peak belongs to quasi-periodic pulses is not clearly exist. In the positive detuning region where two peaks exist, the small peak represents the switch from P1 state to the P2 state where the PRF drops suddenly to the half, therefor the peak represents the end of the continuous range of the pulses. Therefore the path with K = 0.38 offer a convenient continuous range. The second range of injection strength values is important due to its high intensity. Comparing figures 6.8 (a) for the injection strength range between 0.21 and 0.65 and figures 6.9 (a) of injection strength range between 1.9 and 5.8, it is shown that the intensity in the second range is higher than the intensity in the first range. This feature in the second range encourage to use this range, regardless of the shorter obtainable range of the PRF in this range compared with the first range.

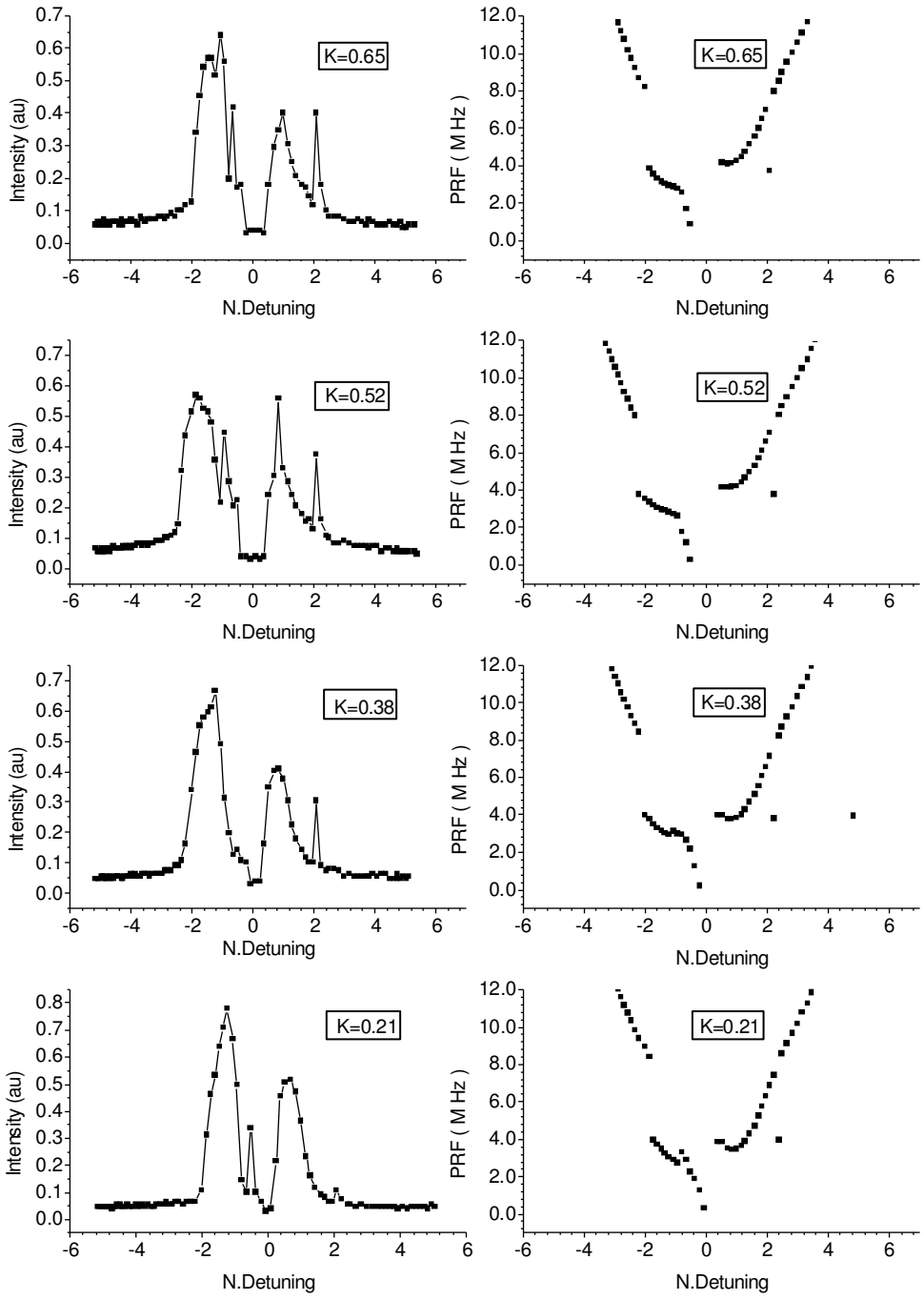

Figure 6.8. (a) The change in intensity by changing the detuning for different values of injection strength for the negative detuning. (b) The change in PRF by changing the detuning for different values of injection strength for the negative and positive detuning for the first range of K.

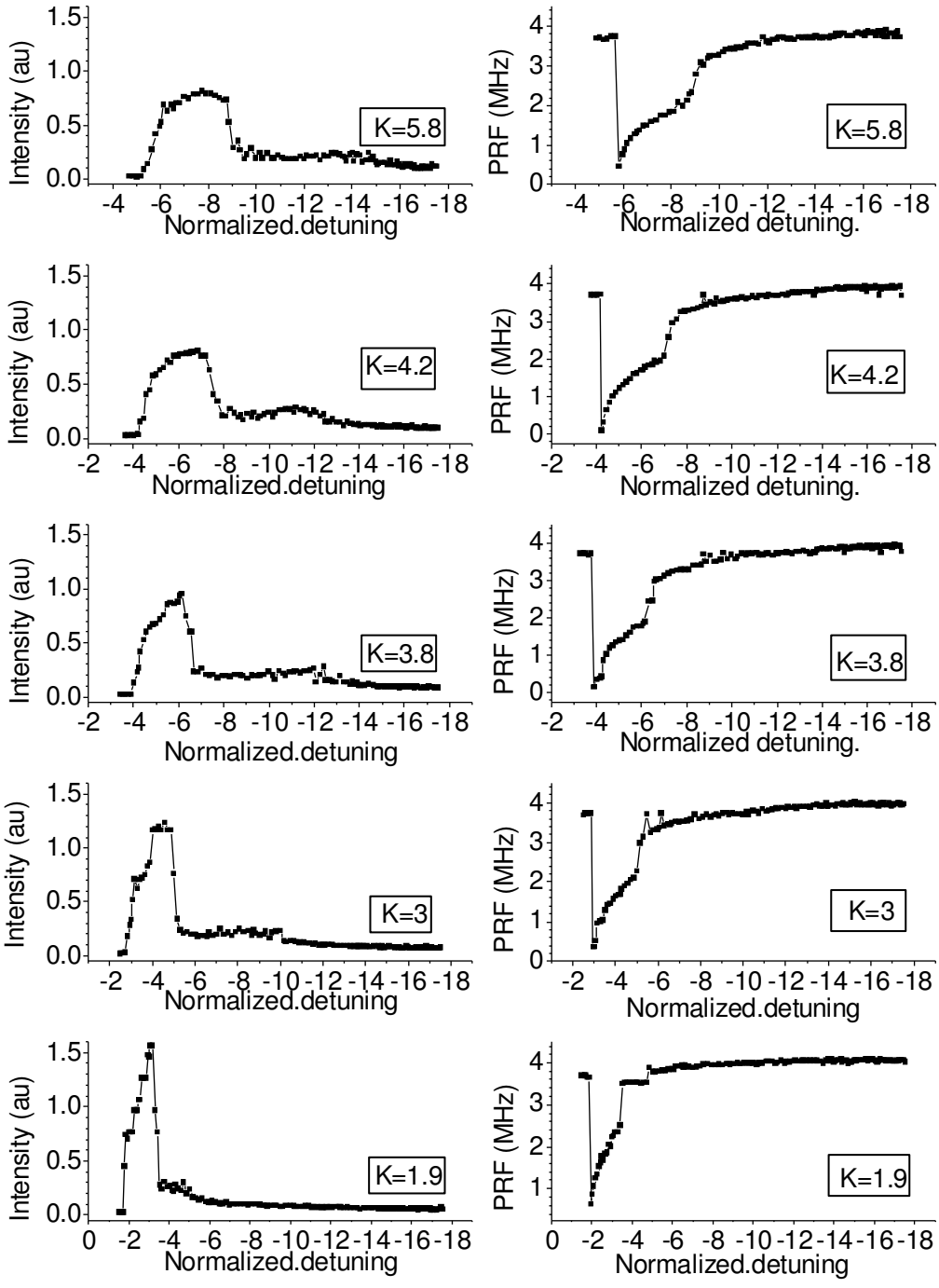

Figure 6.9. (a) The change in intensity by changing the detuning for different values of injection strength for the negative detuning. (b) *The change in PRF by changing the detuning for different values of injection strength for the negative detuning for the second range of K.*

6.5. Conclusion

An optically injected solid-state laser system has been used to generate pulses with a continuously variable pulse repetition frequency by adjusting the frequency detuning between the master and slave laser frequencies. The accessible range of pulse repetition frequency in this system is from approximately 200 kHz up to 7.5 MHz. The experimental curves (figure 6.5, 6.6, 6.7, 6.8, 6.9) reveal that the relation between PRF, intensity and the detuning is a piecewise function which means that different parts have different properties.

Two ranges of injection strength specified in Chapter 5, have been investigated in this study. The two ranges represent the regions on the dynamical map where the system is highly responsive to a change in the frequency detuning. The first range of the injection strength is between 0 and 0.65, can supply a continuous range of 200 kHz up to 7.5 MHz, using 3 piecewise stages shown in figure 6.5, using positive and negative detuning. The waveforms of the pulses in this range are investigated in chapter 5 and are indicated in this chapter.

For the second range of injection strength with injection strength values between 1.9 and 5.8, the attainable continuous range of PRF is between 200 kHz and 4 MHz, using 2 stages. This range possesses good features like the high intensity and the low rate of change. A suggestion to use the pulse intensity as a sensor for monitoring the PRF fluctuations is discussed briefly. More details on this suggestion are explained in chapter 8.

References

1. Kane, D. M., and J. P. Toomey. "Variable pulse repetition frequency output from an optically injected solid state laser." Optics express, vol. 19, no. 5, pp. 4692-4702, 2011.
2. Valling, Simo, Thomas Fordell, and Åsa Marie Lindberg. "Maps of the dynamics of an optically injected solid-state laser." Physical Review A, vol. 72, no. 3, pp. 033810 (1-7), 2005.

3. S. Pearce, and C. L. M. Ireland, “Performance of a CW pumped Nd:YVO4 amplifier with kHz pulses,” Opt. Laser Technol, vol. 35, no. 5, pp. 375–379, 2003.

Chapter 7

Assessing frequency instability of optically pumped $Nd:YVO_4$ and $Nd:GdVO_4$ lasers

7.1. Introduction

The accuracy of the laser optical frequency is very important in many applications, such as optical communications, frequency precision metrology and high resolution spectroscopy. In optically injected lasers the accuracy of the laser frequency is not merely important, but in fact critical: the concept of the operation of the system as a tuneable frequency pulse generator is based on the interaction between the injected and the injection laser. In other words, the optical frequency detuning between the two lasers in the system is an essential parameter to control the pulse repetition frequency of the system output. Methods of active frequency stabilization of the laser frequency are widely used. In optically injected system, these methods can be applied only to the injecting laser. It is not possible to use these techniques to the injected laser because stabilizing components could disturb or prevent the injection process. In addition to this reason, a compact system with few components is preferable in all applications, even when using stabilization techniques. These reasons provide motivation to study passive stabilization effects that are based mainly on maintaining the stability of the optical length of the laser resonator in order, to reduce the frequency instability of the laser.

In this chapter, two aspects are studied. First, the general characteristics of the optical frequency instability of the optically pumped solid state lasers that are used in OISSL. Second, a comparison is made between the frequency instability of optically injected $Nd:YVO_4$ and $Nd:GdVO_4$ lasers. The second is a promising crystal due to its superior thermal properties.

7.2. Frequency instability

Frequency instability, is the result of the random fluctuations in the period of an oscillating signal [1- 4]. A noisy signal of the laser field can be represented mathematically by

$$E(t) = [E_0 + \epsilon(t)]\, sin\, [2\pi\nu_0\, t + \varphi(t)] \tag{7.1}$$

Where E_0, is the peak amplitude, ϵ(t) represents the amplitude fluctuations, φ(t) represents the phase fluctuation or the deviation from the nominal (average) phase $2\pi\nu_0$. The instantaneous frequency $\nu(t)$ of this signal is defined as the instantaneous variation of the phase:

$$\nu(t) = \frac{1}{2\pi}\frac{d}{dt}(\text{Phase}) = \nu_0 + \frac{1}{2\pi}\frac{d}{dt}\varphi(t) \tag{7.2}$$

The second term in equation 7.2 represents the frequency noise of the field. The normalized frequency fluctuation (y (t)), can be described as the deviation $(\nu(t) - \nu_0)$ of the instantaneous frequency $\nu(t)$ from the nominal frequency, normalized to ν_0, that is,

$$\text{y(t)} = \frac{(\nu(t) - \nu_0)}{\nu_0} \tag{7.3}$$

$$\text{y(t)} = \frac{1}{2\pi\nu_0}\frac{d\ \varphi(t)}{dt} \tag{7.4}$$

Equations 7.3, 7.4 indicate that the fractional frequency fluctuation is directly related to phase fluctuations and they in fact describe the same phenomenon in different ways. Since we have random noise processes at play, we can study the characteristics of the fluctuations using various statistical tools such as spectral densities, correlation functions, standard deviations and variances. A normalized frequency, phase fluctuations are used instead of using it itself to compare the frequency, phase noise of any source with different mean frequencies.

7.3. Specifying the frequency instability of oscillating systems

Instability of oscillating systems such as electrical generators, clocks and lasers can be specified and measured in either the frequency domain or the time domain [3,5-9].

7.3.1. Frequency domain

In the frequency domain, frequency and phase instability can be defined and measured as follows [6]: the normalized frequency instability ($S_y(f)$) is the power spectral density (PSD) of normalized frequency fluctuations given as:

$$S_y(f) = \frac{(y_{rms}(f))^2}{BW} \quad (7.5)$$

Where $y_{rms}(f)$, is the measured root-mean-square value of the normalized frequency fluctuations in a specific band of frequencies, BW, containing frequency f ($0 < f < \infty$). BW is the bandwidth used in the measurement of y_{rms} in Hz. The unit of $S_y(f)$, is 1/Hz.

In the same way, normalized phase stability is characterized by the power spectral density of the normalized phase fluctuations,

$$S_\varphi(f) = \frac{(\varphi_{rms}(f))^2}{BW} \quad (7.6)$$

The unit of $S_\varphi(f)$, in rad²/Hz or 1/ Hz, φ_{rms} (f) is the rms value of φ in a Fourier frequency band. The normalized spectral densities of the phase ($S_\varphi(f)$) and the frequency ($S_y(f)$) fluctuations are related by the relation:

$$S_y(f) = \frac{f^2}{\nu_0^2} S_\varphi(f) \quad (7.7)$$

Practically the noise component of the laser radiation can be described by the power spectral density, using Wiener-Khinchin theorem which, state that the power spectral density ($S_y(f)$) can be computed by taking the Fourier transform of auto-correlation functions of the frequency fluctuations.

$$S_y(f) = 4\int_0^\infty R_y(\tau)\cos(2\pi f\tau)d\tau \quad (7.8)$$

where

$$R_y(\tau) = \langle y(t)y(t+\tau)\rangle \quad (7.9)$$

is the auto-correlation function, f is the Fourier frequency.

7.3.2. Time Domain

Working in the time domain can give the stability over a time interval τ for a given application (τ can range from less than milliseconds to months and even years depending on the application). Frequency stability can be measured by calculating the variance of the frequency fluctuations over a time interval τ. In many fields of measurements, instability can be estimated by taking the standard deviation of the data of these measurements. The standard deviation approach is applicable where the results are time independent (stationary data), but if the oscillator data contains time dependent noise (non-stationary data) contributed by a frequency offset, the standard deviation and the mean will not converge to an exact value. This means that there is a change in the standard deviation with each additional measurement, for that reason and in order to estimate the stability in time domain, nonclassical statistic is used. To measure the frequency instability in the time domain two sample deviation called Allan deviation $\sigma_y(\tau)$, which is the square root of Allan variance $\sigma_y^2(\tau)$, is introduced. This deviation is assumed that there is no dead time between average frequency samples (continuous measurements). The deviation for the averaging time τ is:

$$\sigma_y(\tau) = \left[\frac{1}{2}\langle[\overline{y_{k+1}} - \overline{y_k}]^2\rangle\right]^{1/2} \quad (7.10)$$

Where $\overline{y_k}$ Is the value of y(t), averaged over the integration time τ as given by

$$\overline{y_k} = \frac{1}{\tau}\int_{t_k}^{t_{k+1}} y(t)\,dt \quad (7.11)$$

Where $t_k = t_o + \tau k$, (k = 1, 2, 3,...). t_o, some time origin. In equation (7.10), the symbol $\langle\ \rangle$ Indicates the average from k =1 to k = ∞. In practice, and because only a finite number of fractional frequency samples can be produced, the Allan deviation is approximated by

$$\sigma_y(\tau) \cong \left[\frac{1}{2(M-1)}\sum_{k=1}^{M-1}(\overline{y_{k+1}} - \overline{y_k})^2\right]^{1/2} \quad (7.12)$$

where M represents the number of frequency measurements. Equation (7.12) can be expressed in terms of time domain data, by changing the averaging time of the data(τ) and computing the deviation each case. In this way, it is possible to study the strengths and the nature of the noise for any oscillator. Normalized Allan deviations are used instead of using the frequency deviations themselves to compare the frequency, phase noise of sources with different mean frequencies. In this way it is possible to compare, as an example, the normalized fluctuations for different emission wavelengths.

7.4. Power law models

7.4.1. The power law in the frequency domain

Theoretical studies and experimental measurements showed that the spectral density of all precision oscillators, due to the random noise, are the sum of five independent noise processes and may be modeled by the power law model such that

$$S_y(f) = \sum_{\alpha=-2}^{+2} h_\alpha f^\alpha \qquad (7.13)$$

for $0 \leq f \leq f_h$

where h, is a constant, α is an integer and represents the power law exponent, f_h is an upper cutoff frequency. The relation indicates that any oscillator may have several terms of noise sources but usually two or three.

7.4.2. The power law in time domain

The Allan variance can be modeled by sum of four different power laws

$$\sigma_y^2(\tau) = \sum_{\mu=-2}^{1} p_\mu \tau^\mu \quad , \quad \text{where } \mu = -\alpha - 1$$

$$= p_{-2}\tau^{-2} + p_{-1}\tau^{-1} + p_0\tau^0 + p_{+1}\tau^{+1} \qquad (7.14)$$

Figure 7.1, shows the most common noise types. The figure shows the relation between log Allan variance and log τ, where $\sigma_y(\tau) \propto \tau^{\mu/2}$.

In general, five noise types can recognize in the time (or frequency) noise graphs of different oscillating systems, depending on the kind of the system: white phase noise, flicker phase noise, white frequency noise, flicker frequency noise, and random walk frequency noise. The types of noise can be identified from the slope of Allan deviation

line. Identifying the noise types can help to reduce the noise by determining and treating the factors that affect on each of these noises [8, 10, 11].

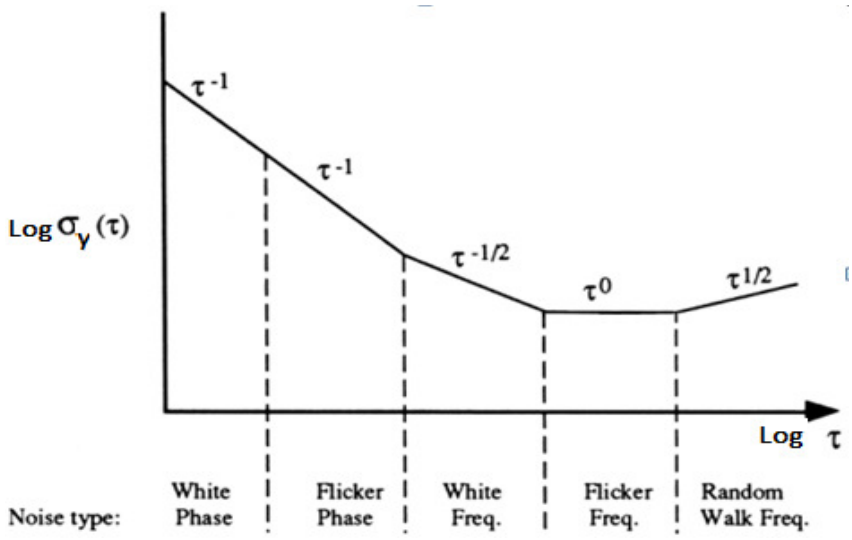

Figure 7.1. The relation between log Allan variance and log τ, where $\sigma_y(\tau) \sim \tau^{\mu/2}$, τ is measurement time interval ,showing a five common noise type. Note that Allan deviation does not distinguish between white phase noise and flicker phase noise. After [8]

Frequency noise can be studied also by measuring the linewidth of the laser, since the linewidth is the result of the phase fluctuations. The linewidth gives an idea of the total noise, but it will not provide full information about the relative magnitude of its phase instabilities because the linewidth depends on the measurement time and for full specification, more data is required [4]. However, measuring the linewidth is the efficient direct way to evaluate the high frequency noise.

7.5. Short-term, medium-term, and long-term instability

In general, the frequency instability is affected by systematic changes and by random noise processes. Systematic variations include periodic and monotonic variations. To study the phase and frequency instability in different devices and systems, the instability is divided into three regimes: short-term, medium-term and long-term instability. Short-term frequency instability refers to the random, non-systematic fluctuations that refer to the region dominated by white phase noise, where the time between observed frequencies (sample time) is less than 0.1 m second (depending on the system). Medium-term frequency instability refers to the region where flicker noise (1/f noise) dominates where the sample time is less than 1 second in general. These limits between terms are according to the experimental observations of the behaviour of the instability in each term. Although both short-term and medium-term frequency instability can be characterized either in the time domain or in the frequency domain, it is preferable to use frequency-domain measurements when the sample time of interest is less than a second. To characterize frequency instability for long sampling time, time-domain measurements are used. The third kind of frequency instability is long-term frequency instability (frequency drift) which includes random-walk frequency-noise processes and systematic changes in the frequency. The long term frequency instability is affected by external parameters such as temperature, humidity, pressure, magnetic field, in addition to the noise that refers to the change in the characteristics of the oscillator elements with the time. As an example, increasing the internal resistance of electric devices with the time, could cause changes in the output characteristics of the device [1, 8, 12]. Table 1 summarizes the information.

Instability term	Short-term instability	Medium-term instability	Long-term instability
Kind of fluctuations	Random, non-systematic fluctuations	Random and systematic fluctuations	Random and systematic fluctuations
Dominated by	White phase noise	Flicker noise	Random-walk frequency-noise processes and the systematic changes
Sample time	~Less than 0.1ms	~Less than a second	~More than a second
Preferable measurements	Frequency domain, linewidth	Time domain, frequency domain	Time domain

Table 7.1. Phase and frequency instability classification in different devices and systems

7.6. Frequency noise in lasers

In general, there are two main kinds of noise in lasers: firstly, inherent noise that includes the quantum noise which is related to the spontaneous emissions of the photons, and the effects of the resonator's factors. The second kind is the technical noise which depends on the ambient conditions, including different sources of noises, mechanical vibrations, pumping power fluctuations and temperature fluctuations. The first kind causes a high to moderate frequency noise (short-term to medium-term instability) while the second causes a low frequency noise (long term instability). In the absence of the technical noise sources (which are difficult to suppress) the quantum noise introduces an emission spectrum of Lorentzian shape. According to the modified Schawlow–Townes equation, for a single longitudinal mode [13-16]:

$$\Delta\nu_{laser} = \frac{2\pi h\nu\,(\Delta\nu_c)^2}{P_{out}} \tag{7.15}$$

where $\Delta\nu_c = (2\pi\tau_c)^{-1}$

In this relation, the theoretical minimum laser linewidth ($\Delta\nu_{laser}$) as a full width at half maximum (FWHM) is inversely proportional to the output power leaving the laser cavity (P_{out}) and proportional to the square of the empty resonator bandwidth ($\Delta\nu_c$). The resonator bandwidth is the full width at half maximum of the resonator's Lorentzian curve for the laseing frequency (ν), where τ_c is the photon lifetime in the resonator.

Random noise due to spontaneous radiation cannot be eliminated and can be considered as an inherent factor that limits the stability of laser frequency. As an example, the theoretical limits of the linewidth of a 5 mm, diode-pumped monolithic Nd: YAG laser at 1064 nm at an output power of 1mW is 1Hz. This linewidth is for empty resonator of $\Delta\nu_c$ =26 MHz. In practice, and due to the instability results from temperature fluctuations and mechanical vibrations, a typical linewidth of 10 kHz during 300 ms observation time, has been achieved [16].

In general, the frequency noise in lasers consists of three kinds of components. At low to moderate frequencies, random-walk ($1/f^2$ noise), flicker ($1/f$ noise) frequency components, while at high frequency, white frequency noise is dominated. Flicker noise depends strongly on the quality factor of the laser (Q factor) and is inversely proportional to Q^2. This proportionality is under ideal conditions. The dependence of flicker noise on the quality factor (Q) of the laser, under normal operation conditions, has been discussed in [28], in which the PSD of the frequency fluctuation is inversely proportional to Q^4.

It is worth mentioning that the contribution of each kind of noise is relatively different between different kinds of lasers. As an example, in solid state lasers, Experiments on Nd: YAG monolithic ring lasers showed the presence of $1/f$, $1/f^2$ components in addition to the white noise [17]. While In semiconductor lasers we can consider the white noise is the dominant frequency noise, which results in Lorentizian line shape, while the presence of the $1/f$, $1/f^2$ component does not perturb the spectral linewidth significantly.

7.7. Frequency instability factors

The laser oscillation frequency is influenced by two essential factors, the laser transition spectral frequency ν_A and the optical resonator resonance frequency ν_C. If the width of the atomic transition spectral line is $\Delta\nu_A$, and the width of the resonator spectral line is $\Delta\nu_C$, and considering that $\Delta\nu_A \gg \Delta\nu_C$, then, according to the relation established by Bennett, the laser resonance frequency can be expressed as [18,19,20]:

$$\nu \approx \nu_C + (\nu_A - \nu_C) \frac{\Delta\nu_C}{\Delta\nu_A} \tag{7.16}$$

This equation shows that the oscillation frequency of the laser depends on both the frequency of the atomic transition spectral lines and the resonance frequency of the resonator. Variations of these two factors induce instability of the laser frequency. The second term in equation (7.16) includes the effect of the spectral linewidth of the resonator and the atomic transition spectral line. The ratio $\frac{\Delta\nu_C}{\Delta\nu_A}$ is called the

frequency pulling factor which in general has a small value (typically, $\frac{\Delta\nu_C}{\Delta\nu_A} \approx 10^{-3}$ [20]). Regardless of the small value of the pulling factor, the resonance frequency of the resonator is very sensitive to the influence of the environment which means that the instability of the laser frequency is mainly depend on the cavity resonance frequency. The laser frequency is determined mainly by the resonator's resonant frequency, i.e,

$$\nu = \nu_C = q \frac{c}{2nL} \tag{7.17}$$

Where c is the light velocity, L is the cavity length, q is the ordinal number of the longitudinal modes and n is the refractive index of the cavity medium. The variation of the oscillation frequency is

$$\Delta\nu = -qc\left(\frac{\Delta L}{2nL^2} + \frac{\Delta n}{2Ln^2}\right) = -\nu\left(\frac{\Delta L}{L} + \frac{\Delta n}{n}\right) \tag{7.18}$$

or

$$\left|\frac{\Delta\nu}{\nu}\right| = \left|\frac{\Delta L}{L}\right| + \left|\frac{\Delta n}{n}\right| \tag{7.19}$$

The above equation shows that the problem of laser frequency instability can be considered as being how to keep the cavity length and the refractive index stable. Many factors lead to a variation of the optical cavity resonance frequency, in optically pumped solid state lasers the influence of temperature change is the most important.

7.8. Influence of temperature change on the frequency instability

The change in temperature due to the heating of the laser material during operation and the fluctuation of ambient temperature, can impact the instability of the laser frequency. The first contribution is caused by the temperature dependence of the refractive index. This factor can be estimated from the value of the thermo-optic coefficient (dn/dT), which is the temperature gradient of refractive index of the laser crystal material. The second contribution is the effect of the temperature on the resonator length. The fluctuation of ambient temperature or the heating of the laser

cavity can make the cavity material stretch or shrink due to the change in temperature and can cause a frequency shift, that is

$$\alpha_l \, \Delta T \; = \; \frac{\Delta L}{L} \propto \; \frac{\Delta \nu}{\nu} \qquad (7.20)$$

Where α_l, the linear expansion coefficient of the resonator material and ΔT is is the temperature variation. A resonator material with a small thermal expansion coefficient is thus clearly preferable to achieve a stable lasing frequency [18]. Equation 20 shows also that any change in the length will translate directly to a change in the frequency.

7.9. Properties of Nd:$GdVO_4$lasers

Recently, many publications have provided information on efficient, free-running, diode-pumped Nd:$GdVO_4$ performance [21, 22, 23]. The $GdVO_4$ crystal has several advantages over an YVO_4 crystal. In addition to a high absorption coefficient around the 808-nm band which can be realized from the absorption cross section values in table 2, Nd:$GdVO_4$ is a higher thermal conductivity, lower thermal expansion coefficient than Nd:YVO_4. The low thermal expansion coefficient is of special interest in the applications which need low instability level like OISSL [21,24]. Table 7.2 shows some of the physical and optical properties of Nd: YAG, Nd:YVO_4, and Nd:$GdVO_4$ laser crystals for different crystallographic directions.

Physical Characteristics	Nd:YAG	Nd:YVO_4	Nd:$GdVO_4$
Nd3+ concentration	1 at. %	1.1 at. %	1.2 at. %
σ_{abs} (10^{-19} cm2)	0.7 at 808 nm	2.3 at 810 nm	3.1–5.2($E//c$) at 808.5 nm
dn/dT (10^{-6} K^{-1})	7.3	[010]:8.5 [100]:8.5 [001]: 3	5.4 [ref.23] ----
Thermal expansion coefficient ($10^{-6}K^{-1}$)	[100]: 8.2 [010]:7.7 [001]: 7.8	[100]:4.43 [010]:4.43 [001]:11.37	1.5 (along *a*) 7.3 (along *c*)
Thermal conductivity (W ▪ m^{-1} ▪ K^{-1})	13 9.76	($E//c$) = 5.23 ($E \perp$c)= 5.10	[110]: 11.7 [001]: 12.3 [ref. 25]

Table 7.2. Physical and optical properties of Nd: YAG, Nd:YVO_4, and Nd:$GdVO_4$ laser crystals. (Data were taken from Ref. 24, except where indicated). Note: Nd: YAG has a cubic system where the lattice system consists of three different axes ($a \neq b \neq c$). For Nd:YVO_4 and Nd:$GdVO_4$, the crystals have tetragonal symmetry ($a = b \neq c$). E//c is where the electric field E is parallel to the optical axis c, E⊥c is for electric field E is perpendicular to the optical axis c. [hkℓ], Miller indices, where the lattice planes are determined by the three integers h, k, and ℓ. A typical crystal is oriented with pumping direction along an a-axis of the crystal where E//c.

7.10. Frequency instability using time domain measurements

7.10.1. Introduction

The experiments in chapters 5 showed that the OISSL does not have extremely strong requirements regarding the short-term frequency instability. As an example, a change in the normalised detuning around ± 0.01 in 1ms produced a pulse repetition frequency (PRF) change equal $\pm$ 0.025 MHz (chapter 5, figure 5.6), which is an acceptable level of change in many applications in the field of materials treatment. For this reason this thesis work will not seek to cover the short term frequency instability. The investigation focused on medium-term and long-term frequency instability of optically pumped Nd:YVO_4 and Nd:$GdVO_4$, working in the time domain as it can be used to study the frequency instability for both medium and long terms. In this study, Allan variance has been used to represent the frequency instability as a function of sampling time.

7.10.2. Frequency noise measurements using two-oscillator technique

As electronic instruments cannot display the variation of the high optical frequency, it is difficult to measure the instability of the laser directly. Heterodyne detection (the beat frequency method), is used as a relative measurement. An efficient way to measure the frequency fluctuation of a laser is by beating the laser output with a reference laser which is either a laser of low noise or, a laser with the a same design and same operation conditions [4, 9]. In this thesis work, beating occurs between the laser and another laser of similar design, as it is difficult to offer a laser with low noise with the same wavelength. Both lasers used in the heterodyne process were operated under as similar conditions as possible. In this way, the measurement yields the output noise from both lasers. With some approximation, it is possible to consider that the measured noise instability is twice that associated with one noisy laser [9].

In this method two beams of light waves from each of the lasers are non-linearly combined in a mixer commonly a photo-diode. In the non-linear detector the output power is proportional to the square of the input amplitudes. Consider two optical fields, $e_1(t)$ and $e_2(t)$ incident on a photodiode, where

$e_1(t) = E_1 \cos(\omega_1 t + \varphi_1)$, and $e_2(t) = E_2 \cos(\omega_2 t + \varphi_2)$, (7.22)

where E_1, ω_1, φ_1 And E_2, ω_2, φ_2 are the amplitude, the frequency and the phase of each of the two fields. The detected power

$$P(t) = (E_1 \cos(\omega_1 t + \varphi_1) + E_2 \cos(\omega_2 t + \varphi_2))^2 \quad (7.23)$$

The photo current generated in the detector is:

$$I(t) = R(E_1 \cos(\omega_1 t + \varphi_1) + E_2 \cos(\omega_2 t + \varphi_2))^2 \quad (7.24)$$

where R is constant for a certain detector

$$I(t) = R\ (\text{constant component} + \text{High frequency components} + (E_1E_2(\cos(\omega_2 - \omega_1) t + \varphi_3))) \quad (7.25)$$

The high frequency components and the time independent component can be filtered out, leaving the intermediate beat frequency component ($E_1E_2\cos((\omega_2-\omega_1) t + \varphi_3)$) to form a frequency signal that can be easily responded to a suitable frequency recording device or to a frequency spectral analyzer [4]. Since the beat component is sensitive to any change in the optical frequencies, it could be used as a monitor to observe the changes in these frequencies and to measure the frequency instability of the oscillators. The time domain measurements are used in this investigation to study the frequency instability characteristics for both $Nd:YVO_4$ and $Nd:GdVO_4$ lasers.

7.11. Instability characterization of Nd:YVO_4 and Nd:$GdVO_4$ lasers

7.11.1. Experimental set-up

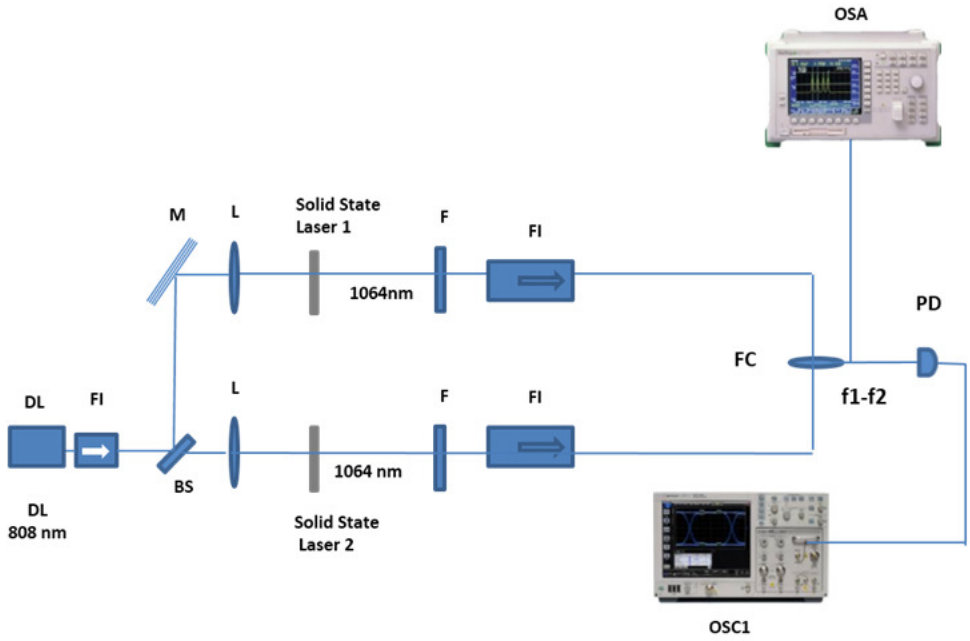

Figure 7.2. The experimental set-up showing the basic apparatus of Instability characterization experiment: DL, Diode laser. BS, beam splitter. F, filter. FI, Faraday isolator. L, lens. M, mirror. OSC, oscilloscope. OSA, Optical spectrum analyzer , PD detectors.FC, fibercoupler

The experimental arrangement for measuring the instability characteristics of the laser is shown in figure 7.2. The two monolithic solid state lasers (with performances explained in 7.9) are pumped by the same diode laser to reduce the effects of the pump power fluctuations. The two single mode output beams of the two solid state lasers are mixed by means of a fibercoupler and connected first to an optical spectrum analyzer (ANRITSU MS9001B1) to ensure that the beat frequency is within the frequency response range of the oscilloscope (6 GHz). In the second step, the beat frequency is detected by the photodetector (New Focus 1554-B--12GHz) which is connected to the oscilloscope (LeCroy Wave MASTER 8600A) to record and analyze the data. Faraday insulators (FI) are used to protect all the laser sources from any feedback effects that could disturb any of the lasers. In this experiment two kinds of solid state lasers are

tested. First, two monolithic Nd:YVO_4 single mode lasers, operated under as similar conditions as possible (same pumping and output power), are used as laser 1 and laser 2 in the diagram. In the second, two monolithic Nd:$GdVO_4$ lasers were used. To isolate the lasers as much as possible from surrounding temperature fluctuations, the lasers are covered by a plastic case. A thin indium foil is used to increase the thermal contact between the laser crystals and the crystal's mounts.

The frequency instability of the laser depends on the time interval considered. In order to characterize the medium and the long term frequency instability of the two kinds of lasers for a wide range of time intervals, two procedures are used to record and collect the data for each type of crystal:

1. In the first, and in order to study the long-term instability of the lasers, the fast Fourier transform (FFT) spectrum of the beat frequency is saved each 0.22 second in the oscilloscope using a sample rate 200MS/s and maximum sample point 1 MS. In this way, 700 values of the beat frequency are saved each 0.22 s to show the frequency fluctuation within approximately 150 seconds. This interval time represents the minimum data saving time of the oscilloscope. The change in the beat frequency for each time interval 0.22 s, for both crystals, is shown in figure 7.3 a, b. From these data it is possible to study the long-term instability of the lasers for sampling time from 0.22 s to 75 s.
2. In the second method and in order to study the Medium-term instability of the lasers, one intensity time trace is saved for both kinds of crystals with sample rate 200MS/s and maximum sample point 10 MS. The data was saved for 0.05 seconds divided into150 parts (60KS for each) and analyzed to find the FFT of the intensity time series for each 0.33 ms interval. Figure 7.5 a, b shows the results for time range less than 0.05 seconds for both crystals, giving the beat frequency each 0.33ms. In this part of the experiment, medium-term instability of the lasers is studied for sampling time from 0.33m s to 0.024 s. These measurements were used in order to assess the frequency instability, over a time intervals τ, that refers to the long and medium terms, to characterize instability for the two crystals, Nd:YVO_4 and Nd:$GdVO_4$.

7.11.2. Instability characterization graphs

In this thesis work, the frequency instability is studied, by computing Allan variance of the beat frequencies as a function of sampling time. As shown in figures 7.4 and 7.6 Allan variance has been found from equation 12 using the data obtained experimentally, as a function of the time intervals (τ) by calculating $\overline{Y_i}$, the average value of the peak frequency (section 7.3.2), over the time interval τ for all data shown in figure 7.3, 7.5. Time intervals from 0.22 s to 75 s and from 0.33 ms to 0.024 s are covered. Figure 7.4 represents the normalized root Allan variance (σ) versus τ using a logarithmic scale, for sampling time from 0.22 s to 75 s, (a) for optically pumped Nd:YVO_4 laser and (b) for optically pumped Nd:$GdVO_4$ laser. Figure 7.6 shows the normalized root Allan variance versus τ using a logarithmic scale for sampling time from 0.33 ms to 0.024 s (a) for optically pumped Nd:YVO_4 laser and (b) for optically pumped Nd:$GdVO_4$ laser. Although there is a small gap of the time interval τ between figures 7.4 and 7.6 that is not covered in this study, the graphs can give a good idea of the frequency instability specifications of the two kinds of lasers. The maximum interval time is half the recorded time because calculating Allan variance needs at least two samples of data.

By comparing the results with figure 7.1. The two basic kinds of noise, the systematic frequency noise and the power-law noise can be distinguished clearly in figures 7.4 and 7.6 which represent normalized root Allan variance versus sampling time in logarithmic scale (normalized σ – τ plot) for both Nd:YVO_4 and Nd:$GdVO_4$ lasers respectively.The systematic noise can be recognized as a sharp drop or a trough in the instability diagrams. Figures 7.4 and 7.6 show many kinds of systematic noise with different response of the two monolithic lasers. In the range of τ from 0.22 s to 75 s, figures 7.3 a, b and 7.4 a, b show a systematic noise at sampling time equal 1 second. This noise could be related to the speed at which the temperature controller works, since the fastest response of this device is 1 second [27]. Another systematic noise appears in figure 7.4, a in normalized σ - τ plot of Nd:YVO_4 at sampling time 10s. The source of this noise is unknown. For the sampling time from 0.33 ms to 0.024 s in figures 7. 5 a, b and figure 7. 6 a, b, a systematic noise appears around 2 $x10^{-2}$ s, the noise is due to electric noise of 50 Hz and the harmonics.

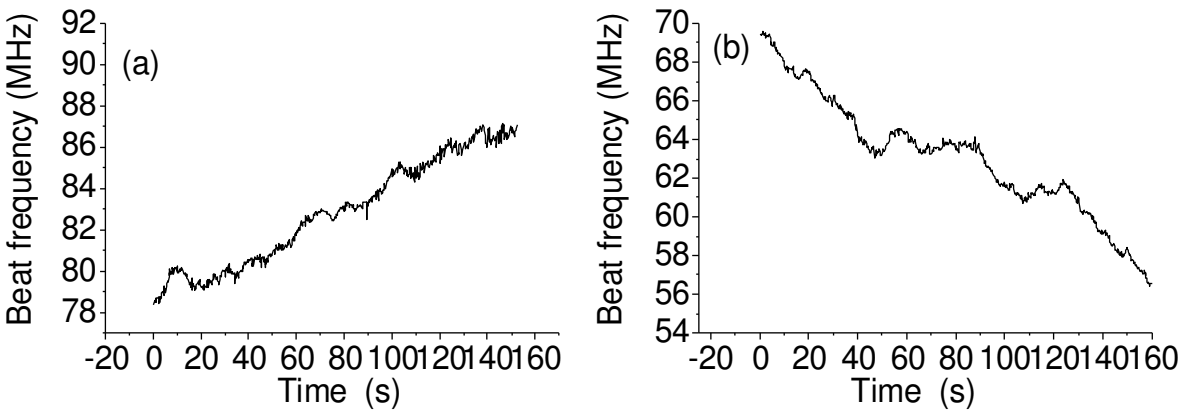

Figure 7.3. The change in beat frequency with time for

(a) Nd:YVO_4 . (b) Nd: $GdVO_4$.

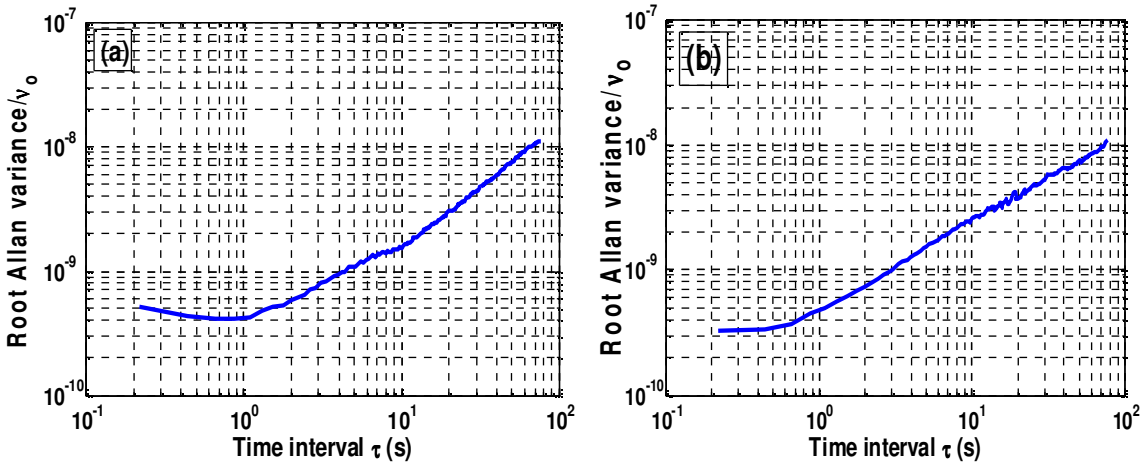

Figure 7.4. Normalized root Allan variance versus sampling time from 0.22s to 75 s. The measured instability is the contribution of two lasers, the real value is; normalized root Allan variance divided by 2.

(a) For Nd:YVO_4 . (b) For Nd: $GdVO_4$.

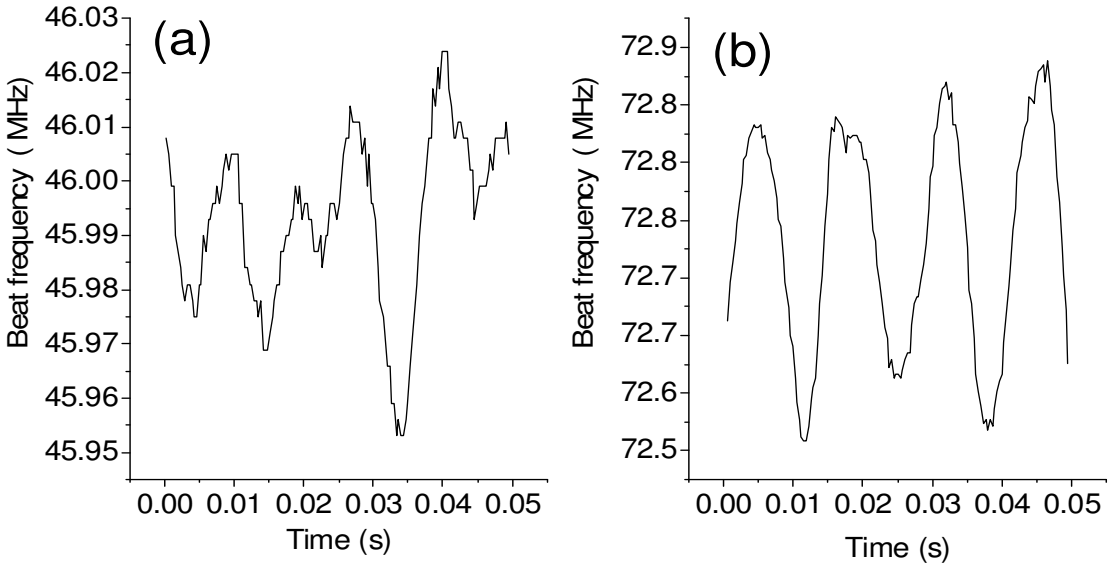

Figure 7.5. The change in beat frequency with time for

(a) $Nd:YVO_4$. *(b) Nd: $GdVO_4$.*

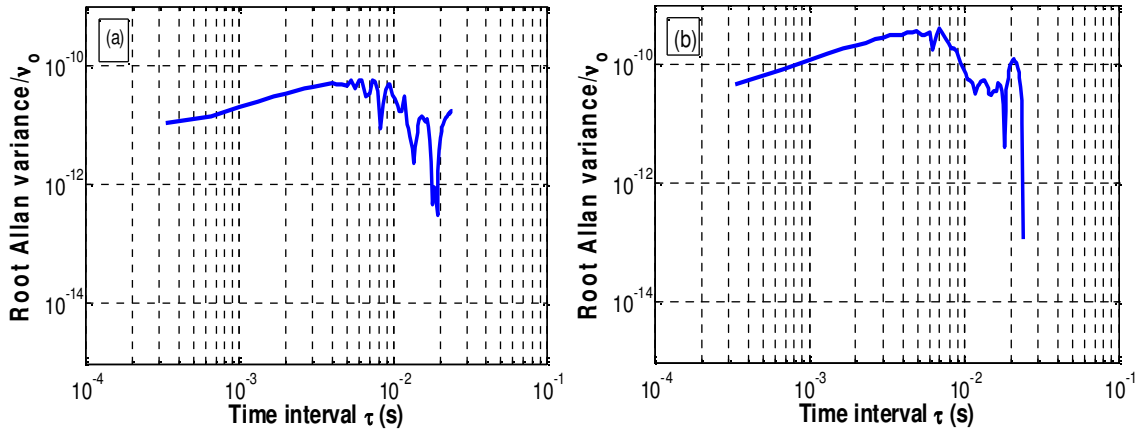

Figure 7.6. Normalized root Allan variance versus sampling time from 0.33ms to 0.024s. The measured instability is the contribution of two lasers ,the real value is; normalized root Allan variance divided by 2.

(a) For $Nd:YVO_4$. *(b) For Nd: $GdVO_4$.*

The power-law noise for both crystals shows two stages of the frequency instability that obey equation 7.14 to a large extent. This can be appreciated by comparing figures 7.4 a, b and 7.6 a, b with figure 7.1. In figures 7.6, if we ignore the effect of the systematic noise appears at 2 $x10^{-2}$ s, an instability caused by flicker noise ($\sigma \propto \tau^{o}$) dominates. In figures 7.4, flicker noise continues until the time interval 1 s. This kind of instability is due to inherent noise that related to the quality factor of the lasers and it is hard to eliminate [28]. It is worth mentioning that the instability due to flicker noise sets the lower limit of instability of any oscillator demonstrates [28, 29]. In general, the minimum measured normalized root Allan variance for the free running $Nd:YVO_4$ laser in the medium term, is 0.5 $x10^{-11}$, and for $Nd:GdVO_4$ laser is 1.5x 10^{-11}, which is approximately the same range of instability of free running optically pumped Nd:YAG ring laser showed in many references [30,31].

In the second stage, for τ more than 1 second, a random-walk frequency-noise dominates where normalized root Allan variance is proportional to $\tau^{1/2}$ ($\sigma \propto \tau^{1/2}$). This noise is mostly due to the temperature fluctuations of the environment and due to insufficient temperature controlling. In this stage, the high thermal conductivity which means higher tendency to dispose the heat and the low Thermal expansion coefficient could play a role in reducing the instability of the laser.

The behaviour of the two optically pumped $Nd:YVO_4$ and $Nd:GdVO_4$ are similar. However, it is expected that the two kinds of crystals have the same instability level in the flicker region due to the similar quality factor of the two kinds of lasers. In the range where random-walk frequency-noise prevails, the high thermal conductivity and the lower linear expansion coefficient of the resonator material of $Nd:GdVO_4$ laser produce approximately the same level of normalized root Allan variance as for $Nd:YVO_4$. The better thermal properties of $Nd:GdVO_4$ laser show effects on the instability behaviour of the crystal that belongs to the systematic noise. A fluctuation at sampling time less than 1 ms shown in figure 7.5a as a trough in the instability curve, is removed in figure 7.5b by using $Nd:GdVO_4$. In similar way, the systematic noise in figure 7.3 a, 7.4 a at a time interval equal 1 s which reduced in figures 7.3b, 7.4b. The results reveal that the good thermal properties have the effect to reduce some of the systematic frequency fluctuations.

The mechanical vibrations, are not considered in this study because optically pumped monolithic lasers are considered to be very stable mechanically, due to the monolithic oscillators and due to the conduction cooling that eliminate the mechanical vibrations [32].

7.12. Conclusions

An evaluation has been made of the frequency noise in free running optically pumped solid state lasers. The investigation included optically pumped Nd:YVO_4 lasers and Nd:$GdVO_4$ lasers. Despite the good thermal properties of these two lasers in general and the Nd:$GdVO_4$ in particular, the two lasers showed a level of frequency instability comparable with other optically pumped solid state lasers.

The study revealed the existence of many kinds of systematic noise, which appears as or troughs in the frequency instability curves which are mostly related to the temperature controlling system. The random-walk frequency-noise which cause high normalized root Allan variance in the related time intervals can be reduced with efficient temperature controlling for the system as a whole. The results presented in this chapter show that the stability requirements for optically injected solid state laser application can be set passively (without using frequency stabilization method), with some efforts to eliminate or reduce the sources of the noise which cause a high frequency instability level. The frequency instability can be reduced in different ways. In this regards,

- Eliminate different sources of systematic noise with the suitable treatment of every kind. Using Nd:$GdVO_4$ laser has proven to help in satisfying this purpose by reducing some of the systematic noise.
- Improve the temperature controlling system to reduce the fluctuation of ambient temperature and the heating of the laser cavity can reduce random-walk frequency-noise.
- Furthermore, optimizing quality factor can reduce the flicker noise for a large degree, since the instability is inversely proportional to Q^2 in general. This is can be done by increasing the resonator length (L) but on the other hand, long resonator means high random walk noise. In this respect, a compromise can be made to design best laser with best frequency instability.

To summarize, the investigation shows that many aspects, particularly that which related to the thermal stabilization of the system still require improvement. Suggestions to refine the frequency instability with more details are explained in chapter 8.

References

1. F. Pikal, Eva S., and F. L. Walls, "Frequency Standards, Characterization." Encyclopedia of RF and Microwave Engineering, 1999.
2. Linder, Bruno. "Basic Concepts and Definitions." Thermodynamics and Introductory Statistical Mechanics: 5-13.
3. Paschotta, Rüdiger. "Noise in Laser Technology." Optik & Photonik. Vol. 4, no. 2, pp. 48-50, 2009.
4. Paschotta, Rüdiger. Encyclopedia of laser physics and technology. Berlin: Wiley-VCH, Vol. 1, 2008.
5. P.P.Bohn, The relationship between phase stability and frequency stability and a method of converting between them, NASA contributor, 1971.
6. IEEE Standard Definitions of Physical Quantities for Fundamental Frequency and Time Metrology Random Instabilities, IEEE Standards Coordinating Committee 27, Sponsored by three Standards Coordinating Committee 27 on Time and Frequency, IEEE Std 1139™, 2008.
7. Rutman, Jacques, and F. L. Walls. "Characterization of frequency stability in precision frequency sources." Proceedings of the IEEE, vol. 79, no. 7, pp. 952-960, 1991.
8. Riley, William J. Handbook of frequency stability analysis. US Department of Commerce, National Institute of Standards and Technology, 2008.
9. Lance, Algie L., Wendell D. Seal, and Frederik Labaar. "Phase noise and AM noise measurements in the frequency domain." Infrared and millimeter waves, vol. 11, pp. 239- 289, 1984
10. Riley, W. J. "The basics of frequency stability analysis." Hamilton Technical Services (2004).
11. Lombard, Michael A. "Fundamentals of time and frequency." The Mechatronics Handbook, volume 2, 2006.

12. International Radio Consultative Committee. Recommendations and Reports of the CCIR, Report 580, PP. 142-150,1986
13. Yariv, Amnon. "Optical Electronics" Rinehart and Winston, New York, PP. 354, 1985.
14. Yamamoto, Y., T. Mukai, and S. Saito. "Quantum phase noise and linewidth of a semiconductor laser." Electronics Letters, vol. 17, no. 9, pp. 327-329, 1981.
15. Schawlow, Arthur L., and Charles H. Townes. "Infrared and optical masers." Physical Review, vol. 112, no. 6, pp 1940-1949, 1958.
16. Koechner, Walter, and Michael Bass. Solid-state Lasers: A Graduate Text. Springer, 2003.
17. Ullrich, Andreas G. "Determination of the instantaneous linewidth of a monolithic Nd: YAG laser from RIN measurements." Photonics Technology Letters, IEEE , vol 3, no. 4, pp. 318-319, 1991.
18. Bennett Jr, W. R. "The physics of gas lasers." NASA STI/Recon Technical Report A, vol. 78, 1977.
19. Xinju, Lan. Laser technology. CRC Press, 2011.
20. Bennett Jr, W. R. "Hole burning effects in a He-Ne optical maser." Physical Review, vol 126, no. 2, pp. 580-594, 1962.
21. Kalisky, Yehoshua Y. The physics and engineering of solid state lasers. Vol. 71. SPIE Press, 2006.
22. Li, M., S. Zhao, K. Yang, G. Li, D. Li, and J. An. "Diode-pumped actively Q-switching and mode-locking Nd: GdVO4 laser." Laser Physics Letters, vol 5, no. 10, pp. 722-725, 2008.
23. He, J. L., J. Du, J. Sun, S. Liu, Y. X. Fan, H. T. Wang, L. H. Zhang, and Y. Hang. "High efficiency single-and dual-wavelength Nd: GdVO4 lasers pumped by a fiber-coupled diode." Applied Physics B, vol 79, no. 3, pp. 301-304, 2004.
24. Zhang, Huaijin, Xianlin Meng, Li Zhu, and Zhaohe Yang. "Growth and thermal properties of Nd: $GdVO_4$ single crystal." Materials research bulletin, vol. 34, no. 10, pp.1589-1593, 1999.
25. Zagumennyi, Alexander I., Yury D. Zavartsev, Pavel A. Studenikin, Ivan A. Shcherbakov, Alexander F. Umyskov, Pavel A. Popov, and Vsevolod B. Ufimtsev. "GdVO4 crystals with Nd3+, Tm3+, Ho3+, and Er3+ ions for diode-pumped microchip laser." In Photonics West. International Society for Optics and Photonics, vol 96, pp. 182-192, 1996.

26. Didierjean, Julien, Emilie Herault, Franšois Balembois, and Patrick Georges. "Thermal conductivity measurements of laser crystals by infrared thermography. Application to Nd: doped crystals." Optics express, vol.16, no. 12, pp. 8995-9010, 2008.
27. USER'S Guide, Precision Thermoelectric Temperature Conroller, ILX LIGHTWAVE,LDT-5412, www.ilxlightwave.com
28. Sayeh, M. R., and H. R. Bilger. "Flicker noise in frequency fluctuations of lasers." Physical review letters, vol. 55, no. 7, pp.700-702, 1985.
29. Uehara, Noboru, and Ken-ichi Ueda. "Frequency stabilization of two diode-pumped Nd: YAG lasers locked to two Fabry-Perot cavities." Japanese Journal of Applied Physics part 1, vol. 33, pp.1628-1628, 1994.
30. Patrick, H., and C. E. Wieman. "Frequency stabilization of a diode laser using simultaneous optical feedback from a diffraction grating and a narrowband Fabry–Perot cavity." Review of scientific instruments, vol. 62, no. 11. pp. 2593-2595, 1991.
31. Arie, Ady, Stephan Schiller, Eric K. Gustafson, and Robert L. Byer. "Absolute frequency stabilization of diode-laser-pumped Nd: YAG lasers to hyperfine transitions in molecular iodine." Optics letters, vol.17, no. 17, pp.1204-1206, 1992.
32. Koechner, Walter. "Solid-state laser engineering". vol. 1. Springer Science, 2006.

Chapter 8

Summary and future work

8.1. Summary

This thesis describes an experimental demonstration of the possibility of using an optically injected solid state-laser to generate optical pulses with a continuous range of pulse repetition frequency. Changing the pulse repetition frequency (PRF) is one of the effective ways of controlling the energy provision rate in various material processing applications. The thesis investigates the capabilities and challenges of this approach in generating pulses.

Chapter 2, presents the optically injected $Nd:YVO_4$ solid state laser studies, while Chapter 3 includes an explanation of the rate equations for the optically injected solid-state laser and the various parameters. The second part describes the diode end-pumped $Nd:YVO_4$ laser and shows the basic requirements of an optically injected solid-state laser system as an optical pulse generator.

The construction of an optically injected solid-state laser system using an optically pumped $Nd:YVO_4$ solid-state lasers is explained in Chapter 4. In addition, a practical method for controlling the frequency detuning between the master and slave lasers, and the injection strength of the injection beam using an acousto-optic modulator (AOM) is explained in detail. Many issues relating to the experimental setup are discussed, such as achieving single mode operation and the effect of pump beam alignment on the optically injected solid-state laser system. The thesis also includes details of the two methods used to quantify the injection strength.

The characteristics of the dynamics of four regions on the dynamical map of the optically injected solid state laser are investigated in Chapter 5. The regions are:

- Period-doubling regime pulses.
- Spiky regime pulses.
- Quasi-periodic regime close to the saddle-node (SN) curve.
- Quasi-periodic regime close to the torus (T)curve.

An experimental demonstration of the behaviour of the dynamics at specific points relating to each of the regions mentioned above is introduced using a direct analysis of real-time traces.

In terms of response of the PRF to the detuning, the results show a high level of response to the changes in detuning for the period-doubling regime (P2, P3) and for the limit cycle regime (P1) in both the positive and the negative detuning regions. Although the limit cycle regime shows a low intensity compared to the period-doubling regime, operating the regime without noise encourages its use as a source of regular pulses in addition to P2 and P3. In this way the PRFs of the two regimes complement each other.

In the spiky region, a kind of bistability is demonstrated between the quasi-periodic and the spiky waveforms which allows the two dynamics to oscillate for the same value of injection parameters. However, this dynamics which has the highest intensity of all the dynamics in this system, showed a very low correlation between the PRF and the detuning and therefore, cannot not be used to generate pulses with a variable PRF. The difference between the frequency values of quasi-periodic and spiky waveforms (f_2-f_1) is used as an indicator to specify the value of the injection strength where the fluctuation between the two waveforms is eliminated, and the rest region can be used to generate pulses. The results show that the frequency difference between the two waveforms drops rapidly to a low value at an injection strength of approximately 2.8 and drops slowly after this value. This means the possibility of using this region with the highest injection strength value to generate regular pulses.

Different correlation coefficients for the PRF and detuning were obtained in the quasi-periodic regime of the region close to the SN and T curves. In general the carrier frequency shows a high correlation, while the envelope frequency shows a lower correlation. In the case of low injection strength, a high level of correlation is seen in the regions close to the SN and T curves. For high injection strength, the correlation coefficient shows low values in the regions close to the SN curve while the correlation coefficient of both frequencies drops very fast with increasing K in the region close to the torus curve. The regions in the (K, $\Delta\omega$) - plane that showed a positive response to the change in detuning are defined in this chapter.

By adjusting the frequency detuning between the free running frequencies of the master and slave laser, an optically injected Nd:YVO_4 solid state laser is used to generate pulses with a continuously variable pulse repetition frequency. The accessible range of pulse repetition frequency in this system is from approximately 200 kHz up to 7.5 MHz. The experimental curves reveal that the relationship between PRF, intensity and detuning is a piecewise function which means that different parts have different properties.

Two ranges of injection strength which have been specified in Chapter 5, are investigated in this chapter. The two ranges represent the regions on the dynamical map where the system is highly response to the change of the frequency detuning. The first range of the injection strength is between 0 and 0.65, and can supply a continuous range of pulse repetition frequency of 200 kHz up to 7.5 MHz, using positive and negative detuning. In the second range, with injection strength values between 1.9 and 5.8, the attainable continuous range of PRF is between 200 kHz and 4 MHz, using 2 stages. This range possesses good features like the high intensity and the low rate of change.

Chapter 7 looks at the optical frequency instability as a function of measurement time, for Nd:YVO_4 and for Nd: $GdVO_4$ by computing the Allan variance of the beat frequency. A normalised root Allan variance versus sampling time from 0.22 s to 75 s and from 0.33 ms to 0.024 s was found for both Nd:YVO_4 and for Nd: $GdVO_4$. These two sampling times represent medium-term and long-term frequency instability. The instability plots are usually a combination of two basic kinds of frequency noise: systematic noise and the power-law noise. The two lasers show a normal level of frequency instability compared to other kinds of optically pumped solid-state lasers despite the good thermal properties of these two lasers in general and the optically pumped Nd:$GdVO_4$ in particular. The study reveals the existence of many kinds of systematic noise mostly relating to the temperature controlling device.

8.2 Future work

The development of this approach to generate optical pulses can be achieved in three aspects:

- By extending the upper limit of pulse repetition frequency to higher frequencies.
- By increasing the average power of the Nd:YVO4 OISSL system.
- By stabilising the output characteristics of the system, including intensity and pulse repetition frequency.

In this regard, the priority should be to stabilise the system, since the offset between the optical frequency of the master and slave laser is a main parameter for determining the output of the optically injected solid state laser system. The investigation in Chapter 7 addresses many types of a systematic and power-law noise that affect on the performance of the system. Investigating the source of each systematic noise and treating it in the suitable way can improve the medium-term and long-term instability. Long term power-law noise (random-walk frequency noise) which is related to the temperature fluctuations of the crystal, can be improved by using a high resolution temperature controller and by refining the thermal conditioning of the solid-state laser as a whole. Medium-term power-law noise (1/f noise) depends strongly on the quality-factor of the solid-state laser ($\propto \frac{1}{Q^2} to \frac{1}{Q^4}$). This noise can be reduced to a large extent by increasing the cavity length of the laser. However, this is not possible with the system used due to the increase of the number of the oscillating longitudinal modes with increasing the cavity length. In addition to increase the random walk noise for the same reason.

A significant improvements in frequency stability and laser efficiency can be achieved by means of the following suggestions:

- Using direct pumping at 880 nm instead of 809 nm can reduce the energy difference between a pump photon and a laser photon. Exciting the ion from the ground state directly to the upper lasing level without relaxation process can reduce this difference. Pumping sources like Ti^{+3}: sapphire or diode laser can be used for this purpose. This method can reduce heat generation by 40% compared with

traditional pumping at 808 nm [1,2]. Laser efficiency can also be improved to 70% by increasing the doping concentration of the laser material.

- Most laser diodes have an output beam with an elliptical cross section. Reducing the ellipticity of the pumping beam has great benefits in terms of increasing laser efficiency and reducing the laser threshold [3]. Increasing laser efficiency and reducing the laser threshold mean increasing the relaxation oscillation frequency and consequently, extending the upper limit of pulse repetition frequency. Many methods can be used to convert the diode elliptical output to a circular beam. Figure 8.1 illustrates the laser diode spot of the diode laser used in the experiments explained in this thesis, before and after using an anamorphic prism pair. The figure shows also a reducing in the number of the transverse modes (the red spots) which is an additional benefit. The power loss caused by such an optical system is about 40% therefore the prism pair is not used in the experiments in this work.

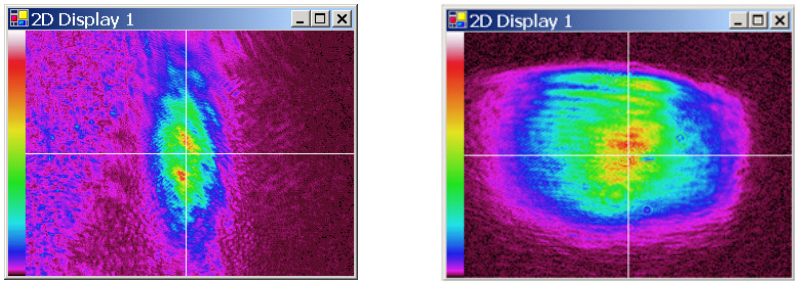

(a) (b)

Figure 8.1. Shows the photo of the laser diode spot before (a) and after (b) using anamorphic prism pair.

A new technique using a micro-cylindrical lens can be applied to circularise the laser beam with a power loss, of approximately 20%, using this technique can offer great benefits [4].

- The correlation between the PRF and the intensity of the system output can be used to stabilize the PRF of the system by using the intensity as a sensor for the PRF fluctuations. In this case a suitable comparative circuit could be used to modify the temperature of the laser crystal.

References

1. Ding, Xin, Rui Wang, Heng Zhang, Xuan-Yi Yu, Wu-Qi Wen, Peng Wang, and Jian-Quan Yao. "High-efficiency Nd: YVO_4 laser emission under direct pumping at 880nm." Optics Communications,vol. 282, no. 5, pp. 981-984, 2009.
2. Lavi, R., Y. Tzuk, S. Jackel, E. Lebiush, I. Paiss, and M. Apter. "High-Efficiency 880nm Diode Direct-Pumping of Nd: YVO_4 Grazing Incidence Oscillators." In CLEO/Europe'00 Conference. 2000.
3. Laporta, Paolo, and Marcello Brussard. "Design criteria for mode size optimization in diode-pumped solid-state lasers." IEEE Journal of Quantum Electronics, vol. 27, no. 10, pp. 2319-2326, 1991.
4. LASER DIODE TECHNICAL NOTE 1, Beam Circularization and Astigmatism-correction. http://www.coherent.com/downloads/LaserDiodeTechNote1

Appendix (A)

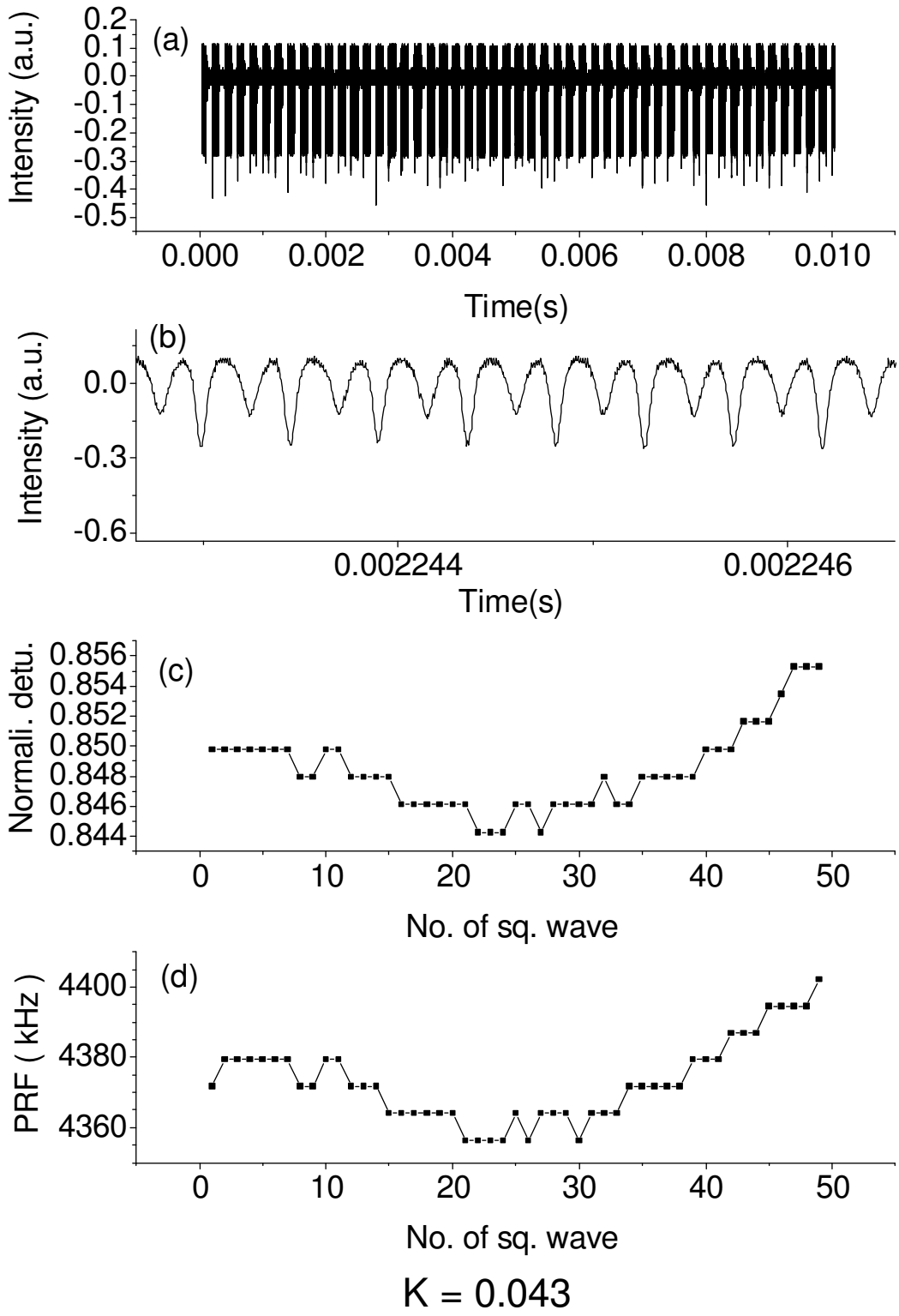

Figure A1. (a) The intensity level for 50 squares of pulses; (b) pulses waveform; (c) the change in frequency detuning in 10ms; (d) the change in PRF in 10ms. (The relations for the injection parameters K=0.043, Δω=- 0.85).

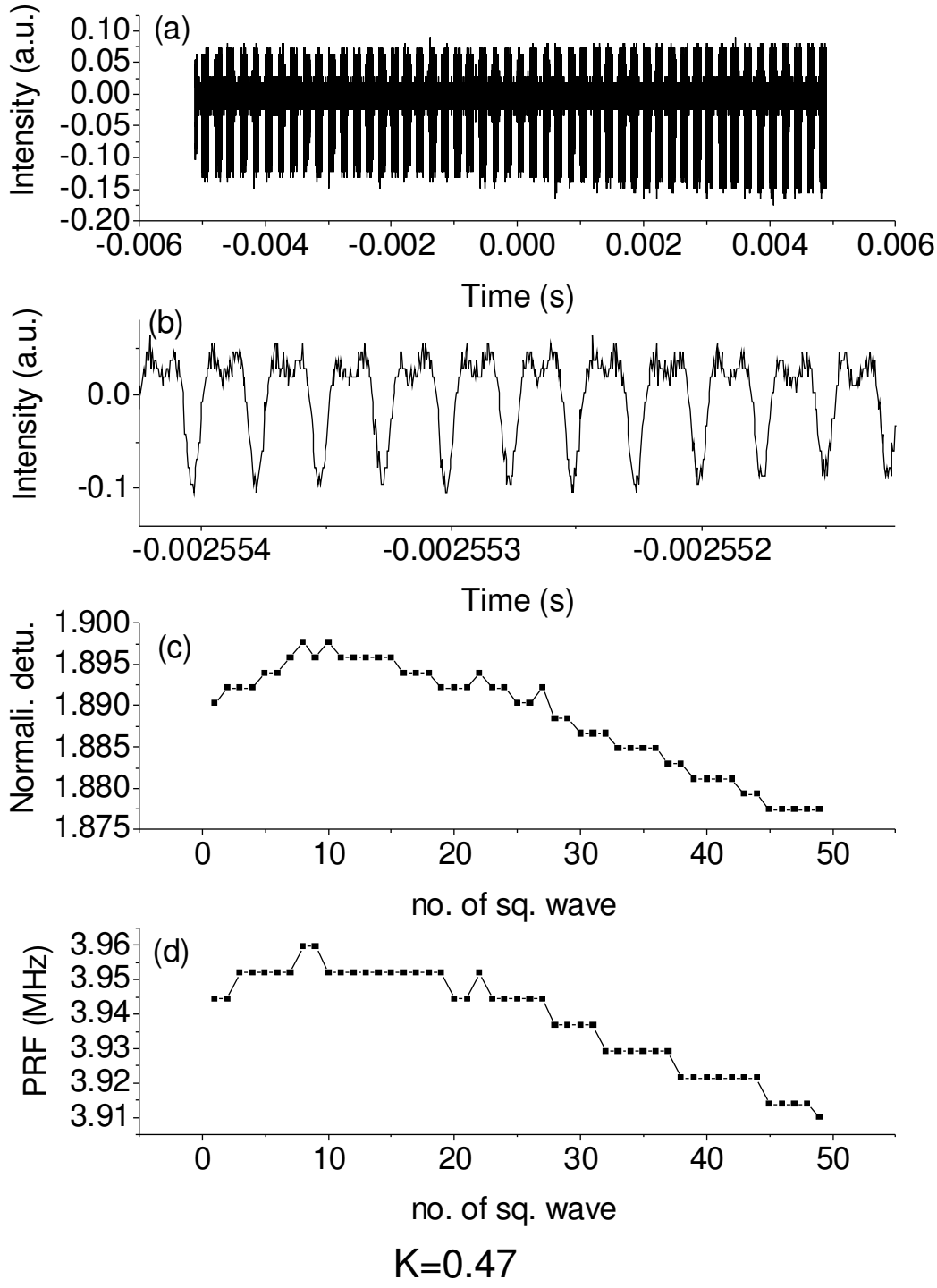

Figure A2. (a) The intensity level for 50 squares of pulses; (b) pulses waveform; (c) the change in frequency detuning in 10ms; (d) the change in PRF in 10ms. (The relations for the injection parameters K=0.47, Δω=- 1.89).

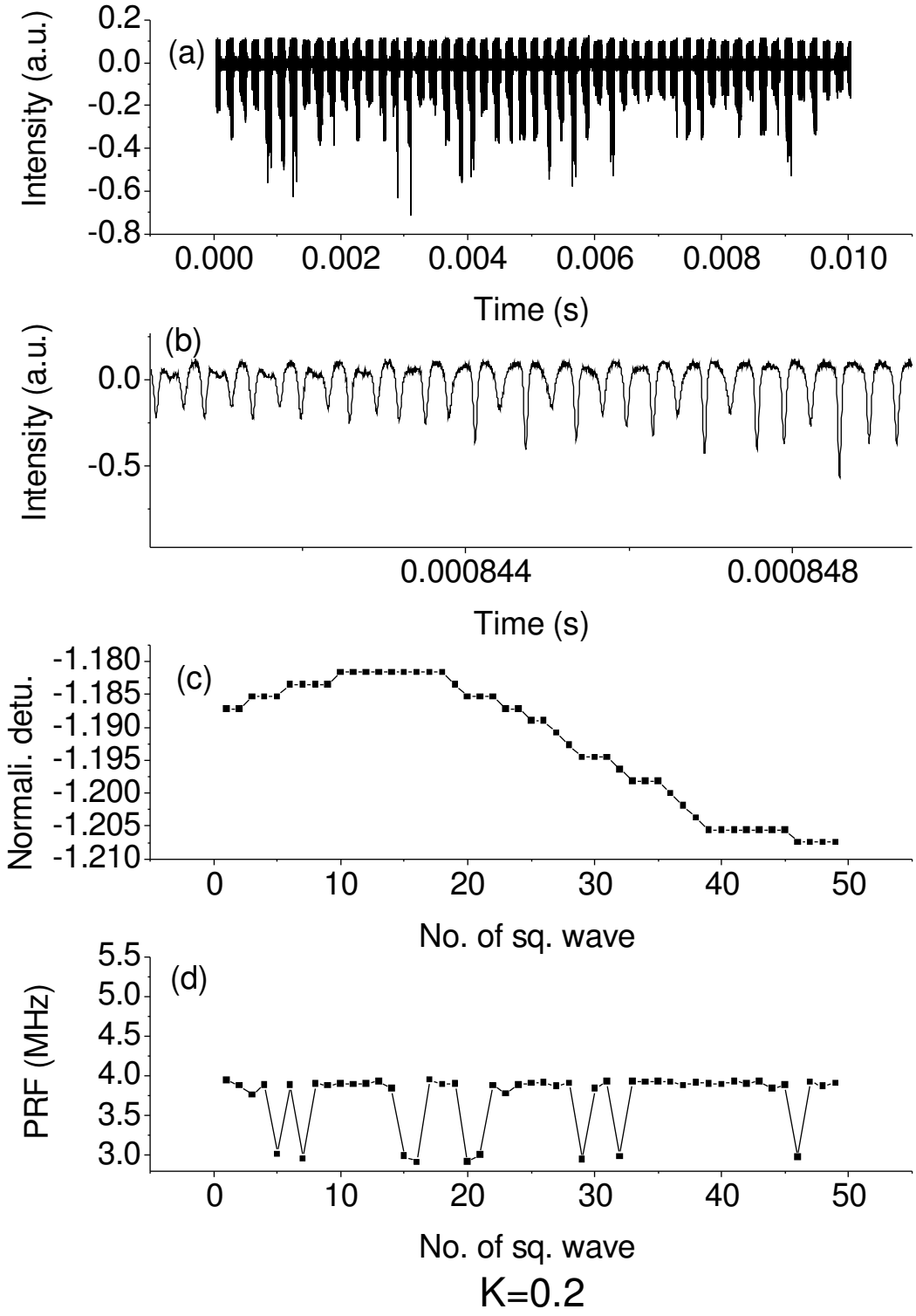

Figure A3. (a) The intensity level for 50 squares of pulses; (b) pulses waveform; (c) the change in frequency detuning in 10ms; (d) the change in PRF in 10ms. (The relations for the injection parameters K=0.2, Δω=- 1.19).

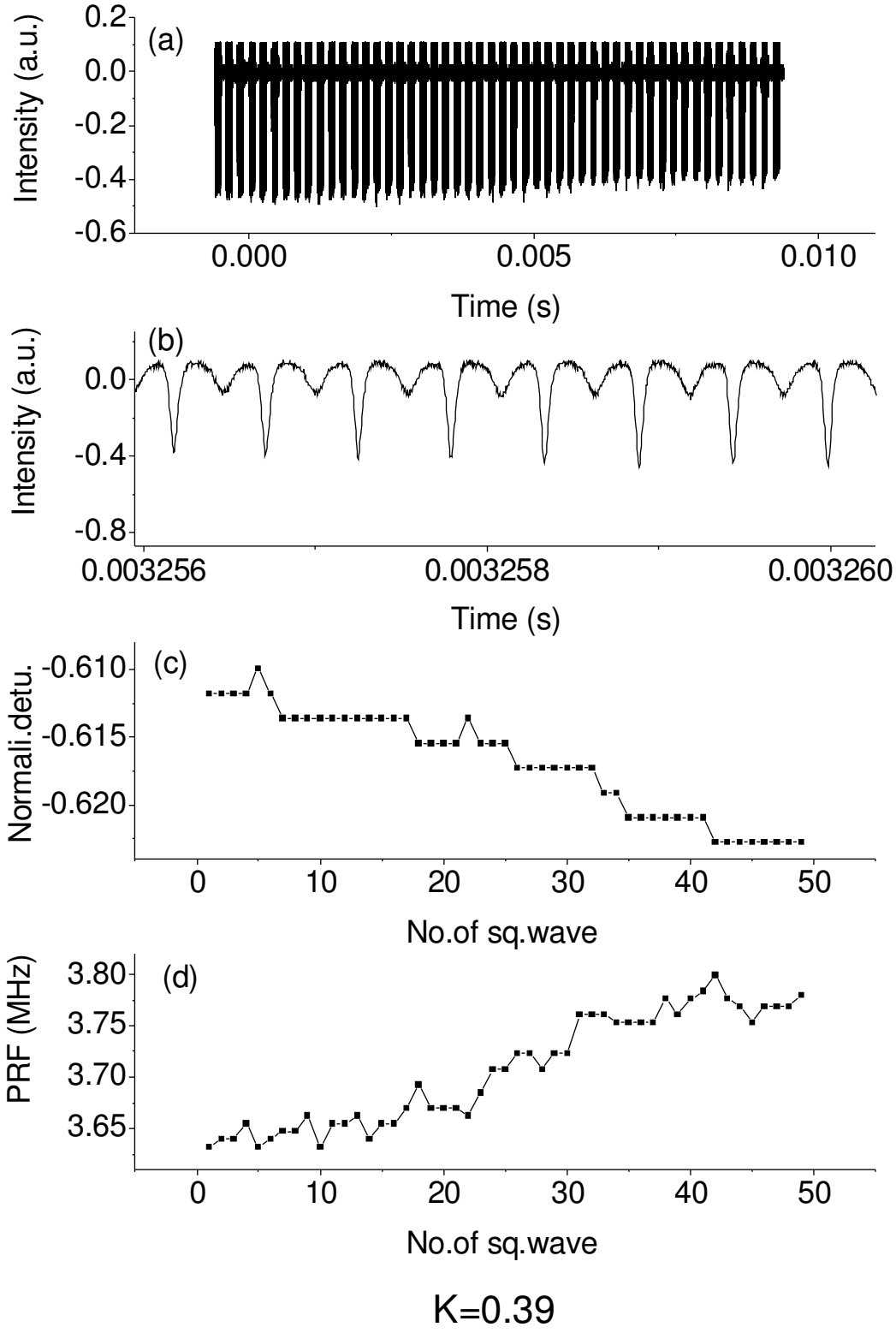

Figure A4. (a) The intensity level for 50 squares of pulses; (b) pulses waveform; (c) the change in frequency detuning in 10ms; (d) the change in PRF in 10ms. (The relations for the injection parameters K=0.39, Δω=- 0.62).

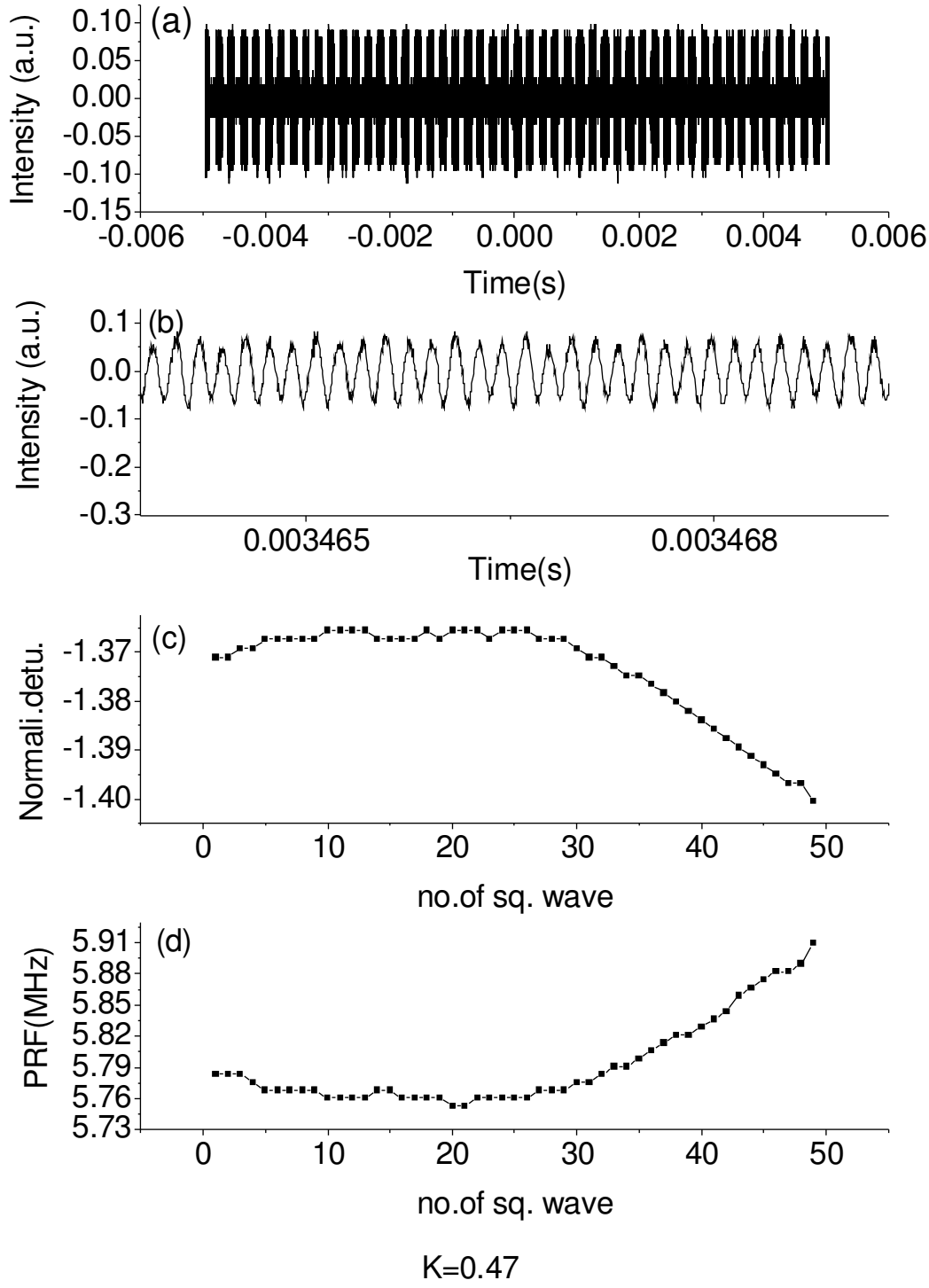

Figure A5. (a) The intensity level for 50 squares of pulses; (b) pulses waveform; (c) the change in frequency detuning in 10ms; (d) the change in PRF in 10ms. (The relations for the injection parameters K=0.47, Δω= - 1.38).

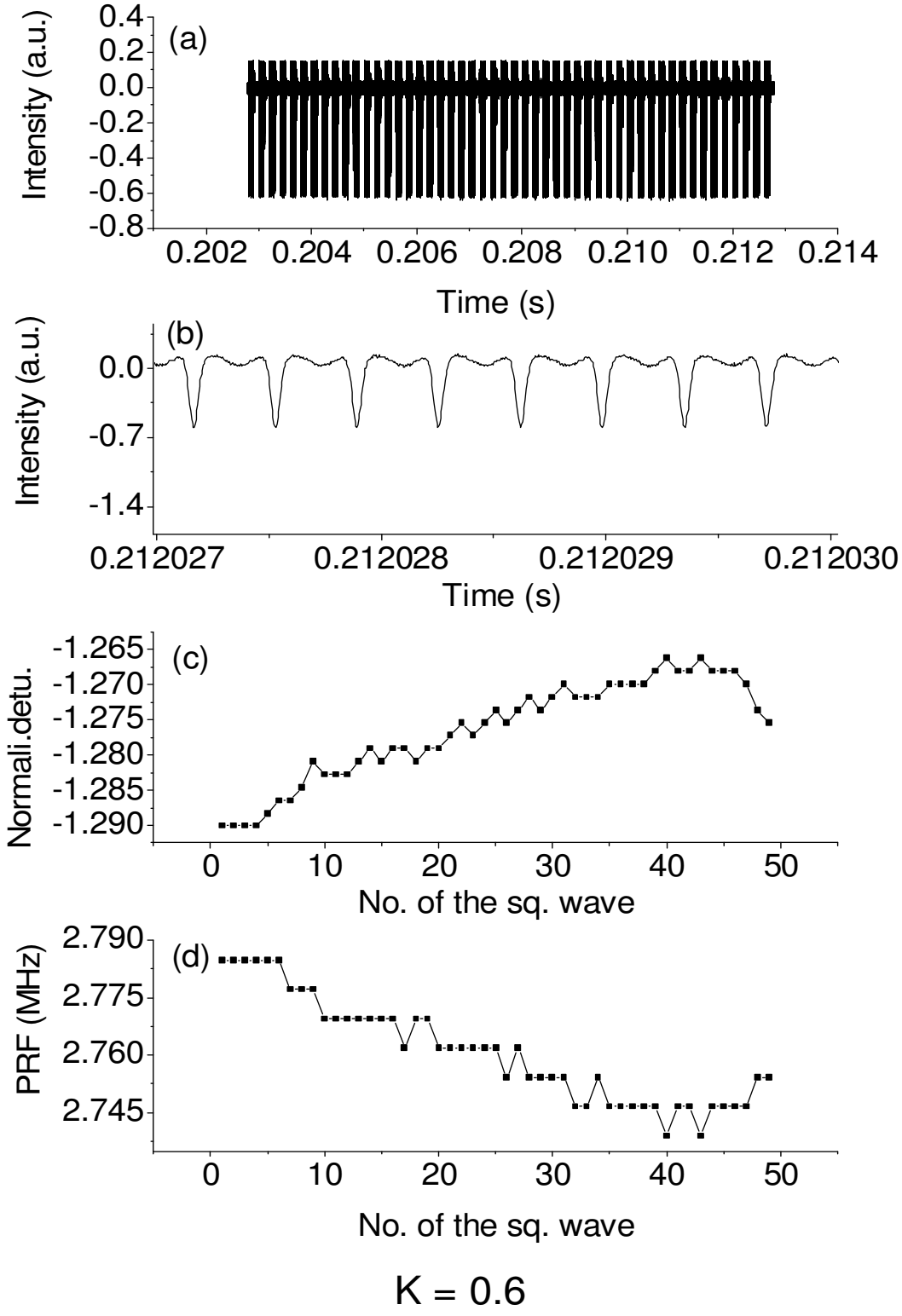

Figure A6. (a) The intensity level for 50 squares of pulses; (b) pulses waveform; (c) the change in frequency detuning in 10ms; (d) the change in PRF in 10ms. (The relations for the injection parameters K=0.6, Δω=- 1.27).

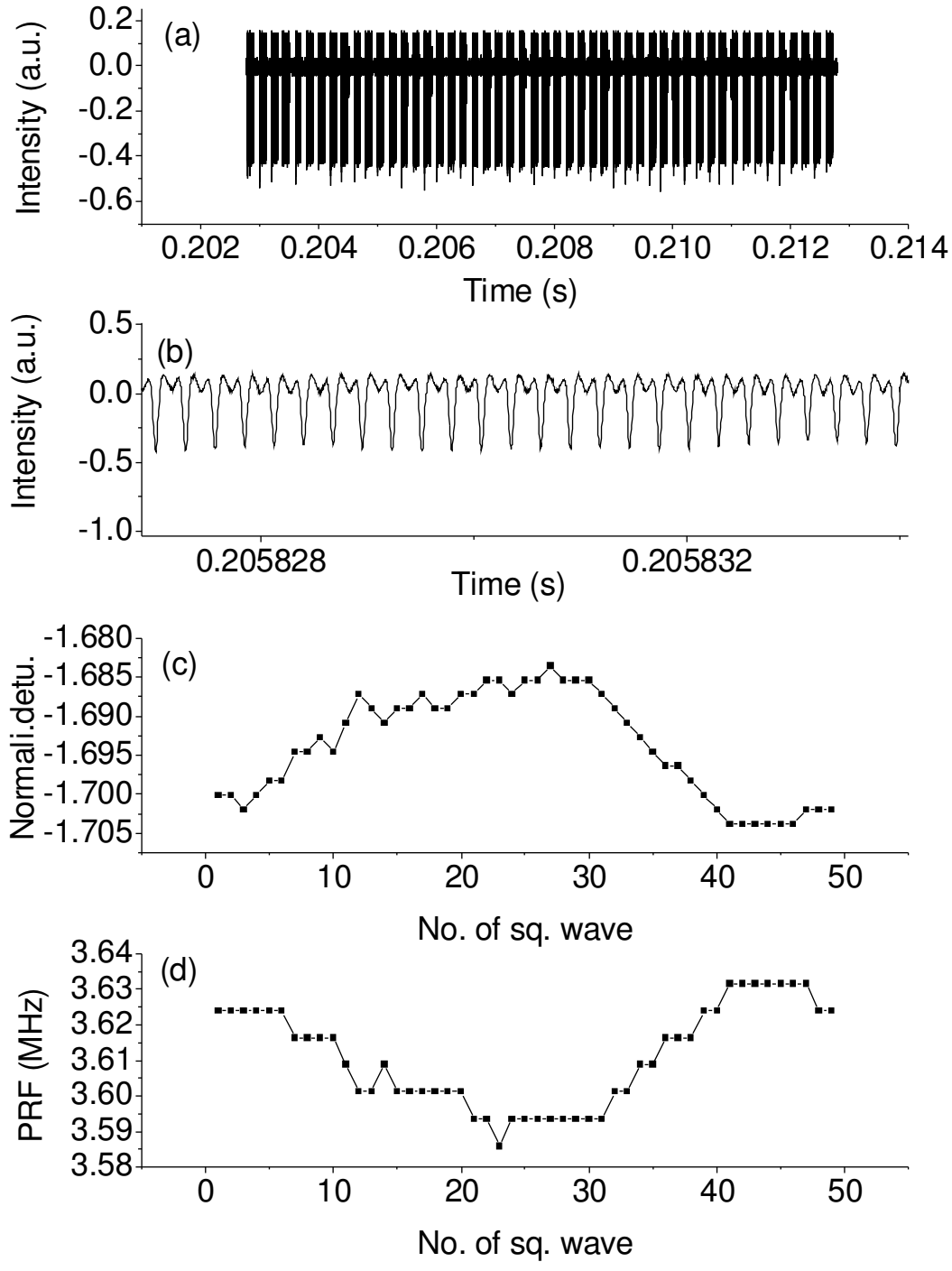

Figure A7. (a) The intensity level for 50 squares of pulses; (b) pulses waveform; (c) the change in frequency detuning in 10ms; (d) the change in PRF in 10ms. (The relations for the injection parameters K=0.6, Δω=- 1.69).

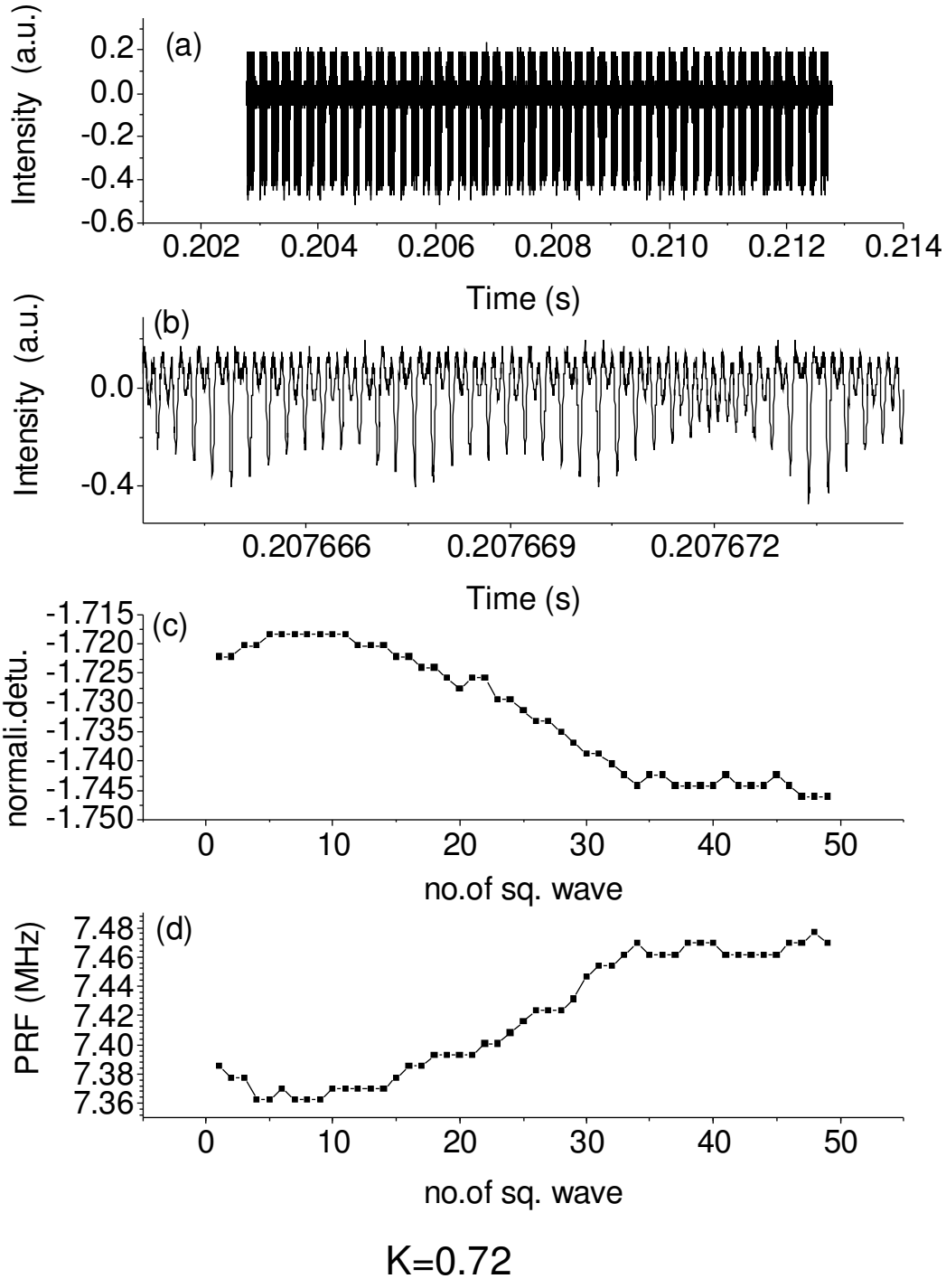

Figure A8. (a) The intensity level for 50 squares of pulses; (b) pulses waveform; (c) the change in frequency detuning in 10ms; (d) the change in PRF in 10ms. (The relations for the injection parameters K=0.72, Δω=- 1.73).

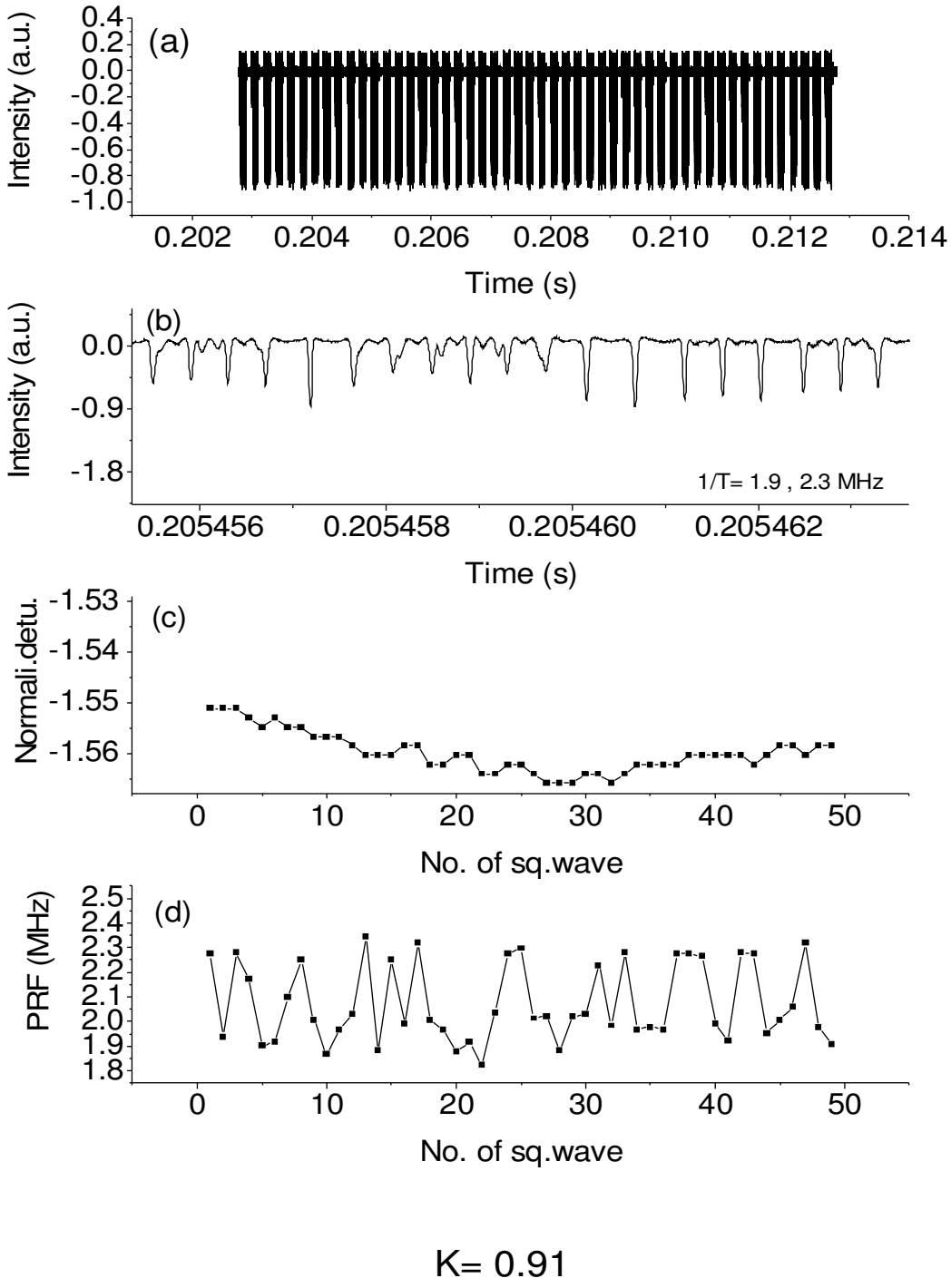

Figure A9. (a) The intensity level for 50 squares of pulses; (b) pulses waveform; (c) the change in frequency detuning in 10ms; (d) the change in PRF in 10ms. (The relations for the injection parameters K=0.91, Δω=- 1.55).

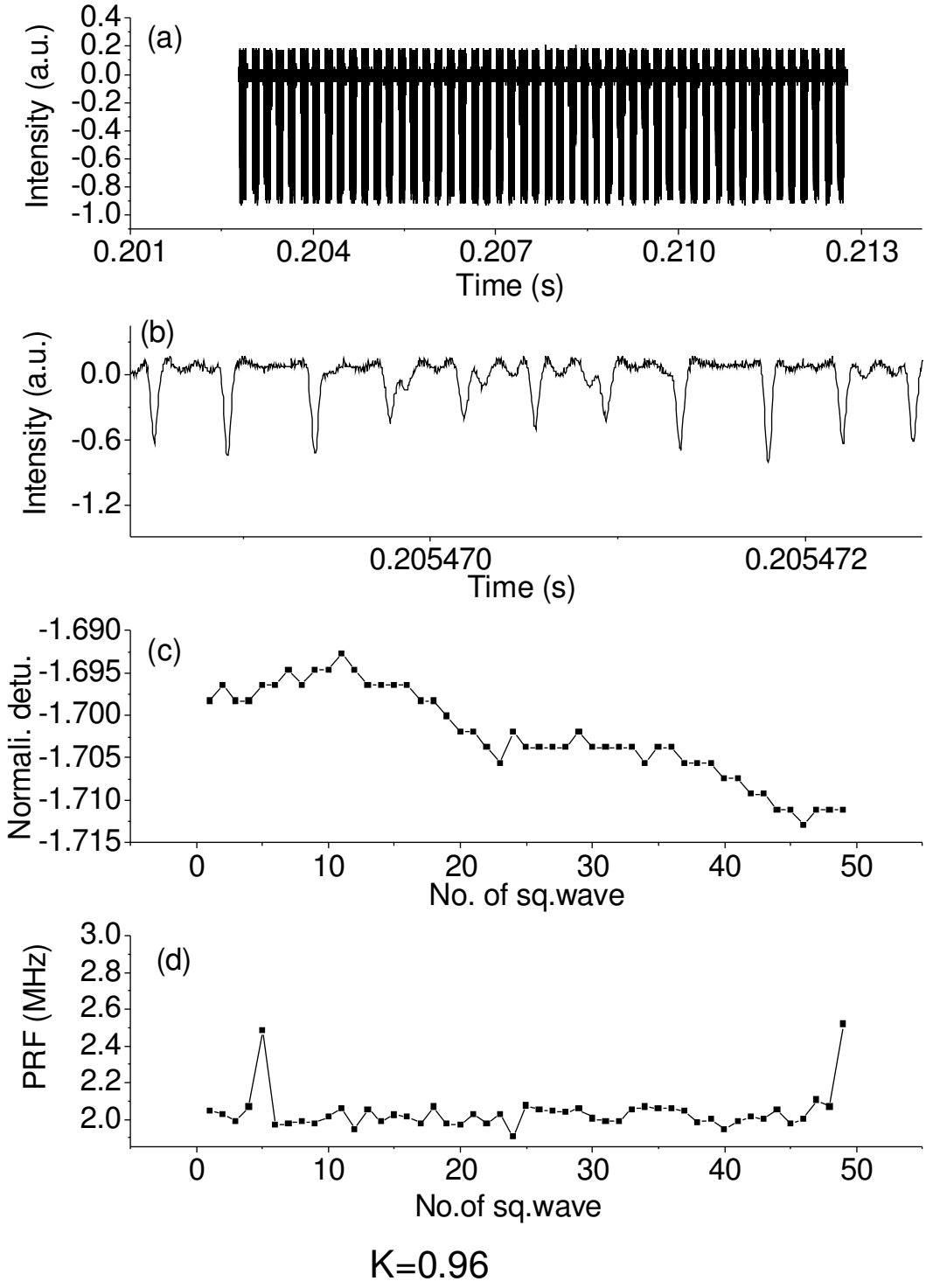

Figure A10. (a) The intensity level for 50 squares of pulses; (b) pulses waveform; (c) the change in frequency detuning in 10ms; (d) the change in PRF in 10ms. (The relations for the injection parameters K=0.96, Δω=- 1.96).

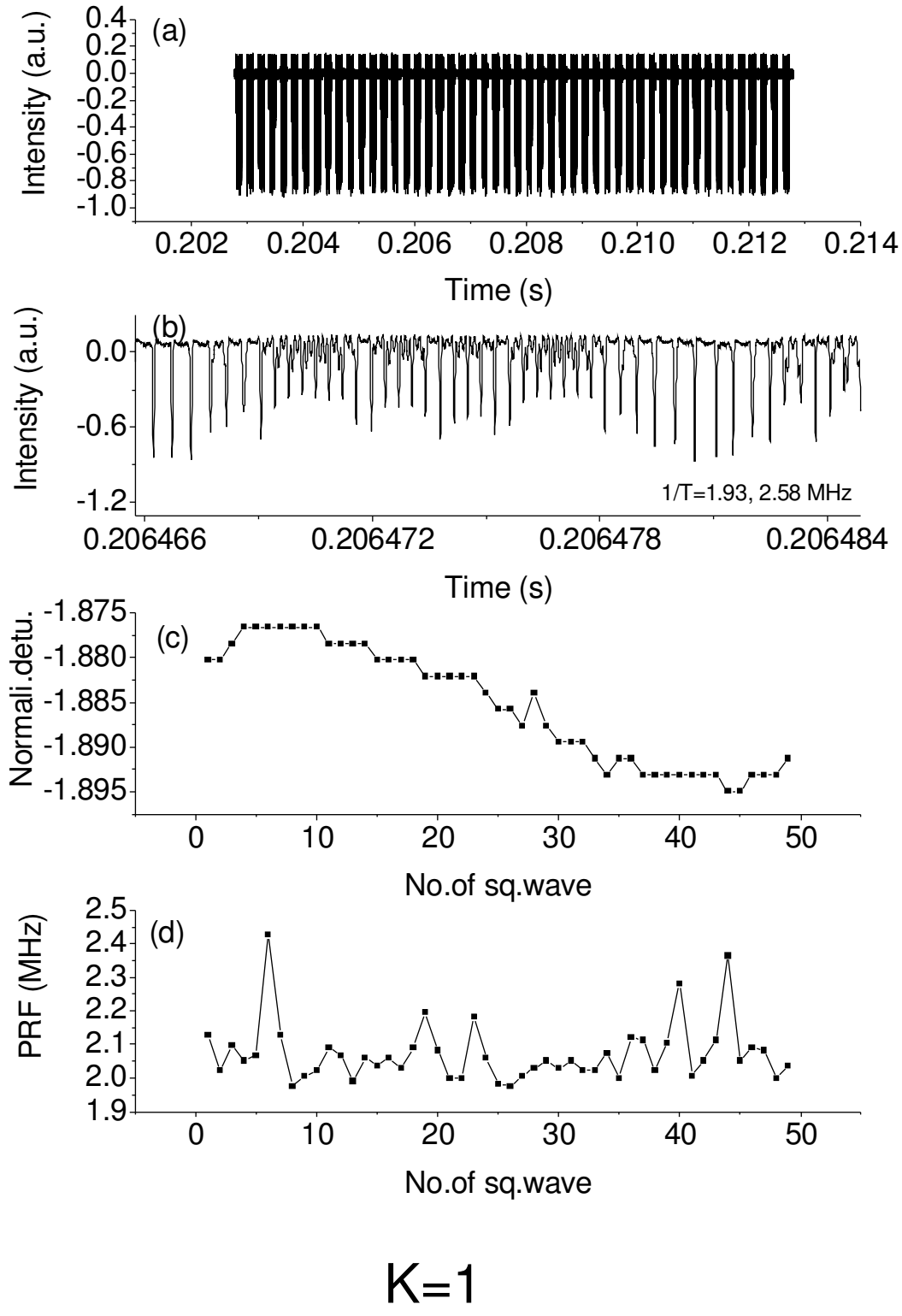

Figure A11. (a) The intensity level for 50 squares of pulses; (b) pulses waveform; (c) the change in frequency detuning in 10ms; (d) the change in PRF in 10ms. (The relations for the injection parameters K=1, Δω=- 1.88).

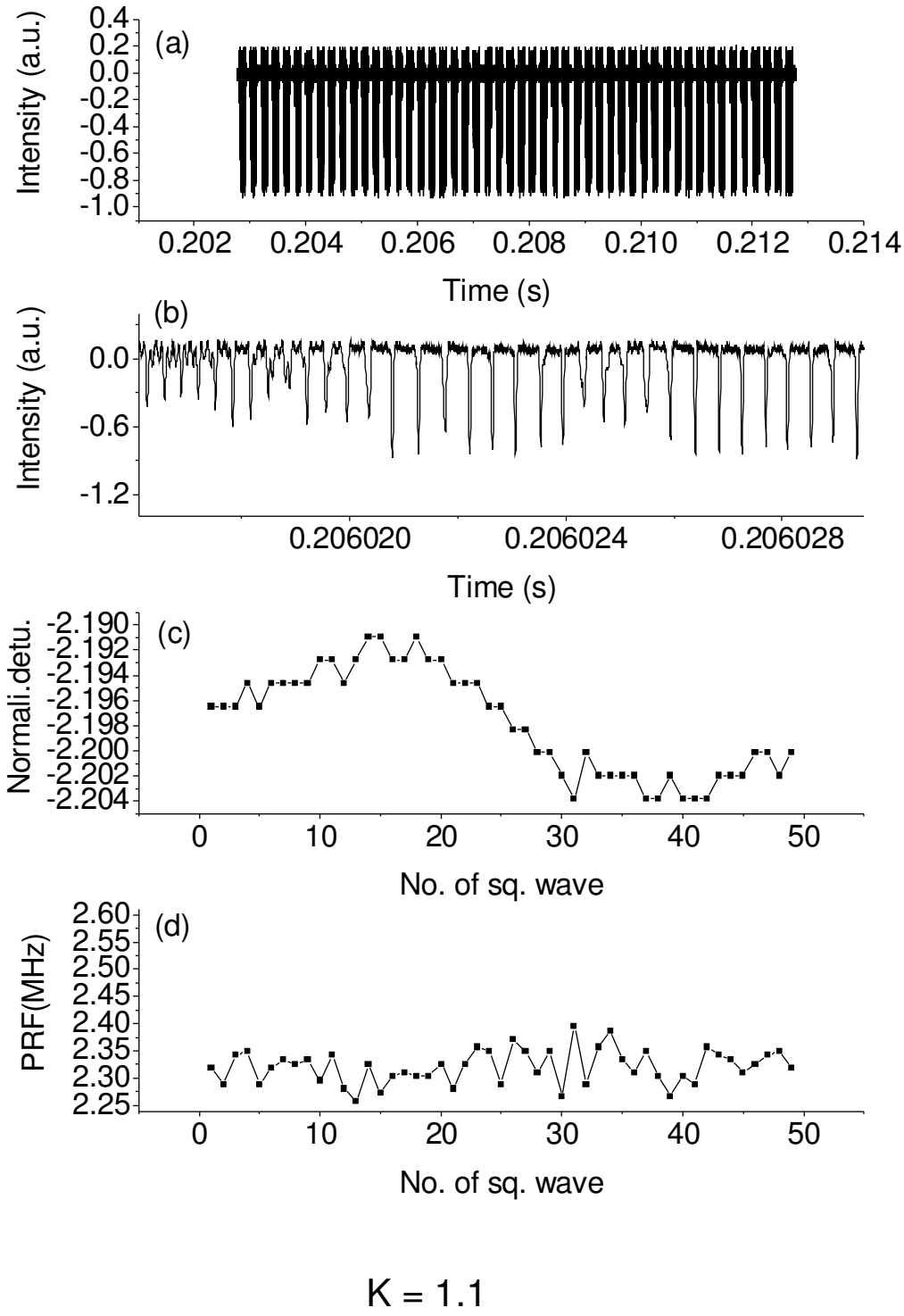

Figure A12. (a) The intensity level for 50 squares of pulses; (b) pulses waveform; (c) the change in frequency detuning in 10ms; (d) the change in PRF in 10ms. (The relations for the injection parameters K=1. 1, Δω=- 2.1).

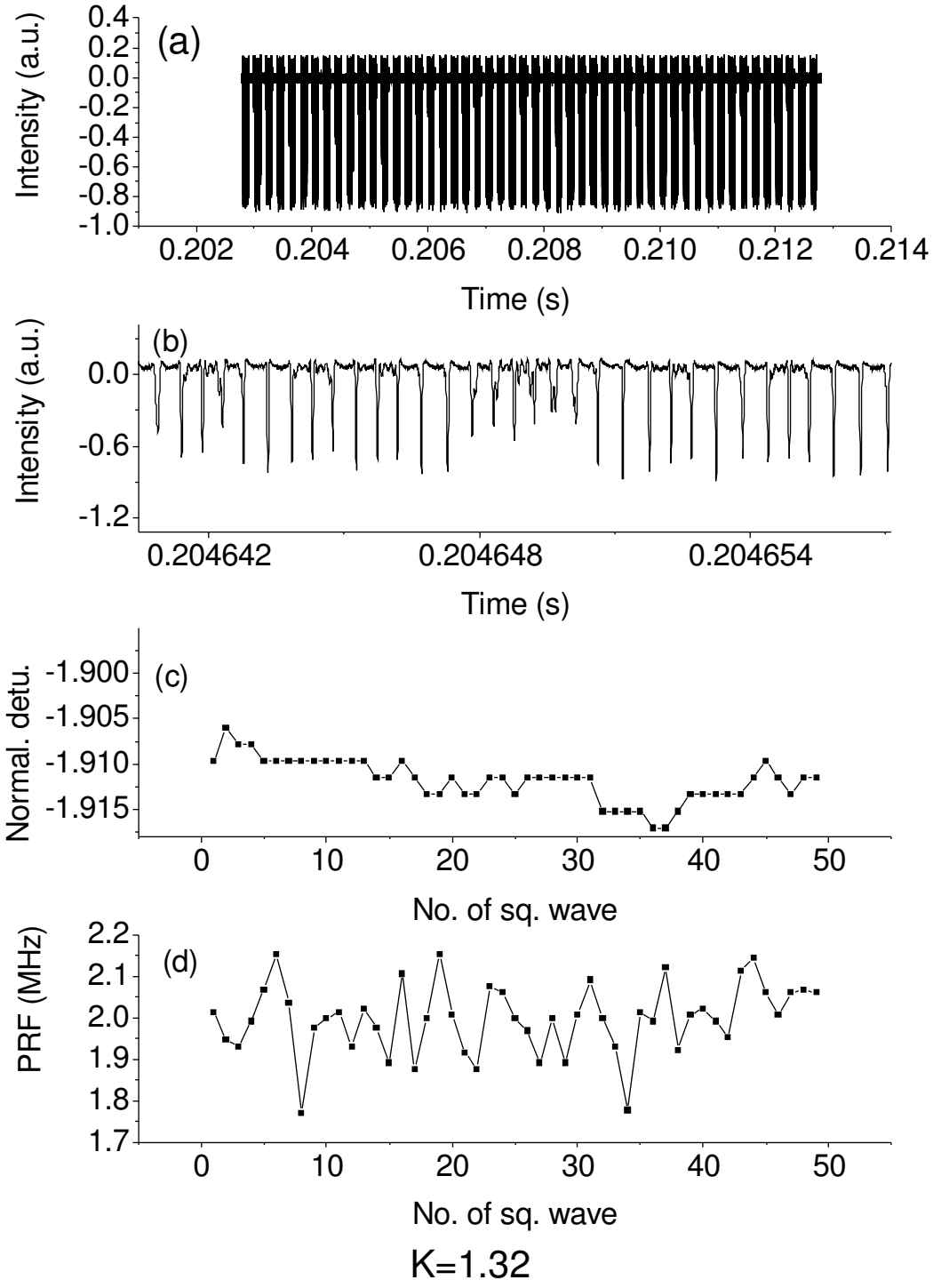

Figure A13. (a) The intensity level for 50 squares of pulses; (b) pulses waveform; (c) the change in frequency detuning in 10ms; (d) the change in PRF in 10ms. (The relations for the injection parameters K=1.32, Δω= -1.9).

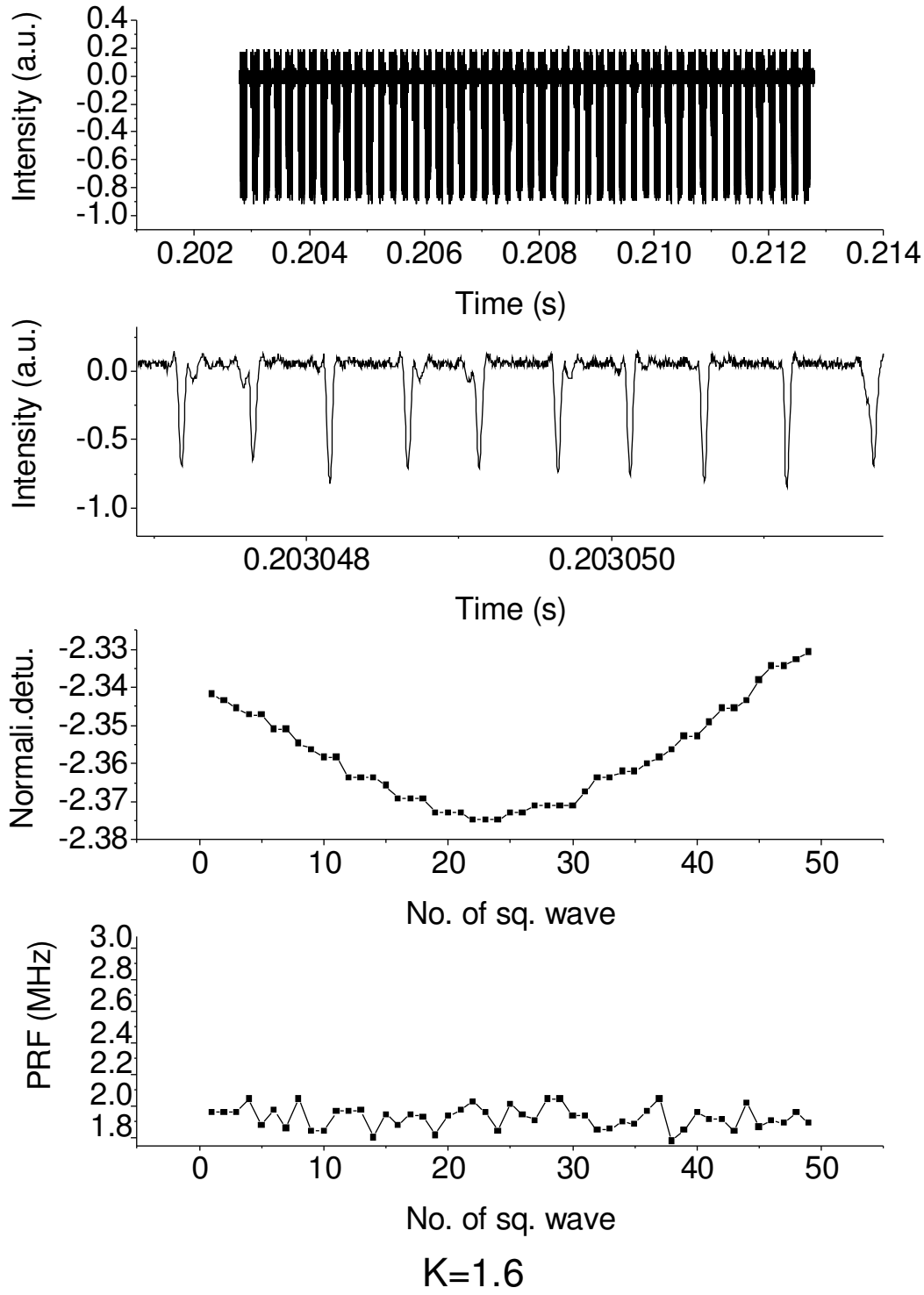

Figure A14. (a) The intensity level for 50 squares of pulses; (b) pulses waveform; (c) the change in frequency detuning in 10ms; (d) the change in PRF in 10ms. (The relations for the injection parameters K=1.6, Δω=- 2.3).

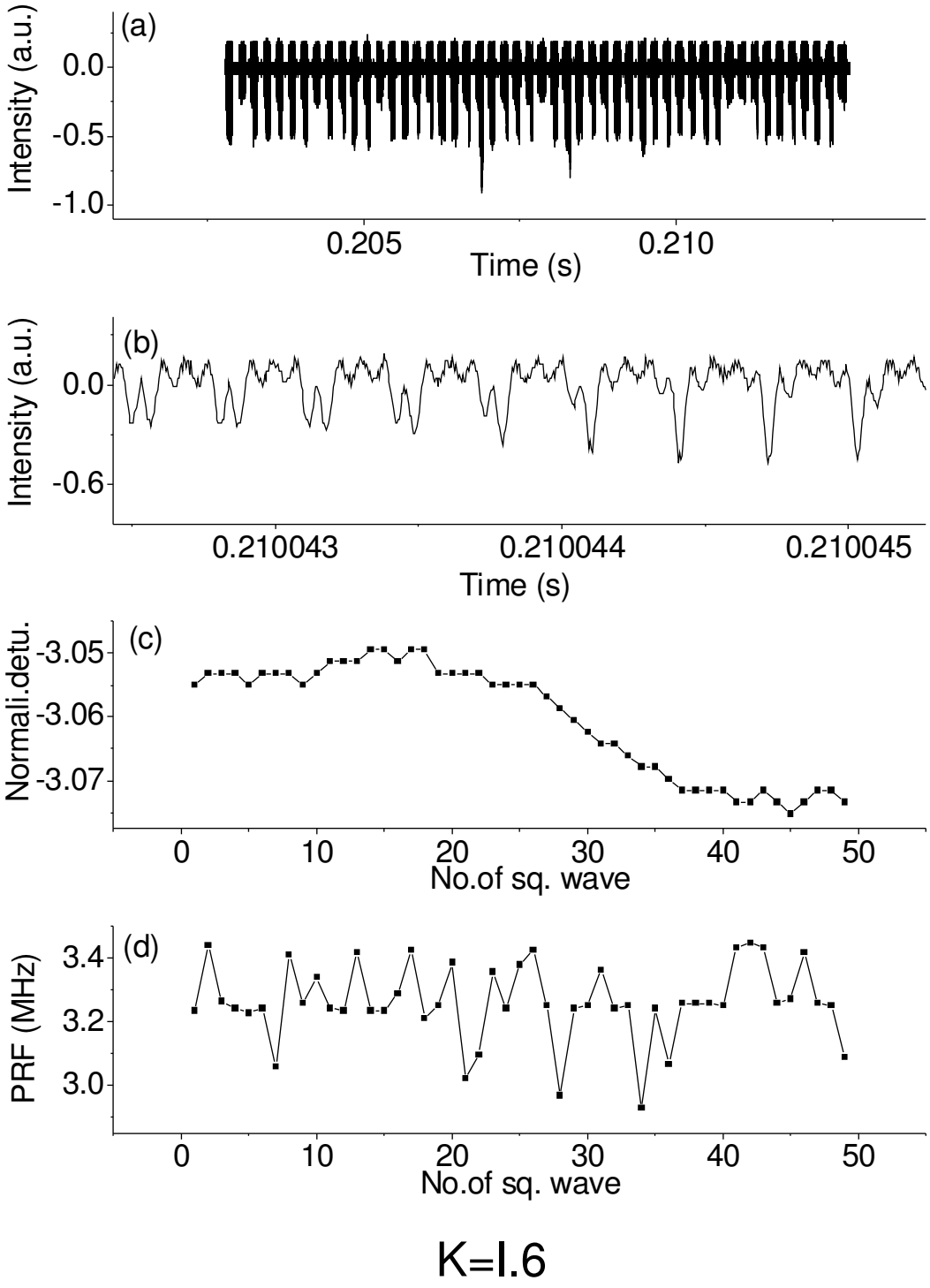

Figure A15. (a) The intensity level for 50 squares of pulses; (b) pulses waveform; (c) the change in frequency detuning in 10ms; (d) the change in PRF in 10ms. (The relations for the injection parameters K=1.6, Δω=- 3.05).

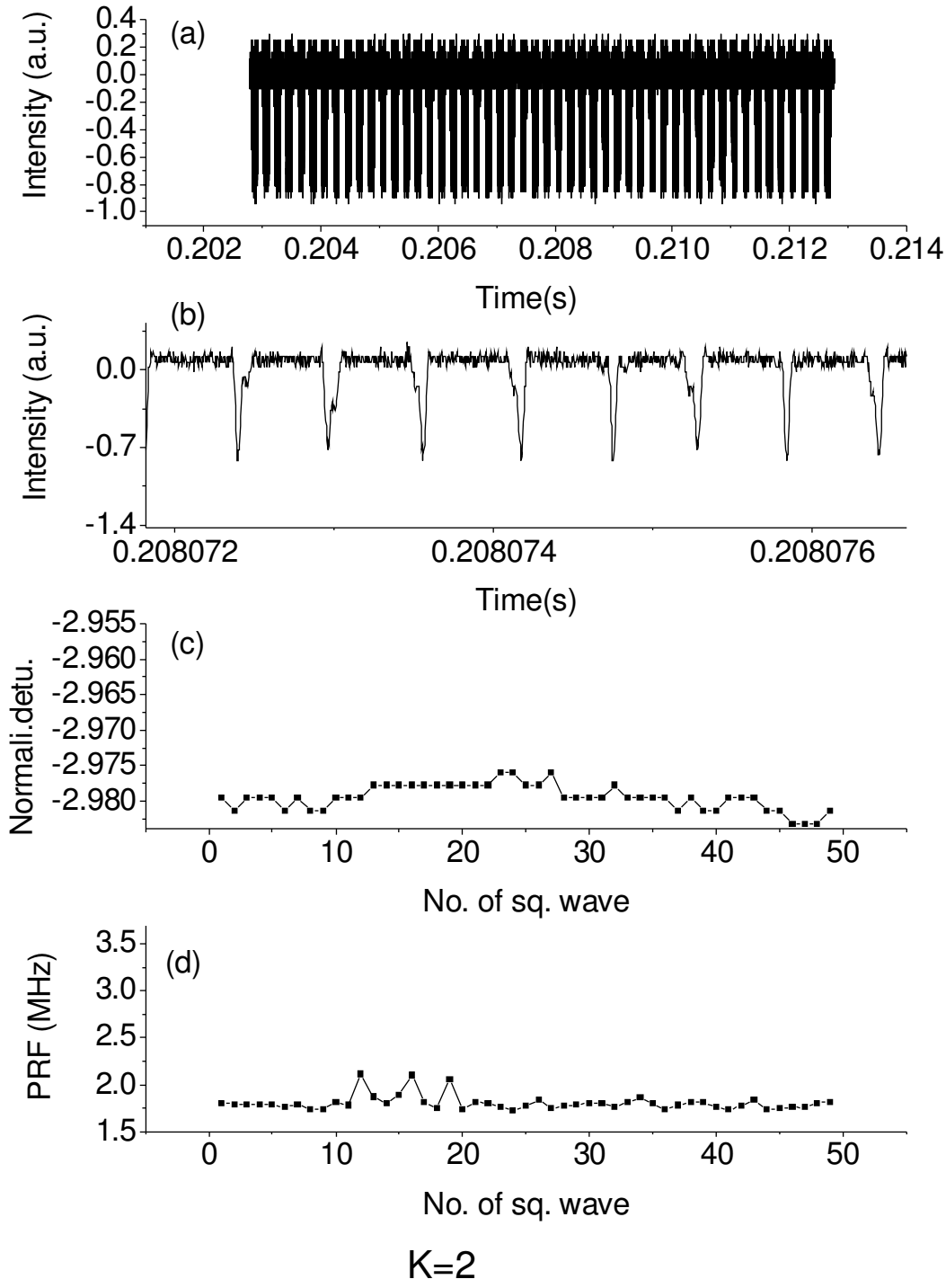

Figure A16: (a) The intensity level for 50 squares of pulses; (b) pulses waveform; (c) the change in frequency detuning in 10ms; (d) the change in PRF in 10ms. (The relations for the injection parameters K=2, Δω=- 2.98).

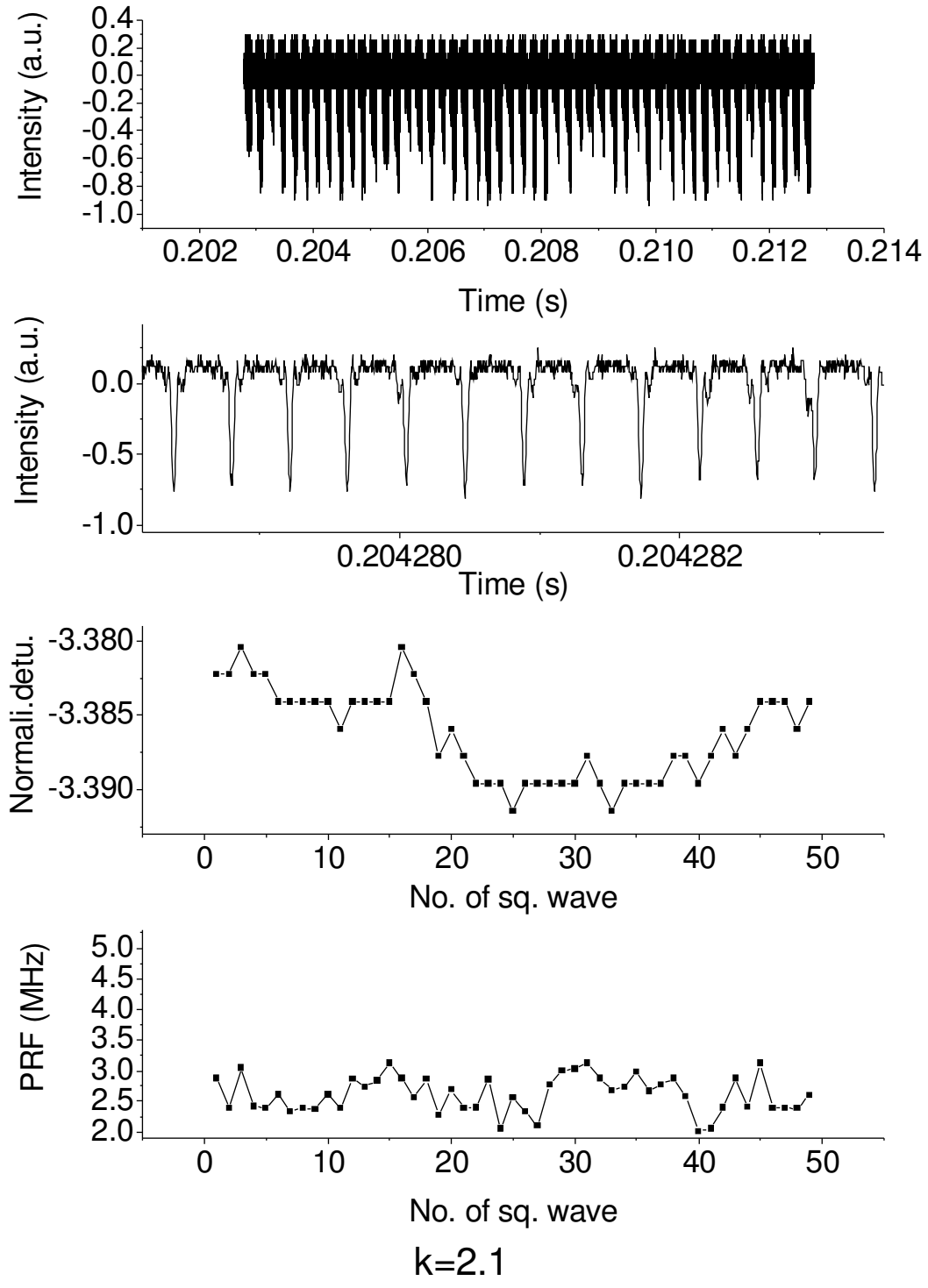

Figure A17 *(a) The intensity level for 50 squares of pulses; (b) pulses waveform; (c) the change in frequency detuning in 10ms; (d) the change in PRF in 10ms. (The relations for the injection parameters K=2. 1, Δω=- 3.38).*

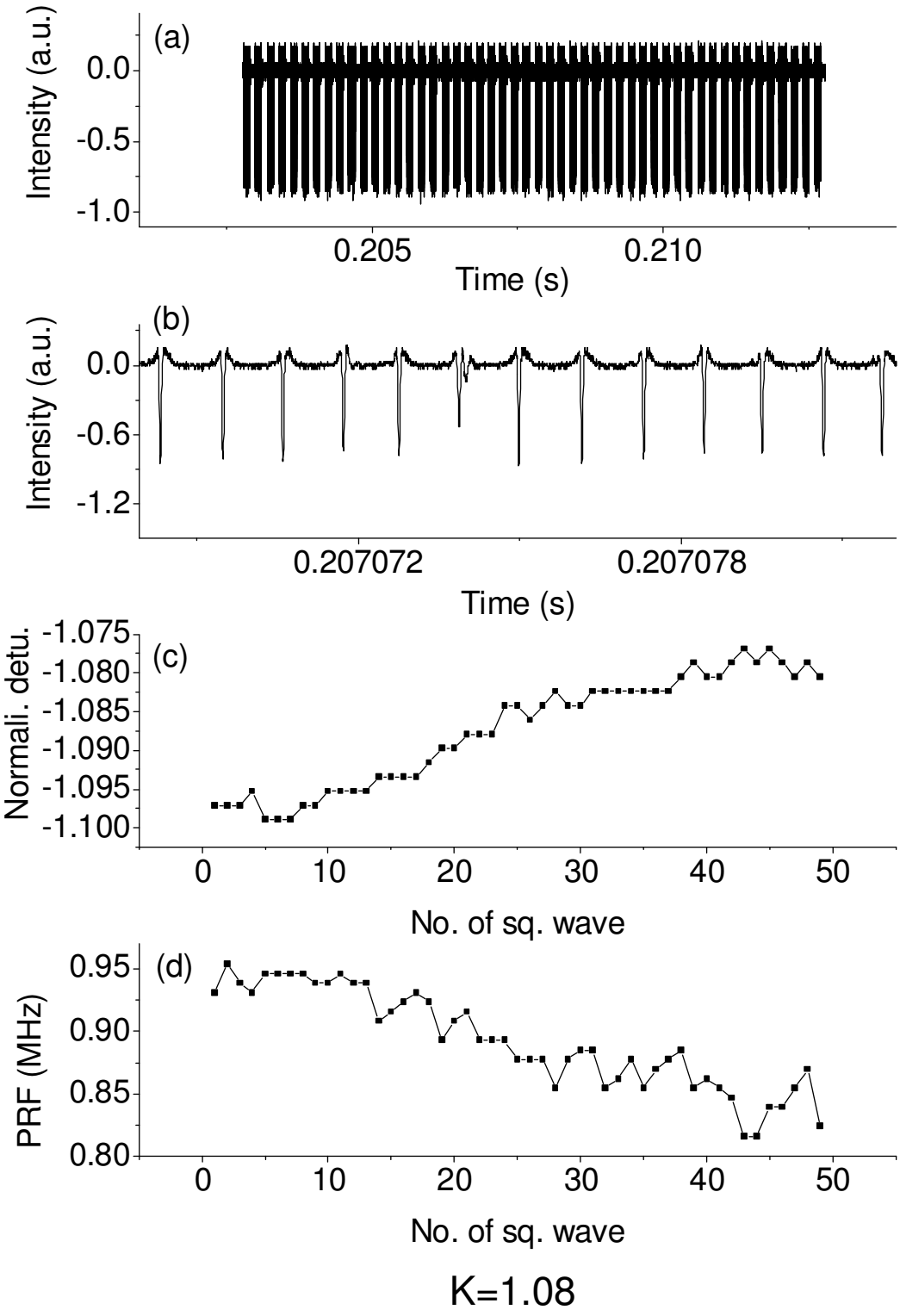

Figure A18 *(a) The intensity level for 50 squares of pulses; (b) pulses waveform; (c) the change in frequency detuning in 10ms; (d) the change in PRF in 10ms. (The relations for the injection parameters K=1.08 ,Δω=- 1.08).*

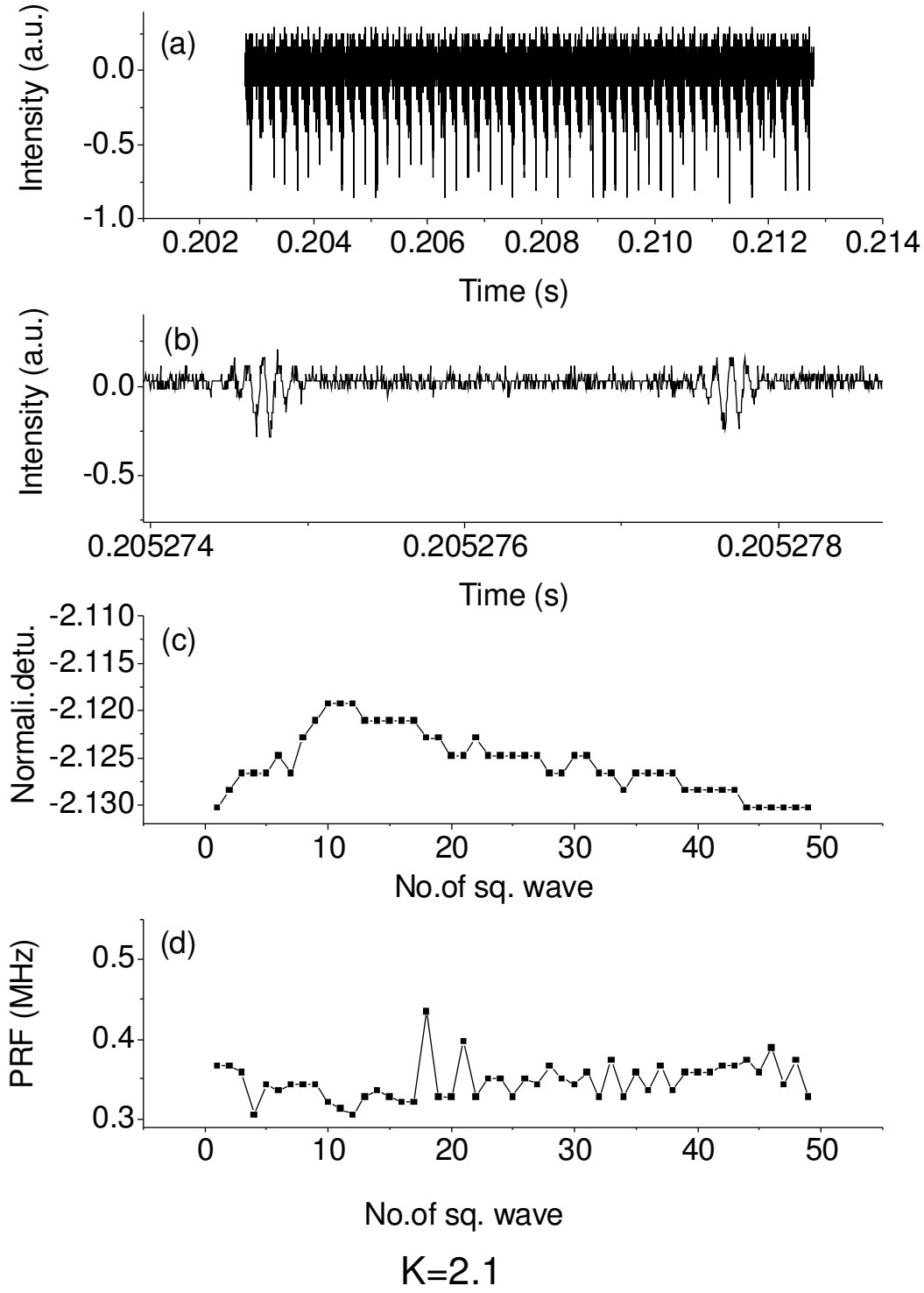

***Figure* A19** *(a) The intensity level for 50 squares of pulses; (b) pulses waveform; (c) the change in frequency detuning in 10ms; (d) the change in PRF in 10ms. (The relations for the injection parameters K=2.1 ,Δω=- **2.1**).*

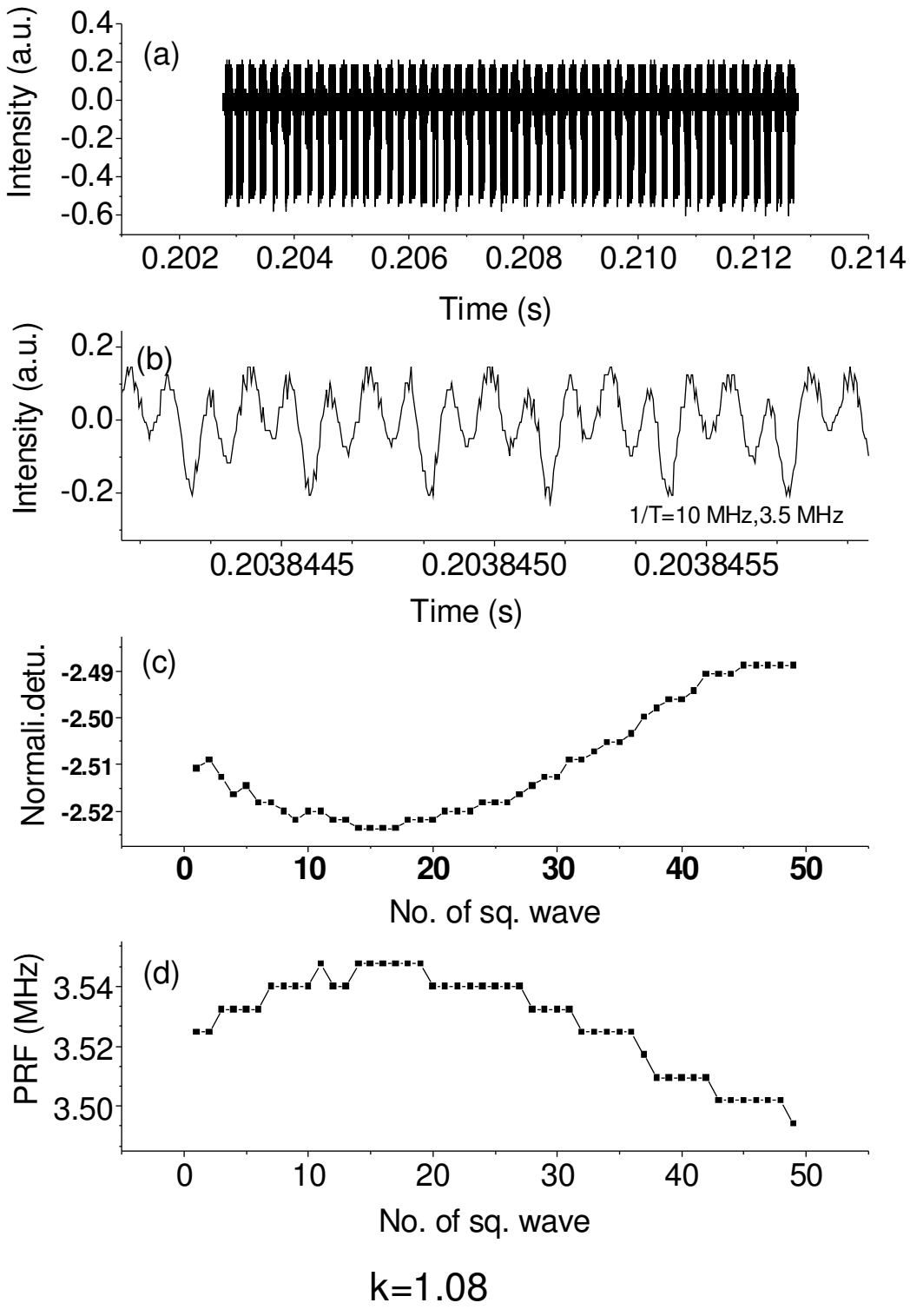

Figure A20 *(a) The intensity level for 50 squares of pulses; (b) pulses waveform; (c) the change in frequency detuning in 10ms; (d) the change in PRF in 10ms. (The relations for the injection parameters K=1.08 ,Δω=- 2.53).*

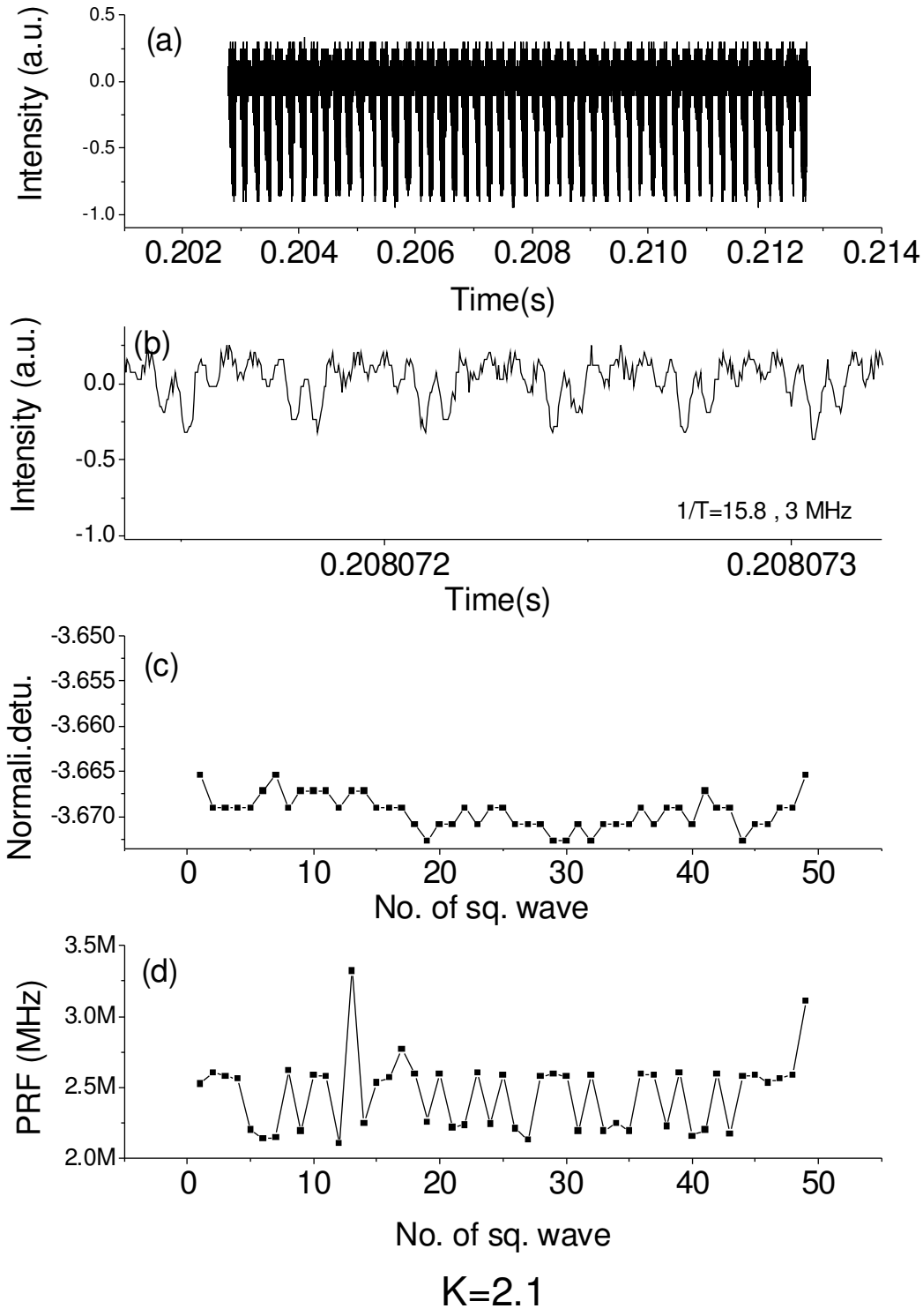

Figure A21 *(a) The intensity level for 50 squares of pulses; (b) pulses waveform; (c) the change in frequency detuning in 10ms; (d) the change in PRF in 10ms. (The relations for the injection parameters K=2.1 ,Δω=- 3.65).*